PRESSURIZED WATER REACTOR OWNERS GROUP

PWROG-15091-NP
Revision 1

Framatome Inc. NON-PROPRIETARY
WESTINGHOUSE NON-PROPRIETARY CLASS 3

Subscale Brine Test Program Report

Analysis Committee

PA-ASC-1188

November 2019

Westinghouse

framatome

Framatome Inc. NON-PROPRIETARY
WESTINGHOUSE NON-PROPRIETARY CLASS 3

PWROG-15091-NP
Revision 1

Subscale Brine Test Program Report

PA-ASC-1188

James P. Spring*
Safety Analysis

November 2019

Reviewer: Danial Utley*
LOCA Integrated Services II

Approved: Kent W. Bonadio*, Manager
LOCA Integrated Services II

Approved: Jay D. Boardman*, Program Director
PWR Owners Group PMO

*Electronically approved records are authenticated in the electronic document management system

Westinghouse Electric Company LLC
1000 Westinghouse Drive
Cranberry Township, PA 16066, USA

Framatome Inc.
3315 Old Forest Road
Lynchburg, VA 24501

ACKNOWLEDGEMENTS

This report was developed and funded by the PWR Owners Group under the leadership of the participating utility representatives of the Analysis Committee. The author thanks the PWR Owners Group GSI-191 Technical Integration Group Engaged in Research (TIGER) Team for their support and contributions to this program; Mr. Jeffrey Brown, the late Mr. Phillip Grissom, Mr. Dana Knee, Mr. Ernie Kee, Mr. Kenneth Greenwood, Mr. Timothy Croyle, and associate members; Mr. Kurt Flaig and Mr. Paul Leonard. The authors gratefully acknowledge and recognize the Framatome technical team who supported this effort; Mr. Adam Spontarelli and Mr. Gordon Wissinger, as well as Mr. Jay Boardman, PWR Owners Group Program Manager, Mr. Paul Stevenson, Ms. Danielle Page Blair and Mr. John Maruschak, Project Managers, for their guidance and encouragement throughout the process of developing this report. The authors also gratefully acknowledge all the members of the Churchill staff for their efforts in making this test program a success.

LEGAL NOTICE

This report was prepared as an account of work performed by both Framatome Inc. and Westinghouse Electric Company LLC. Neither Framatome Inc., nor Westinghouse Electric Company LLC, nor any person acting on its behalf:

1. Makes any warranty or representation, express or implied including the warranties of fitness for a particular purpose or merchantability, with respect to the accuracy, completeness, or usefulness of the information contained in this report, or that the use of any information, apparatus, method, or process disclosed in this report may not infringe privately owned rights; or

2. Assumes any liabilities with respect to the use of, or for damages resulting from the use of, any information, apparatus, method, or process disclosed in this report.

COPYRIGHT NOTICE

DISTRIBUTION NOTICE

This report was prepared for the PWR Owners Group. This Distribution Notice is intended to establish guidance for access to this information. This report (including proprietary and non-proprietary versions) is not to be provided to any individual or organization outside of the PWR Owners Group program participants without prior written approval of the PWR Owners Group Program Management Office. However, prior written approval is not required for program participants to provide copies of Class 3 Non-Proprietary reports to third parties that are supporting implementation at their plant, and for submittals to the NRC.

PWR Owners Group
United States Member Participation* for PA-ASC-1188

Utility Member	Plant Site(s)	Participant	
		Yes	No
Ameren Missouri	Callaway (W)	X	
American Electric Power	D.C. Cook 1 & 2 (W)	X	
Arizona Public Service	Palo Verde Unit 1, 2, & 3 (CE)	X	
Dominion Energy	Millstone 2 (CE)	X	
	Millstone 3 (W)	X	
	North Anna 1 & 2 (W)	X	
	Surry 1 & 2 (W)	X	
	V.C. Summer (W)	X	
Duke Energy Carolinas	Catawba 1 & 2 (W)	X	
	McGuire 1 & 2 (W)	X	
	Oconee 1, 2, & 3 (B&W)	X	
Duke Energy Progress	Robinson 2 (W)	X	
	Shearon Harris (W)	X	
Entergy Palisades	Palisades (CE)	X	
Entergy Nuclear Northeast	Indian Point 2 & 3 (W)	X	
Entergy Operations South	Arkansas 1 (B&W)	X	
	Arkansas 2 (CE)	X	
	Waterford 3 (CE)	X	
Exelon Generation Co. LLC	Braidwood 1 & 2 (W)	X	
	Byron 1 & 2 (W)	X	
	Calvert Cliffs 1 & 2 (CE)	X	
	Ginna (W)	X	
FirstEnergy Nuclear Operating Co	Beaver Valley 1 & 2 (W)	X	
	Davis-Besse (B&W)	X	
Florida Power & Light \ NextEra	St. Lucie 1 & 2 (CE)	X	
	Turkey Point 3 & 4 (W)	X	
	Seabrook (W)	X	
	Pt. Beach 1 & 2 (W)	X	
Luminant Power	Comanche Peak 1 & 2 (W)	X	

PWR Owners Group
United States Member Participation* for PA-ASC-1188

Utility Member	Plant Site(s)	Participant	
		Yes	No
Pacific Gas & Electric	Diablo Canyon 1 & 2 (W)	X	
PSEG – Nuclear	Salem 1 & 2 (W)	X	
So. Texas Project Nuclear Operating Co.	South Texas Project 1 & 2 (W)	X	
Southern Nuclear Operating Co.	Farley 1 & 2 (W)	X	
	Vogtle 1 & 2 (W)	X	
Tennessee Valley Authority	Sequoyah 1 & 2 (W)	X	
	Watts Bar 1 & 2 (W)	X	
Wolf Creek Nuclear Operating Co	Wolf Creek (W)	X	
Xcel Energy	Prairie Island 1 & 2 (W)	X	

* **Project participants as of the date the final deliverable was completed. On occasion, additional members will join a project. Please contact the PWR Owners Group Program Management Office to verify participation before sending this document to participants not listed above.**

PWR Owners Group
International Member Participation* for PA-ASC-1188

Utility Member	Plant Site(s)	Participant	
		Yes	No
Asociación Nuclear Ascó-Vandellòs	Asco 1 & 2 (W)	X	
	Vandellos 2 (W)	X	
Centrales Nucleares Almaraz-Trillo	Almaraz 1 & 2 (W)	X	
EDF Energy	Sizewell B (W)	X	
Electrabel	Doel 1, 2 & 4 (W)	X	
	Tihange 1 & 3 (W)	X	
Electricite de France	58 Units	X	
Elektriciteits Produktiemaatschappij Zuid-Nederland	Borssele 1 (Siemens)	X	
Eletronuclear-Eletrobras	Angra 1 (W)	X	
Emirates Nuclear Energy Corporation	Barakah 1 & 2	X	
Hokkaido	Toman 1, 2 & 3 (MHI)	X	
Japan Atomic Power Company	Tsuruga 2 (MHI)	X	
Kansai Electric Co , LTD	Mihama 3 (W)	X	
	Ohi 1, 2, 3 & 4 (W & MHI)	X	
	Takahama 1, 2, 3 & 4 (W & MHI)	X	
Korea Hydro & Nuclear Power Corp.	Kori 1, 2, 3 & 4 (W)	X	
	Hanbit 1 & 2 (W)	X	
	Hanbit 3, 4, 5 & 6 (CE)	X	
	Hanul 3, 4 , 5 & 6 (CE)	X	
Kyushu	Genkai 2, 3 & 4 (MHI)	X	
	Sendai 1 & 2 (MHI)	X	
Nuklearna Electrarna KRSKO	Krsko (W)	X	
Ringhals AB	Ringhals 2, 3 & 4 (W)	X	
Shikoku	Ikata 2 & 3 (MHI)	X	
Taiwan Power Co.	Maanshan 1 & 2 (W)	X	

* **Project participants as of the date the final deliverable was completed. On occasion, additional members will join a project. Please contact the PWR Owners Group Program Management Office to verify participation before sending this document to participants not listed above.**

FOREWARD

This technical report was prepared in support of final resolution of Generic Safety Issue (GSI) – 191 and is incorporated into WCAP-17788 by reference to provide justification for the cold leg break in-vessel debris limit as described in Section 7 of WCAP-17788, Volume 1.

WCAP-17788 is comprised of six volumes. All six volumes of Revision 0 of the technical report were submitted to the U.S. Nuclear Regulatory Commission (US NRC) with the objective of obtaining a Safety Evaluation (SE) on the complete report (all six volumes). The US NRC initiated a review of the technical report and issued a number of Requests for Additional Information (RAIs). A number of RAI questions were also asked for this technical report. Responses to those RAIs were prepared and submitted. In the middle of 2019, the US NRC informed the PWROG that an SE would not be issued on WCAP-17788. Rather, the US NRC would accept licensees referring to WCAP-17788 in their response submittals to Generic Letter (GL) 2004-02 (ADAMS Accession Number ML042360586), accompanied by a statement demonstrating the applicability of the referenced portion of WCAP-17788 to their specific PWR unit.

Additionally, the US NRC has used information contained in WCAP-17788, along with other information, to prepare a Technical Evaluation Report (TER) that concludes in-vessel debris effects are of low safety significance. The US NRC has used the TER to support closure of GSI-191 (ADAMS Accession Number ML19203A303). In lieu of an SE, the TER was published in Volume 1 of WCAP-17788, Revision 1.

To support use of WCAP-17788 by PWROG members, Revision 1 of WCAP-17788 was prepared and includes the TER, all RAIs and their responses, as well as modifications to the text of the report committed to in the RAI responses. As noted previously, WCAP-17788 has not received an US NRC SE. However, all six volumes of WCAP-17788 have been amended to Revision 1 and are made available to participating PWROG members for their use in responding to GL 2004-02 for the PWR units they operate.

All RAIs and their responses are included in an appendix to the applicable volumes. It is noted that Volume 2 was not reviewed in detail by the US NRC, and as a result, an RAI was not provided for this volume of the technical report. It is also noted that sections of technical report PWROG-15091 Revision 0, "Subscale Brine Test Program Report" were reviewed as supporting information to WCAP-17788. RAIs and their responses related to PWROG-15091 are included in the applicable WCAP-17788, Volume 1 appendix. Revision 1 of PWROG-15091 was also prepared and includes a modification to the text as committed to in the RAI response.

This report may reference AREVA. Since Revision 0 of this report was generated, AREVA has changed their name to Framatome Inc.

TABLE OF CONTENTS

LIST OF TABLES

LIST OF FIGURES

1 EXECUTIVE SUMMARY

Westinghouse and the Pressurized Water Reactor Owners Group (PWROG) have designed and built the subscale brine test facility to investigate the influence that fibrous debris collection at the core inlet has on density-driven mass transport between the core and lower plenum regions of a reactor vessel. The goal of the test program was to obtain concentration distribution data in the core and lower plenum regions of the test facility such that the exchange flow rate across the core inlet geometry could be calculated. Debris bed pressure drop data was also collected throughout the testing. The experiments will provide insight into the physical phenomena occurring in a reactor vessel following a postulated large cold leg break (CLB) loss-of-coolant accident (LOCA) and the results will be used to justify an in-vessel debris limit for the large CLB scenario.

A number of natural convection experiments and analyses have been completed that are relevant to the subscale brine testing. In Section 3, these experiments and analyses are reviewed to introduce the physical phenomena of buoyancy-driven exchange (countercurrent) flow which is the primary mechanism for core-to-lower plenum mass transport investigated by the subscale brine testing.

The subscale brine testing is intended to study the density-driven flow patterns governed by the concentration gradient of boron solutes that develop between the core and lower plenum. While it would be preferable to use varying concentrations of borated solution as the working fluid, the subscale test facility is not able to operate at the conditions necessary to study the borated solution concentrations of interest, nor is it equipped to insulate against the heat losses associated with elevated temperatures. Additionally, there are difficulties associated with the accurate measurement of these solution concentrations. Instead, various borated solution concentrations at 212°F will be simulated through the use of an aqueous salt solution at room temperature. Justification of this approach and selection of the aqueous salt solution is provided in Section 4.

The test facility was constructed at the Westinghouse thermal hydraulic test laboratory located in Churchill, Pennsylvania. The design consists of a 4 inch inner-dimension, square cross-section flow column that houses the tested fuel geometry, which is roughly one-quarter of a full-area fuel assembly. The vertical column was fabricated with clear polycarbonate sidewalls to provide optical access. For testing, debris-laden flow was injected from the bottom of the test column and directed upwards through the fuel geometry. Brine was injected downstream of the simulated core region using a sparger designed to uniformly inject the brine across the entire test column cross-section. Additional details associated with the brine test facility design, operation, and test conditions are contained in Section 5.

In the testing, the density gradient that develops between the core and the lower plenum due to the build-up of boron solutes in the core was simulated using a potassium bromide (KBr) solution. Flow through the test column was scaled based on the boil-off rate calculated for prototypic Post-LOCA conditions. For tests that had brine injection, the flow rate was reduced during each test consistent with the decay heat curve. For tests conducted with debris only (no brine injection) the flow rate was held constant at a value consistent with decay heat boil-off

calculated at 20 minutes post-LOCA. Fibrous debris loadings of 2.5 – 22.5 grams per full-area fuel assembly (g/FA) arriving at the core inlet were considered in the testing, which is consistent with the range of debris loads expected to enter the reactor vessel following a large CLB scenario. A limited number of tests were completed with fibrous and particulate debris to understand the impact that particulate debris has on the resulting debris bed and the core-to-lower plenum buoyancy-driven exchange process.

A total of 46 production experiments were completed using the subscale brine test facility. The test program was broken into two test series. Test Series 1 was completed using a core inlet geometry representative of Westinghouse fuel components, and Series 2 was completed using a geometry representative of AREVA fuel components. Section 6 presents the detailed test matrix, and Sections 7 through 11 present and analyze the test data obtained during the program, which includes tests conducted with debris injection only, brine injection only, and tests with both debris and brine injection.

The subscale brine test program was successful in improving the state of knowledge of density-driven mass transport between the core and the lower plenum in the presence of in-vessel debris. The testing considered a broad range of conditions prototypic of those expected to occur following a postulated large CLB LOCA and considered both Westinghouse and AREVA core inlet geometries by using prototypic fuel components.

The debris only test results demonstrate that debris beds formed under low-flow conditions prototypic of a large CLB scenario result in minimal head loss with the maximum pressure drop achieved across the debris bed being less than [ ]^{a,c} when experimental uncertainty was considered. The addition of particulate debris was shown to have [ ]^{a,c} for the low fibrous debris loadings considered in this testing.

The brine test results demonstrate [

]^{a,c} Densimetric Froude number provides the relative importance of inertia to buoyancy forces. As Froude number reduces buoyancy forces become more dominate. In this scenario, a reduction in upward liquid velocity or an increase in density difference results in a reduction in Froude number. [

]^{a,c}

2 INTRODUCTION

Westinghouse and the PWROG have designed and built the subscale brine test facility to investigate the influence that fibrous debris collection at the core inlet has on density-driven mass transport between the core and lower plenum regions of a PWR reactor vessel. The goal of the test program was to obtain concentration distribution data in the core and lower plenum regions of the test facility such that the exchange flow rate across the core inlet geometry could be calculated. Debris bed pressure drop data was also collected throughout the testing. The experiments will provide insight into the physical phenomena occurring in a reactor vessel following a postulated large CLB LOCA and the results will be used to justify an in-vessel debris limit for the large CLB scenario.

The subscale brine test facility is an adiabatic, separate effects test facility that takes advantage of an existing test apparatus constructed by Westinghouse and the PWROG for resolution of in-vessel debris effects under Nuclear Regulatory Commission (NRC) Generic Safety Issue 191 (GSI-191) (Reference 2-1). The brine test facility was designed to simulate the post-LOCA density gradient that exists between the core and lower plenum by using a high density brine solution that is injected downstream from the core inlet geometry. The injected brine will create the necessary density gradient to transport mass through the core inlet geometry. The testing investigated how this density-driven transport mechanism is influenced by the presence of debris collection at the core inlet.

This report provides details of the test facility design, the experimental setup, and the results obtained. Analysis is provided to quantify the influence of in-vessel debris on the density-driven mass transport (exchange rate) between the core and the lower plenum regions of a reactor vessel.

2.1 BACKGROUND

Assessment of post-LOCA long-term core cooling (LTCC) has gained considerable regulatory attention over the last decade. Extended power uprates (EPUs) have provided the opportunity for the NRC to challenge some of the common approaches, assumptions and simplifications used in the analyses that support the plant methods and timing for boric acid precipitation control (BAPC). The entire U.S. PWR fleet uses boron as a reactivity control method and is subject to the potential for BAP in the reactor vessel under certain post-LOCA scenarios. The common approach for demonstrating adequate BAPC in a post-LOCA scenario includes the use of simplified methods with conservative boundary conditions and assumptions. These methods are used with limiting scenarios in calculations that determine the time at which appropriate operator action must be taken to initiate an active boric acid dilution flow path or alternately, to show that BAP will not occur.

Prior to 2004, the majority of PWR licensees used Westinghouse topical report CENPD-254, "Post LOCA Long Term Cooling Model" (Reference 2-2) or a similar method to demonstrate adequate BAPC. However, this topical report has since been suspended for use by the NRC due to the discovery of non-conservative modeling assumptions (Reference 2-3). Licensees who relied on CENPD-254-P or similar methods were requested by the NRC to perform an

evaluation to confirm that sufficient margin exists and that they remain in compliance with the regulations and their design basis.

In response to the NRC request, and in accordance with the stated NRC expectations, the PWROG funded a program to review and qualitatively evaluate the BAPC analysis-of-record (AOR) for each participating licensee to confirm that post-LOCA BAP would not occur and those regulatory requirements are met. As suggested by the staff, these evaluations used insights from analyses performed for the Waterford 3 EPU, along with recent analyses for the Beaver Valley and Ginna EPUs, to show that existing calculations are conservative and post-LOCA BAP would not occur with the existing plant mitigation measures. The results from this evaluation were submitted to the NRC in OG-06-200 (Reference 2-3), which concluded that sufficient margin exists in the methodology and assumptions to prevent the boric acid concentration in the reactor vessel from exceeding the solubility limit before established operator actions are completed.

One of the margins credited in the evaluation presented in OG-06-200 was the lower plenum volume. However, the closure of GSI-191 has brought crediting this margin into question due to a potential technical issue regarding the influence of in-vessel debris following a postulated large CLB. The potential technical issue, as identified by the NRC, centers on whether a debris bed formed at the core inlet, could cut off communication between the core and lower plenum and prevent the transport of high concentration boric acid into the lower plenum. This must be addressed for the evaluations contained in OG-06-200 to remain valid for plants in which lower plenum volume was credited.

This test program is intended to investigate the impact of in-vessel debris on the transport of mass between the core and the lower plenum. Ultimately, the results from this program will be used to define an in-vessel fibrous debris limit for the large CLB scenario such that communication between the core and lower plenum will continue.

2.2 PROTOTYPIC SCENARIO

For typical plant designs (Westinghouse 2-loop Upper Plenum Injection (UPI) plants excluded), the limiting scenario for BAP is a large cold leg (pump discharge) break where the downcomer is eventually filled and the excess safety injection (SI) flows out of the break. The SI flow into the core region is largely limited to that quantity boiled-off in the core to remove decay heat. The steam generated in the core travels around the intact hot leg(s) (or through the Reactor Vessel Vent Valves (RVVVs) in B&W-designed plants) to exit the break. Boric acid left behind accumulates in the core region and the boric acid concentration in the core region increases. Eventually, the core region boric acid concentration increases to the point that it is high enough to overcome the kinetic energy associated with the upward flow from the lower plenum needed to replace boil-off. At this point, buoyancy-driven mass transport occurs between the core and the lower plenum. Higher concentration boric acid from the core region is exchanged with lower concentration boric acid from the lower plenum. During this time, the core and upper plenum are filled with a two-phase mixture whose liquid content is dependent on the degree of voiding in the core and upper plenum region. The degree of voiding is a function of the core decay heat, the reactor coolant system (RCS) pressure, and the pressure drop around the loop (or through

the RVVVs), as it affects the hydrostatic balance between the downcomer head and the collapsed liquid level in the core. At low RCS pressures and high decay heat levels, the boiling in the core is vigorous, and the volume of liquid in the core region is smaller. As the decay heat drops off, the boiling becomes less vigorous and more liquid is retained in the core region.

Westinghouse U.S. 2-loop plants differ from typical PWR designs because they utilize low pressure upper plenum safety injection (i.e., UPI). For these plants, the limiting large break LOCA BAP scenario is a hot leg break where the cold leg high pressure SI may be terminated at or prior to sump recirculation. This scenario is relevant only with the very conservative assumption that all UPI flow in excess of core boil-off bypasses the core region and flows directly out of the break (i.e., no mixing in the core and upper plenum). Under this scenario, buoyancy-driven mass transport from the core to the lower plenum is still relevant and will increase the effective mixing volume used to predict the build-up of boric acid in the reactor vessel.

2.3 POST-LOCA BORIC ACID PRECIPITATION ANALYSIS METHODOLOGY

For Westinghouse-designed and CE-designed plants, BAP calculations are used to determine the appropriate time to switch some or all the emergency core cooling system (ECCS) sump recirculation flow to the hot leg or to otherwise show that BAP will not occur. For B&W-designed plants, BAP calculations are used to justify plant-specific active boric acid dilution methods or limitations on the dilution methods (e.g., plant specific auxiliary pressurizer spray flows, protection of the sump screens, prevention of potential water-hammer scenarios in the decay heat piping, challenges to Net Positive Suction Head (NPSH) limits for Low Pressure Injection (LPI) pumps, hot and cold fluid mixing limits, prevention of BAP inside the decay heat cooler).

Current post-LOCA boric acid analysis methodologies do not consider the effects of GSI-191 in-vessel debris. The current analysis methods assume that the coolant entering the reactor vessel is free of any debris constituents. Further, the analyses do not account for any effects that in-vessel debris may have on the mixing and transport phenomena associated with BAP.

The NRC has identified the lack of GSI-191 considerations in the current post-LOCA analysis methodologies as a potential technical issue. The technical issue is focused on the impact of in-vessel debris on the effective mixing volume used to calculate the build-up of boric acid in the reactor vessel. Typical Westinghouse methods assume that the lower plenum volume is part of the effective mixing volume and if the lower plenum volume is removed, the build-up of boric acid in the reactor vessel is accelerated. Providing additional experimental information to help address this potential technical issue is the focus of this testing activity.

2.4 REFERENCES

2-1 WCAP-17788-P/NP (Proprietary/Non-Proprietary), "Comprehensive Analysis and Test Program for GSI-191 Closure (PA-SEE-1090) – Subscale Head Loss Test Program Report," July 2015.

2-2 CENPD-254-P, "Post-LOCA Long Term Cooling Evaluation Model," June 1980.

2-3 NRC letter dated November 23, 2005, D. S. Collins to G. C. Bischoff, "Suspension of NRC Approval for use of Westinghouse Topical Report CENPD-254-P, Post LOCA Long Term Cooling Model, Due to Discovery of Non-Conservative Modeling Assumptions During Calculation Audit."

2-4 OG-06-200, "Suspension of NRC Approval for Use of Westinghouse Topical Report CENPD-254-P, Post LOCA Long Term Cooling Model, Due to Discovery of Non-Conservative Modeling Assumptions During Calculation Audit, PA-ASC-0290," June 2006.

3 REVIEW OF PREVIOUS WORK

A number of natural convection experiments and analyses have been completed that are relevant to the subscale brine testing. In this section, these experiments and analyses are reviewed to introduce the physical phenomena of buoyancy-driven exchange (countercurrent) flow which is the primary mechanism for core-to-lower plenum mass transport investigated by the subscale brine testing.

3.1 BUOYANCY-DRIVEN EXCHANGE FLOW THROUGH SMALL OPENINGS IN A HORIZONTAL PARTITION

In Reference 3-1, Epstein completed an experimental study of buoyancy-driven exchange flow through a single opening in a horizontal partition. In the experiments, a density-driven exchange flow was obtained by placing brine in a tank above the partition and fresh water in a second tank below the partition. For opening aspect ratios (L/D) in the range of 0.01 to 10, where L and D are the length of the opening and the diameter of the opening, respectively, Epstein concluded that the exchange flow rate, for all practical purposes, was independent of viscosity. This enables the purely buoyancy-driven volumetric exchange rate, Q_{cc}, to be correlated with respect to Froude number (dimensionless exchange rate) and the aspect ratio:

$$\frac{Q_{cc}}{(D^5 g\,\Delta\rho/\bar{\rho})^{1/2}} = \frac{0.055\left[1+400(L/D)^3\right]^{1/6}}{\left(1+0.00527\left[1+400(L/D)^3\right]^{1/2}\left[(L/D)^6+117(L/D)^2\right]^{3/4}\right)^{1/3}} \quad \text{Eq. 3-1}$$

where the left hand side of Eq. 3-1 is the densimetric Froude number with g being the gravitational constant, $\Delta\rho$ the density gradient between the two fluids, and $\bar{\rho}$ the average density.

Also in Reference 3-1, Epstein extended the experimental study to consider buoyancy-driven exchange flow between two compartments separated by a horizontal partition with two openings, which can result in more complex flow patterns than those observed in the experiments that considered a single opening.

For flow through each opening in a multi-opening system, the flow may be unidirectional and form a convective loop, as illustrated in Figure 3-1(a). On the other hand, simultaneous unidirectional flow and countercurrent (bidirectional) flow may occur, as illustrated in Figure 3-1(b). Under certain conditions, it is also possible to obtain bidirectional flow through all openings, as illustrated in Figure 3-1(c). It is relevant to note that the bidirectional flow shown in Figure 3-1(b) is different from that encountered in a system with a single opening in that in the former case the upward flow rate is not equal to the downward flow rate. With downward unidirectional flow occurring in opening 2, continuity demands that the upward flow exceed the downward flow within opening 1.

It is apparent from Epstein's work (Reference 3-1) that the flow within any opening of a multi-opening system may be bidirectional if the unidirectional flow established throughout the system

is not high enough to prevent the opposing flow in the opening. In other words, some minimal unidirectional, "purging" or "flooding" velocity is required to prevent countercurrent flow within the opening. In the flow configuration shown in Figure 3-1(a), the strength of the unidirectional convective loop is sufficient to prevent the downward flow of the heavier liquid into opening 1 and the upward flow of lighter liquid into opening 2. To the contrary, in the situation depicted in Figure 3-1(b), the loop flow is not strong enough to oppose the downward movement of the heavier fluid at opening 1.

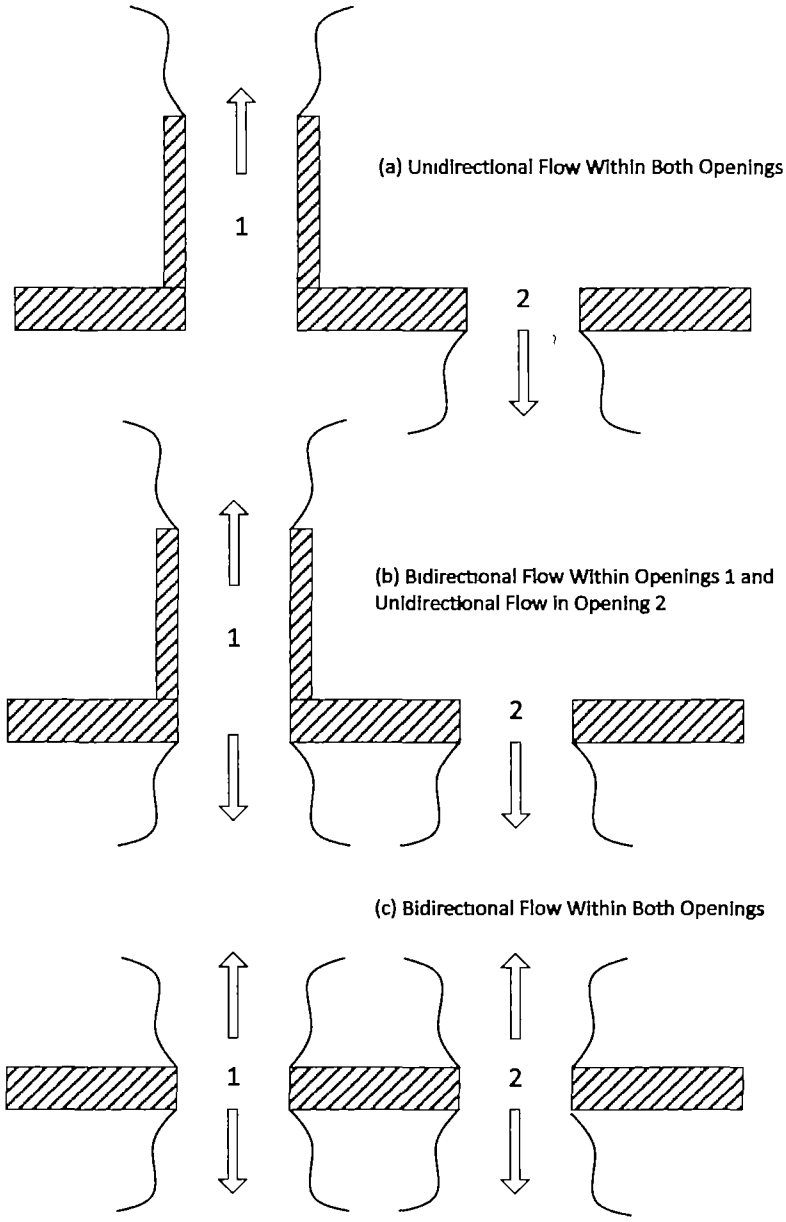

Figure 3-1 Illustration of Observed Flow Configurations with the Two-Opening System (Reproduced from Reference 3-1)

Epstein has shown in Reference 3-1 that an expression for the exchange flow rate for the unidirectional flow configuration shown in Figure 3-1(a) can be obtained by application of the Bernoulli equation. The derivation is not repeated here but assuming there is no net volumetric flow to each compartment and that the entrance loss coefficients for the openings are the same and equal to 1/2, the following equation can be written to determine the unidirectional volumetric flow rate, Q_u:

$$Q_u = 0.805\left[\frac{A_1^2 g\Delta\rho L}{\rho_L + \rho_H(A_1/A_2)^2}\right]^{1/2} \quad \text{Eq. 3-2}$$

where A_1 and A_2 are the areas of openings 1 and 2, respectively. L is the length of the gravitational head of the system, and ρ_L and ρ_H are the light and heavy fluid densities, respectively. The coefficient of 0.805 on the right hand side of Eq. 3-2 has been reduced by 30% of the value derived from the Bernoulli equation. This was done based on experimental results obtained in Reference 3-1 which showed that the exchange flow was about 70 percent of the theoretical predicted by Eq. 3-2 when a coefficient of 1.15 was used. Apparently additional contractions and losses reduce the exchange flow rate through the system (Reference 3-1).

3.2 COMBINED BUOYANCY-DRIVEN EXCHANGE FLOW AND FORCED FLOW THROUGH SMALL OPENINGS IN A HORIZONTAL PARTITION

Reference 3-2 is a continuation of the work completed by Epstein in Reference 3-1 and provides an empirical formula for the one-way (unidirectional) purging flow rate that is necessary to prevent countercurrent exchange flow (bidirectional) within a single opening in a horizontal partition. The empirical correlation developed yields the magnitude of the buoyant component of this combined flow in terms of the pure countercurrent flow rate determined in Reference 3-1 and the flooding flow rate for the opening. Reference 3-2 also demonstrates, through an experimental study, that the correlation for combined flow through a single opening can be extended to successfully predict the convection patterns that develop within more complex geometries with multiple openings.

As a means of introducing the empirical correlation for simultaneous forced flow and reverse buoyancy-driven flow through a horizontal partition, Reference 3-2 first considers the simpler case of combined flow in an opening in a vertical partition. Using hydraulic theory, Reference 3-2 determined that the buoyancy-driven component of combined convection, Q_{BF}, through a single opening in a vertical partition can be represented by the following expression:

$$Q_{BF} = Q_{cc}(1 - Q_u/q)^m \quad \text{Eq. 3-3}$$

where Q_{cc} is the purely buoyancy-driven exchange flow rate across the partition (i.e., the exchange flow rate without a forced convection component), Q_u the one-way (unidirectional) buoyancy-driven exchange flow rate, q the flooding, or purging, flow rate and m some constant exponent. It is noted that the buoyant flow $Q_{BF} \rightarrow 0$ as the flooding limit $Q_u = q$ is approached and that the condition of purely buoyantly-driven countercurrent flow is reached when $Q_u = 0$.

In view of the mingling of the heavy and light fluid streams in a vertical orientation, it is not possible to derive a similar functional relationship that is applicable to openings in horizontal partitions. However, it is reasonable to assume that Q_{BF} through openings in a horizontal partition will conform closely to Eq. 3-3.

With the theoretical groundwork complete, Reference 3-2 performs a series of combined flow experiments to determine empirical correlations for the flooding flow rate and the constant exponent contained in Eq. 3-3. Similar to the expression for purely buoyantly-driven exchange flow found by Epstein in Reference 3-1, the expression for the flooding flow rate is:

$$\frac{q}{(D^5 g\,\Delta\rho/\bar{\rho})^{1/2}} = \frac{0.19\left[1+4000(L/D)^3\right]^{1/9}}{\left(1+0.05091(L/D)^{16/7}\left[1+4000(L/D)^3\right]^{4/9}\right)^{1/4}} \quad \text{Eq. 3-4}$$

And the constant value for the exponent, m, in Eq. 3-3 is 2.3.

In the case of a multi-opening system like that shown in Figure 3-1, Reference 3-2 has shown that Eq. 3-3 is also applicable. In the case where the flooding flow rate, q, is greater than the unidirectional flow Q_u, Figure 3-1(b) applies and the total exchange flow, Q, is:

$$Q = Q_u + Q_{BF} \quad \text{Eq. 3-5}$$

Solving Eq. 3-5 for Q_{BF} and substituting into Eq. 3-3 yields:

$$Q = Q_u + Q_{cc}(1 - Q_u/q)^{2\,3} \quad \text{Eq. 3-6}$$

Conversely, if the flooding flow rate is less than the unidirectional flow, Figure 3-1(a) applies and the total exchange flow rate is only the unidirectional flow:

$$Q = Q_u \quad \text{Eq. 3-7}$$

3.3 CORE-TO-LOWER PLENUM BORON TRANSPORT MODEL

Using the empirical relations presented in the previous section, a two-region model has been created to predict the boric acid concentrations in the core and lower plenum by assuming liquid-density-gradient-gravity-driven exchange flow through the lower core plate. Each region is assumed to be well mixed and therefore, the boric acid concentration and temperature in each region is assumed to be uniformly distributed throughout. The core is assumed to be at saturation temperature while the lower plenum can be either saturated or subcooled, depending on the user specified initial condition. In this scenario, the flow required to make-up for boil-off is defined as the unidirectional flow, Q_u, (i.e., an externally supplied flow) and bidirectional flow is present in all of the lower core plate holes such that the total exchange flow rate is determined using Eq. 3-5. The problem is depicted schematically in Figure 3-2.

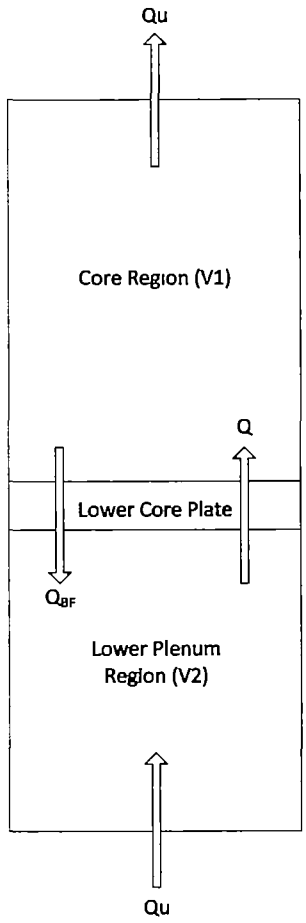

Figure 3-2 Control Volumes used in the Two-Region Transport Model

Inception of boric acid transport is determined by two factors. First, the density gradient between the core and lower plenum due to solute concentration differences must overcome the density gradient caused by the temperature difference between the core and lower plenum if subcooling exists in the lower plenum region. Second, since there is upflow through the reactor vessel due to the makeup of liquid boil-off, the buoyancy-driven exchange flow in the downward direction must be larger than the boil-off flow rate in the upward direction such that the downward flow can penetrate through the lower core plate and into the lower plenum. By modeling the inception in this fashion, both the effects of subcooling in the lower plenum and upward liquid kinetic energy due to the makeup of boil-off are accounted for.

It is expected that if a debris bed forms at the core inlet, it will provide an additional resistance to the inception of boric acid transport. This resistance is currently not accounted for in the two-region boric acid transport model.

The volumetric flow of make-up water through the lower plenum and into the core is Q_u, which is equal to the boil-off rate, and the source concentration (weight fraction) of boric acid into the lower plenum from the sump is denoted by the symbol M_o. The quantity of interest is the

concentration of boric acid in the core, M_1, as a function of time, t, within the core region. In order to predict this concentration, the following simplifying assumptions are made:

1. The lower plenum and core regions are well mixed and the boric acid concentration and temperature profiles within these regions are spatially uniform.

2. The lower core plate represents the only resistance to buoyancy-driven transport between the core and lower plenum.

3. The Boussinesq approximation is invoked such that the variation of liquid density with liquid temperature and solute concentration appears only in the buoyancy terms and all other terms that contain density are represented with an effective density which is defined as the average density between the core and lower plenum.

4. The water in the core instantaneously rises to saturation temperature and remains there throughout the transient.

5. The volumetric coefficient of thermal expansion of water, β and the boric acid expansion coefficient, k are known.

The boil-off flow, Q_u through the vessel is essentially an externally supplied flow that passes through the lower core plate and carries boric acid into the core region. Initially, the boric acid concentration in the core increases with time at a rate directly proportional to Q_u. However, when the boric acid in the core becomes sufficiently concentrated, the density of the core solution exceeds that of the solution in the lower plenum. This density difference induces a buoyancy-driven, countercurrent downflow of the heavier core liquid and consequential upflow of the lighter liquid through the openings in the lower core plate.

3.3.1 Model Equations

In accordance with the assumptions presented in the previous section, the following linear expression for the density difference, $\Delta\rho_{21}$ between the liquid in the lower plenum (region 2) and the reactor core (region 1) can be written as:

$$\Delta\rho_{21} = \rho\beta(T_2 - T_{sat}) + \rho k(M_1 - M_2) \tag{3-8}$$

where T and M refer to the temperature and boric acid weight fraction, respectively. ρ is the effective constant density of the liquid solution in the vessel and is defined as the average between the lower plenum and core densities:

$$\rho = \frac{(\rho_1 + \rho_2)}{2} \tag{3-9}$$

The term Q_u represents the net upward flow through the lower core plate required for make-up due to boil-off of liquid in the core region. It is the difference between the actual upward flow

through the plate, Q and the buoyancy-driven downward flow from the core to the lower plenum, Q_{BF}. A volumetric flow balance across the lower core plate requires that:

$$Q_u = Q - Q_{BF} \tag{3-10}$$

The countercurrent flow occurs within each opening (hole) in the lower core plate. Denoting N as the number of holes in the plate and assuming that each hole in the plate has the same diameter, Q_u/N may be regarded as an externally imposed, upward forced flow opposite to the downward buoyant flow, Q_{BF}/N in each opening. This is the flow pattern that was studied experimentally by Epstein and Kenton as described in Section 3.2.

The time histories of the solute concentrations, M_i, and the temperatures, T_i, in each region are given transient solute mass and liquid energy balances. Applying the correlations for Q_{BF} along with Eq. 3-10, the transient mass and liquid energy balances can be simplified to form a set of nonlinear equations that are functions of T_i, M_i, Q_{BF}, and Q_u which can be solved numerically for a set of given initial and boundary conditions.

3.3.2 Inception Criteria

In view of Eq. 3-8, when $\Delta\rho_{21} \leq 0$ the system is stably stratified and the buoyancy-driven back flow, Q_{BF} is zero, that is:

$$Q_{BF} = 0 \qquad \text{when } \Delta\rho_{21} \leq 0 \tag{3-11}$$

Also, when the destabilizing density difference, $\Delta\rho_{21}$ is positive but small, the buoyancy-driven back flow is not large enough to penetrate the upward makeup flow, Q_u through the core plate and the net downward transport rate is again zero:

$$Q_{BF} = 0 \qquad \text{when } q_{21} \leq Q_u \tag{3-12}$$

Eqs. 3-11 and 3-12 define the inception criteria for the transport of higher concentration boric acid from the core to lower plenum. If the liquid in the lower plenum is not subcooled, then $\Delta\rho_{21} \geq 0$ and Eq. 3-12 is the only criterion that has to be met, and transport between the core and lower plenum will occur sooner in the transient. If subcooling exists in the lower plenum, $\Delta\rho_{21} \leq 0$ and the concentration gradient between the core and lower plenum will have to overcome the oppositely opposing temperature gradient in addition to Eq. 3-12, and inception will occur later in the transient.

3.3.3 Plant Simulation

Using a typical Westinghouse 3-loop PWR plant model, an analysis using the boron transport model described above is performed to estimate the boric acid concentration gradient required to initiate buoyancy-driven exchange flow across the lower core plate. This analysis is performed using 10 CFR 50 Appendix K decay heat, prototypic dimensions, and it assumes the exchange flow from the core mixes in the entire lower plenum volume. The lower plenum liquid

temperature is set to 130°F. The application of subcooling in the lower plenum results in a larger concentration gradient between the core and lower plenum at the inception time which in turn delays the onset of exchange flow.

Results from this simulation show that the inception to buoyancy-driven transport from the core to the lower plenum occurs within 1000 seconds (0.28 hours) following the postulated LOCA when the concentration gradient between the core and lower plenum is roughly 8.5 wt% boric acid. This result is consistent with observations from available experimental data which indicates an approximate 8.5 wt% concentration gradient at the inception time. A comparison of this run to results from a typical licensing basis calculation is provided in Figure 3-3 (see Reference 3-3 for a discussion on typical licensing basis BAP calculations). As the figure shows, the core boric acid concentration from the prediction using the core-to-lower plenum boron transport model initially increases at a faster rate compared to the typical licensing basis calculation, because the effective mixing volume is smaller. After the inception time, the core concentration build-up rate slows as the lower plenum concentration begins to increase. Just after 10000 seconds, the core boric acid concentration predicted with the boron transport model crosses the concentration predicted by the licensing basis calculation and remains below it for the remainder of the transient. The lower plenum concentration trend follows the core concentration but remains roughly 8.5 wt% lower for the remainder of the transient. The hot leg switchover time predicted using the boron transport model is 8.32 hours which is almost 2 hours longer than that predicted by the licensing basis type calculation.

If communication (exchange flow) between the core and lower plenum begins before a resistive debris bed forms, some credit can be taken for the lower plenum volume. In addition, when the core boric acid concentration becomes high enough to overcome the temperature gradient between the core and lower plenum, as well as the upward force generated by the upward makeup flow, the system becomes unstable. This instability may generate oscillations in the flow field, around the core inlet which could serve to breakup or prevent a debris bed from forming. It is shown in Figure 3-4 that the magnitude of the countercurrent exchange flow between the core and lower plenum overcomes that required to replace boil-off within the first 10000 seconds of the transient. Given that the countercurrent exchange flow is greater than the upward flow required to replace boil-off, it can be postulated that the exchange flow would break-up any existing debris bed or prevent one from forming. This behavior will be investigated as part of the subscale brine testing.

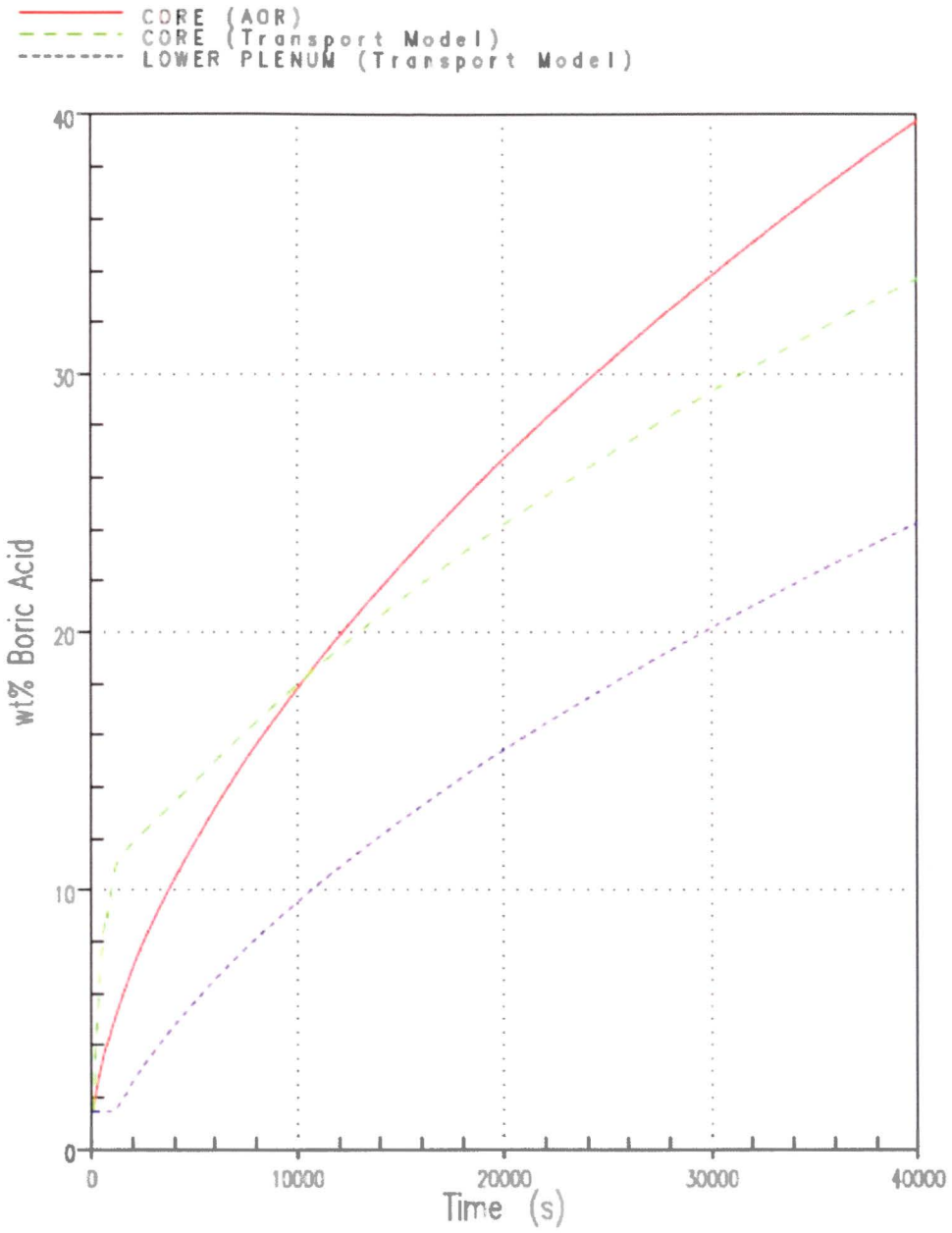

Figure 3-3 Predicted Boric Acid Concentration Build-Up from Boron Transport Model

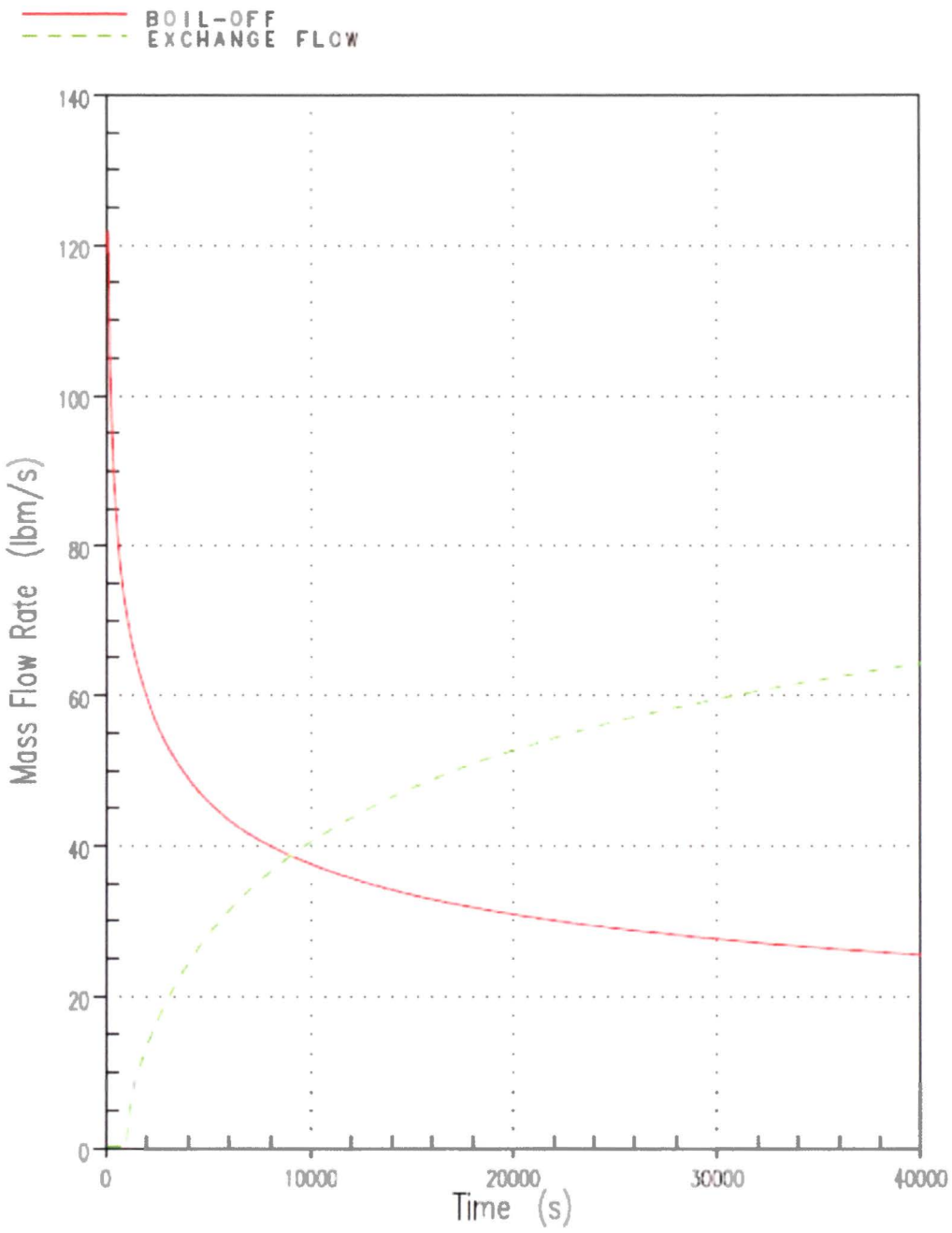

Figure 3-4 Boil-off Rate Compared to the Core-to-Lower Plenum Exchange Flow Rate Predicted by the Boron Transport Model

3.4 REFERENCES

3-1 Epstein, M. "Buoyancy-Driven Exchange Flow Through Small Openings in Horizontal Partitions," J. Heat Transfer 110, pp. 885-893, 1988.

3-2 Epstein, M. and Kenton, M. A. "Combined Natural Convection and Forced Flow through Small Openings in a Horizontal Partition: With Special Reference to Flows in Multi-Compartment Enclosures," J. Heat Transfer 111, pp. 980-987, 1989.

3-3 OG-13-205, "NRC Technical Concerns Regarding Boric Acid Precipitation in the Presence of In-Vessel Fibrous Debris and the Consequential Effects on Long-Term Core Cooling (PWROG PA-SEE-1090 and PA-SEE-1072)," May 2013.

4 SELECTION OF WORKING FLUID

4.1 INTRODUCTION

The subscale brine testing is intended to study the density-driven flow patterns governed by the concentration gradient of boron solutes that develop between the core and lower plenum. While it would be preferable to use varying concentrations of borated solution as the working fluid, the subscale test facility is not able to operate at the conditions necessary to study the borated solution concentrations of interest, nor is it equipped to insulate against the heat losses associated with elevated temperatures. Additionally, there are difficulties associated with the accurate measurement of these solution concentrations. Instead, various borated solution concentrations at 212°F will be simulated through the use of an aqueous salt solution at room temperature, an approach which has been used with success in the density-driven experiments of Epstein (Reference 3-1), Epstein and Kenton (Reference 3-2), and Mercer and Thompson (Reference 4-1).

4.2 WORKING FLUID PROPERTIES

The goal of the brine testing is to gain insight into the behavior of the RCS coolant near the core inlet under large CLB conditions. Therefore, the choice of working fluid at room temperature should replicate as closely as possible the properties of varying concentrations of borated solutions at 212°F and near atmospheric conditions. The primary thermodynamic properties of interest for this buoyancy-driven experiment are density and viscosity.

Four different aqueous salt solutions are examined: sodium chloride (NaCl), potassium bromide (KBr), potassium chloride (KCl), and sodium bromide (NaBr). All properties of these salt solutions are found in Reference 4-2. The boric acid (H_3BO_3) densities and viscosities are found in Reference 4-3.

4.2.1 Density

Figure 4-1 presents comparisons of the density and density gradient between varying concentrations of the four salt solutions and boric acid. Because this is a buoyancy-driven experiment, it is the density gradient, rather than the absolute value of the density, that is most important. Therefore, the working fluid should cover the full range of density gradients resulting from boric acid concentrations between zero and the solubility limit defined in Reference 4-3. Figure 4-1 shows that this is the case for all four salt solutions. The solubility limits for buffered and unbuffered boric acid at 212°F are contained in Table 4-1 below.

Table 4-1 Buffered and Unbuffered Boric Acid Solubility Limits		
Coolant	Boron Concentration	
	ppm	wt%
Boric Acid	47,121	27.0
Boric Acid, NaOH (pH 7)	113,532	64.9
Boric Acid, NaOH (pH 10)	69,891	40.0
Boric Acid, TSP	67,753	38.8
Boric Acid, NaTB	51,552	29.5

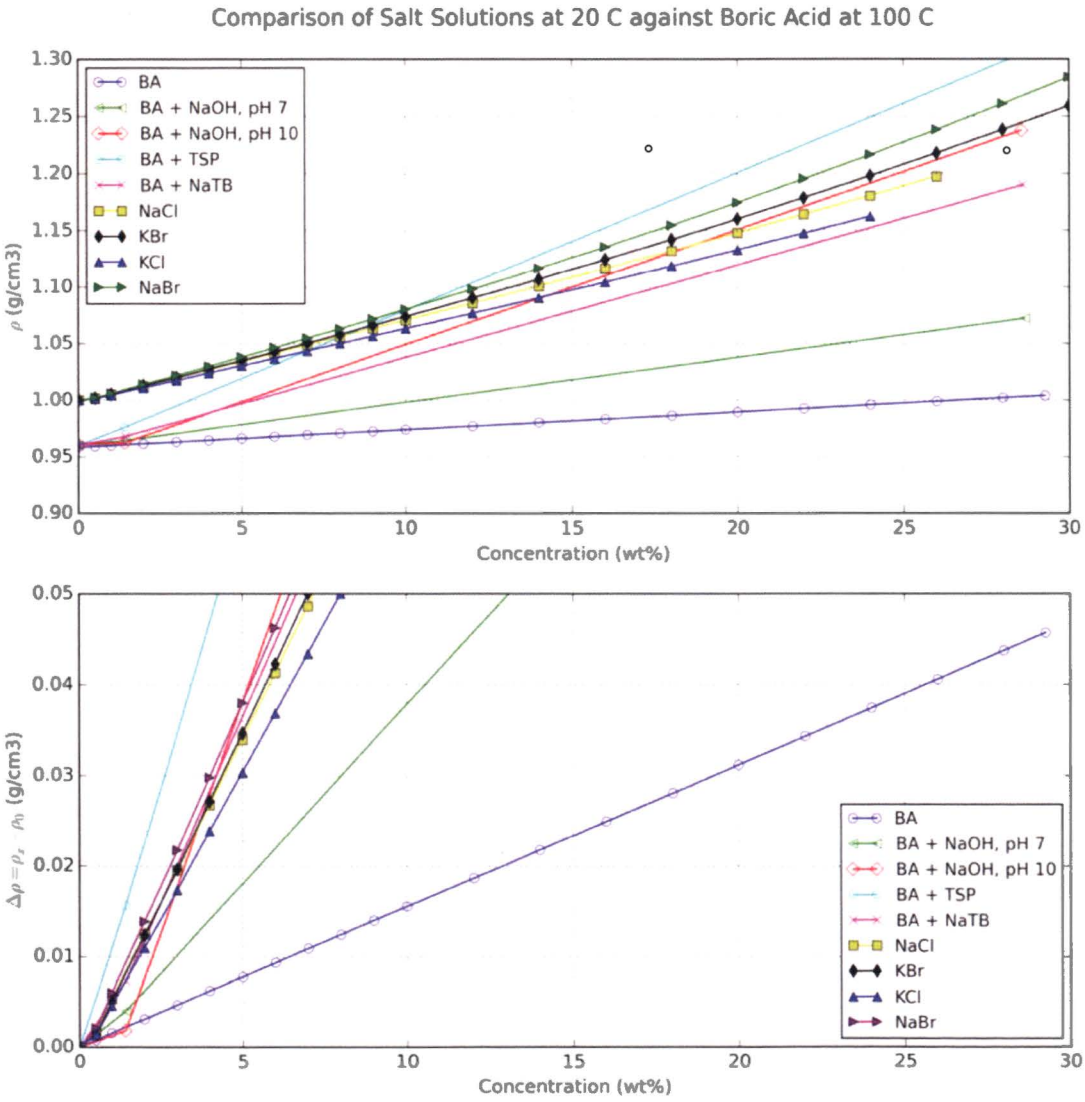

Figure 4-1 Density Comparison

4.2.2 Dynamic Viscosity

Data for the viscosity of boric acid solutions at 212°F is limited. With points at 0, 1.44, and 25.7 wt% boric acid, it is assumed that a linear relationship exists over the full range of concentrations.

The viscosity for all four salt solutions is approximately two to five times that of the boric acid solution being simulated as shown in Figure 4-2. This is due to the dependence of viscosity on temperature and the difference between the test facility and post-LOCA liquid temperatures in the reactor vessel. Without being able to replicate the absolute viscosity, it's important that the relative trend of viscosity as a function of mass percent be similar to that of boric acid. In other words, as the solution concentration increases, so should the dynamic viscosity. Sodium Bromide seems to best fit this goal, as it has a nearly linear increasing viscosity over the range of interest, whereas NaCl has a non-linear increasing relationship, KCl has a slightly decreasing then increasing relationship, and KBr has a decreasing relationship.

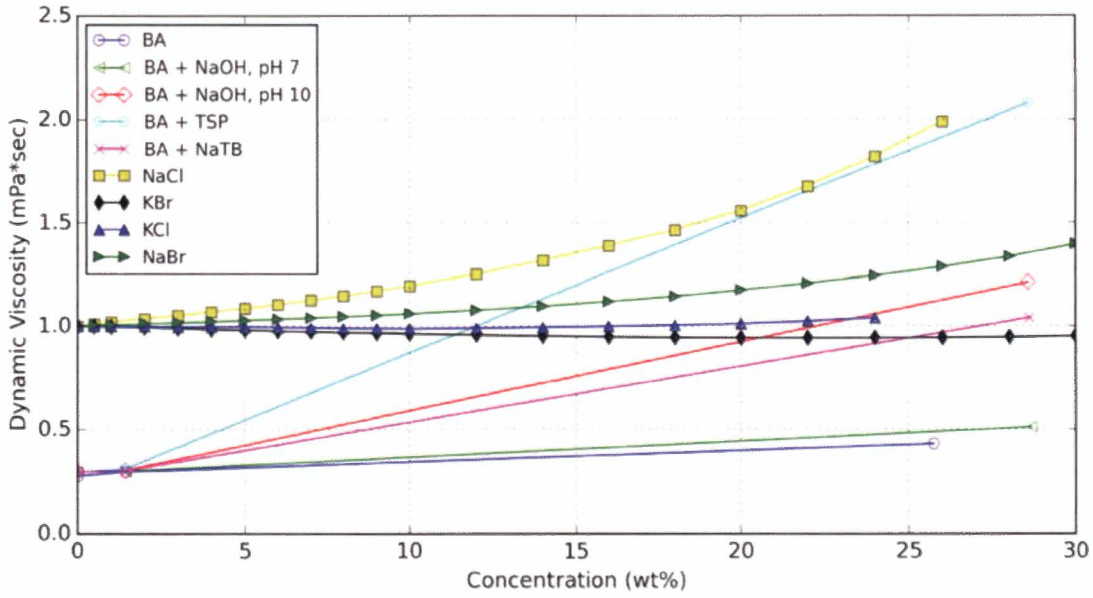

Figure 4-2 Viscosity Comparison

These differences in the absolute viscosity can be put into perspective through dimensional analysis. Tritton makes clear that when the Grashof number (Gr) is large, viscous forces are negligible compared with the buoyancy and inertial forces (Section 14.5 of Reference 4-4):

$$Gr = \frac{g \cdot \beta \cdot (C_1 - C_0) \cdot L^3}{\nu^2} \quad (4\text{-}1)$$

where,

$$\beta = -\frac{1}{\rho}\left(\frac{\partial \rho}{\partial C}\right)_{T,p} \quad (4\text{-}2)$$

and

g is the acceleration due to gravity

C_0 is the concentration of the species at position 0

C_1 is the concentration of the species at position 1

L is the characteristic length

ν is the kinematic viscosity

ρ is the fluid density

C is the concentration of the species

While the viscosity of the boric acid solution being simulated may be as much as five times greater than that of the salt solution, it is still a relatively small value. With the kinematic viscosity being on the order of $\sim 10^{-7}$ m²/s, squaring this term results in a large Grashof number under the conditions being tested. Such a finding is again consistent with Tritton, who stated that even for very small temperature differences (1°C), the Grashof number for water will be on the order of $\sim 10^{3}$, causing vigorous convection currents to arise.

A sample calculation reflecting the brine testing conditions is provided in order to demonstrate the dominance of buoyant forces. A characteristic length of 0.5 inches is used in the following calculations, as this reflects the length of the bottom nozzle, which serves as the separation between the corresponding chemical concentrations.

$$\beta = \frac{1}{1000\,\frac{kg}{m^3}} \times \frac{99.6\,\frac{kg}{m^3}}{29.27\,wt\%}$$

$$Gr = \frac{\left(9.81\frac{m}{s^2}\right)\left(0.0034\,wt\%^{-1}\right)(1.0-0.0wt\%)\left(0.0127m^3\right)}{\left(3.214\times10^{-7}\frac{m^2}{s}\right)^2}$$

$$Gr = 1.281 \times 10^{6} \ @0.5wt\%\ H_3BO_3$$

The same calculation is performed for KBr:

$$\beta = \frac{1}{1000\,\frac{kg}{m^3}} \times \frac{374.3\,\frac{kg}{m^3}}{40.0\ wt\%}$$

$$Gr = \frac{\left(9.81\frac{m}{s^2}\right)\left(0.0094\ wt\%^{-1}\right)\left(1.0-0.0wt\%\right)\left(0.0127m^3\right)}{\left(7.648\times10^{-7}\frac{m^2}{s}\right)^2}$$

$$Gr = 1.908 \times 10^5 \ \ @0.5wt\%\ KBr$$

This calculation is performed at varying solute concentrations in order to generate Figure 4-3, which shows the Grashof numbers much greater than 1 over the full range of concentrations analyzed. It is noted that using a larger length scale would only result in higher values of Grashof number.

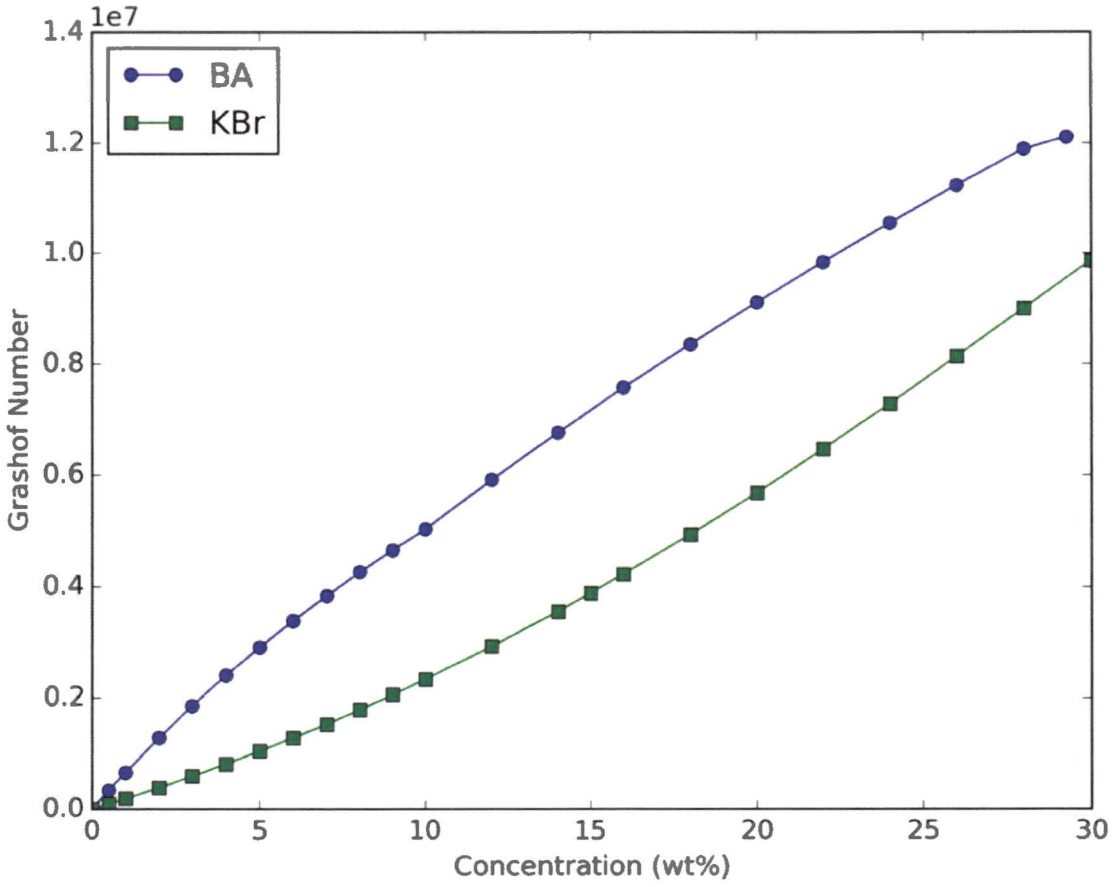

Figure 4-3 Grashof Number Comparison

It's also important to consider that in the proposed brine testing, the salt solution will be injected in the presence of a counter-current flow, in which the Froude number (Fr) can be used to predict the onset of density-driven flow by providing the relative importance of inertia to buoyancy forces (Reference 4-4).

$$Fr = \sqrt{\frac{\overline{\rho} \cdot U^2}{g \cdot L \cdot \Delta\rho}} \tag{4-3}$$

Where $\overline{\rho}$ is the average density between the two fluids, U the fluid velocity, and $\Delta\rho$ the density difference of the two fluids.

The formulation of the Froude number reinforces the fact that so long as the density gradient is equivalent between the salt solution and the boric acid solution being simulated, the fluid behavior will be similar as well.

4.2.3 Electrical Conductivity

The electrical conductivity will serve as the means of concentration measurement. Data for aqueous KBr as a function of concentration is provided in Section 5-71 of Reference 4-2, and is repeated in Table 4-2 below.

Table 4-2 Electrical Conductivity of Aqueous Potassium Bromide

Concentration (wt%)	Conductivity (mS/cm)
0.5	5.2
1	10.2
2	19.5
5	47.7
10	95.6
15	144
20	194

The conductivity is also provided in Figure 4-4 for convenience. A linear fit is made by omitting the data above 10 wt%. The resulting fit has an R^2 value of 0.9997. Based on the figure, the linear curve fit reasonably represents the data above 10 wt% as well.

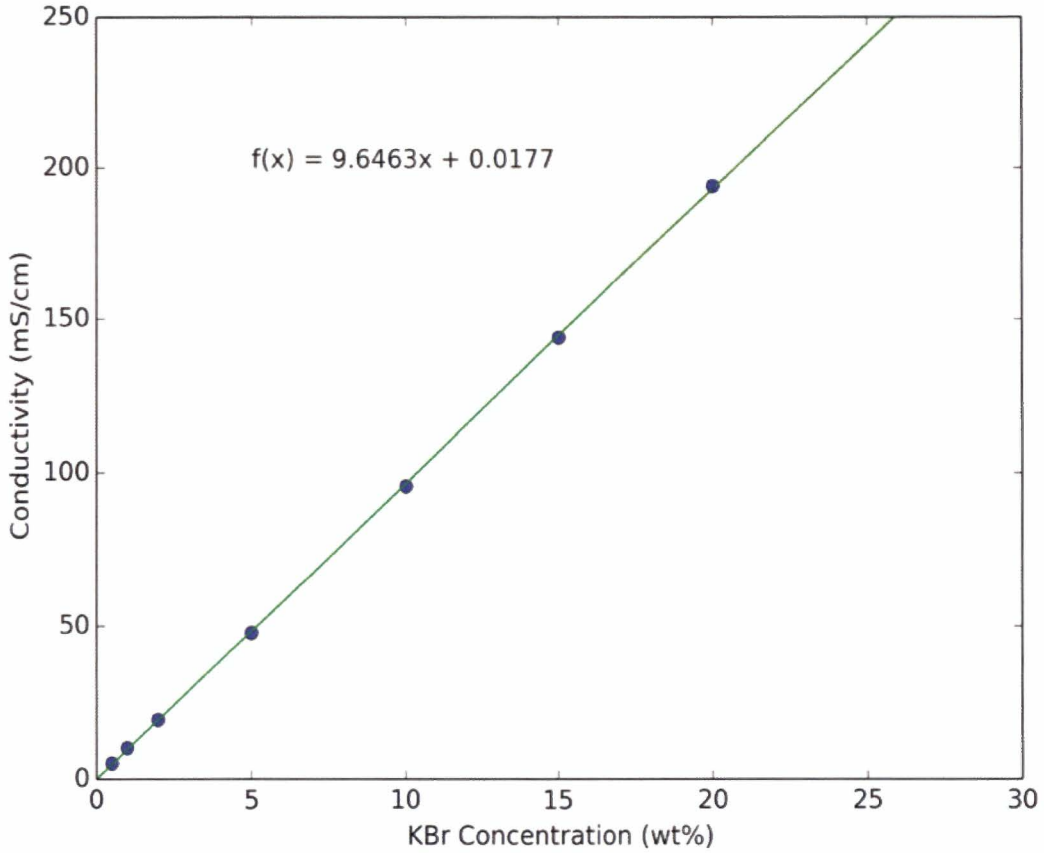

Figure 4-4 Potassium Bromide (KBr) Conductivity versus Concentration

4.3 CONCLUSIONS

The use of a salt solution to model the buoyancy-driven behavior of a differing fluid is a common approach, employed by Epstein (Reference 3-1), Epstein and Kenton (Reference 3-2), Mercer and Thompson (Reference 4-2), and Steckler et al. (Reference 4-5). Steckler showed through dimensional analysis that for Reynolds numbers greater than $\sim 10^4$, the molecular transport terms of the governing equations become negligible. Based on these insights and the comparisons of density and viscosity, as well as the electrical conductivity, it was determined that all four salt solutions would well suit the needs of this testing. However, due to practical purposes, potassium bromide (KBr) is selected as the working fluid for the brine testing.

A linear fit is performed in Eq. 4-4 below for the density gradient of KBr as a function of wt% KBr. Similarly, a linear fit is performed between the wt% of KBr at 68°F versus wt% boric acid at 212°F in Eq. 4-5. Given a wt% of KBr, the solution to Eq. 4-5 represents the wt% of boric acid that would produce the same density gradient. For example, a 3 wt% solution of KBr at 68°F would produce the same density gradient as a 12.78 wt% solution of boric acid at 212°F. This trend is shown graphically in Figure 4-5.

$$\Delta\rho_{KBr} = 0.0092 \times wt\%_{KBr} - 0.0132 \quad (4\text{-}4)$$

$$wt\%_{H_3Bo_3} = 4.7213 \times wt\%_{KBr} - 1.3837 \quad (4\text{-}5)$$

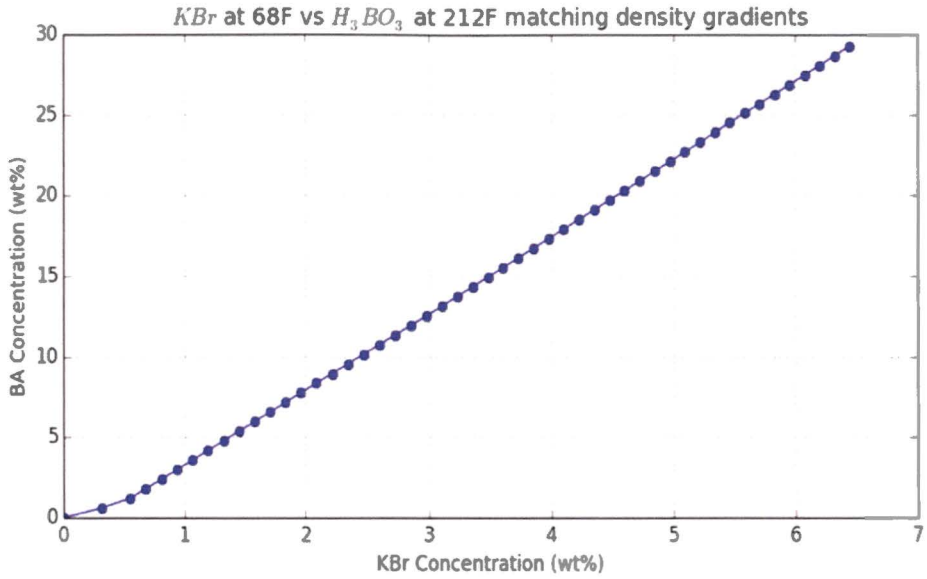

Figure 4-5 Boric Acid Concentration versus Potassium Bromide (KBr) Concentration

4.4 REFERENCES

4-1 A. Mercer and H. Thompson, "An Experimental Investigation of Some Further Aspects of the Buoyancy-Driven Exchange Flow Between Carbon Dioxide and Air Following a Depressurization Accident in a Magnox Reactor, Part I: The Exchange Flow in Inclined Ducts," J. Br. Nuclear Energy Society, 1975.

4-2 David R. Lide, CRC Handbook of Chemistry and Physics, CRC Press, 89th Edition, 2008.

4-3 WCAP-17021-NP, Rev. 1, "Summary of Tests to Determine the Physical Properties of Buffered and Un-buffered Boric Acid Solutions," January 2010.

4-4 D. J. Tritton, "Physical Fluid Dynamics," Oxford Science Publications, Second Edition, 1988.

4-5 K. D. Steckler, H. R. Baum, J. G. Quintiere, "Salt Water Modeling of Fire Induced Flows in Multicompartment Enclosures," NBSIR 86-3327, 1986.

5 TEST FACILITY DESCRIPTION

5.1 OVERVIEW

The test facility was constructed at the Westinghouse thermal hydraulic test laboratory located in Churchill, Pennsylvania. Figure 5-1 shows a schematic of the subscale brine test facility. The design consists of a 4 inch inner-dimension, square cross-section column that houses the tested capture geometry. The vertical column was fabricated with clear polycarbonate sidewalls to provide optical access. For all testing, flow was injected from the bottom of the test column and directed upwards through the tested capture geometry. Brine was injected downstream of the simulated core region using a sparger designed to uniformly inject the brine across the entire flow column cross-section.

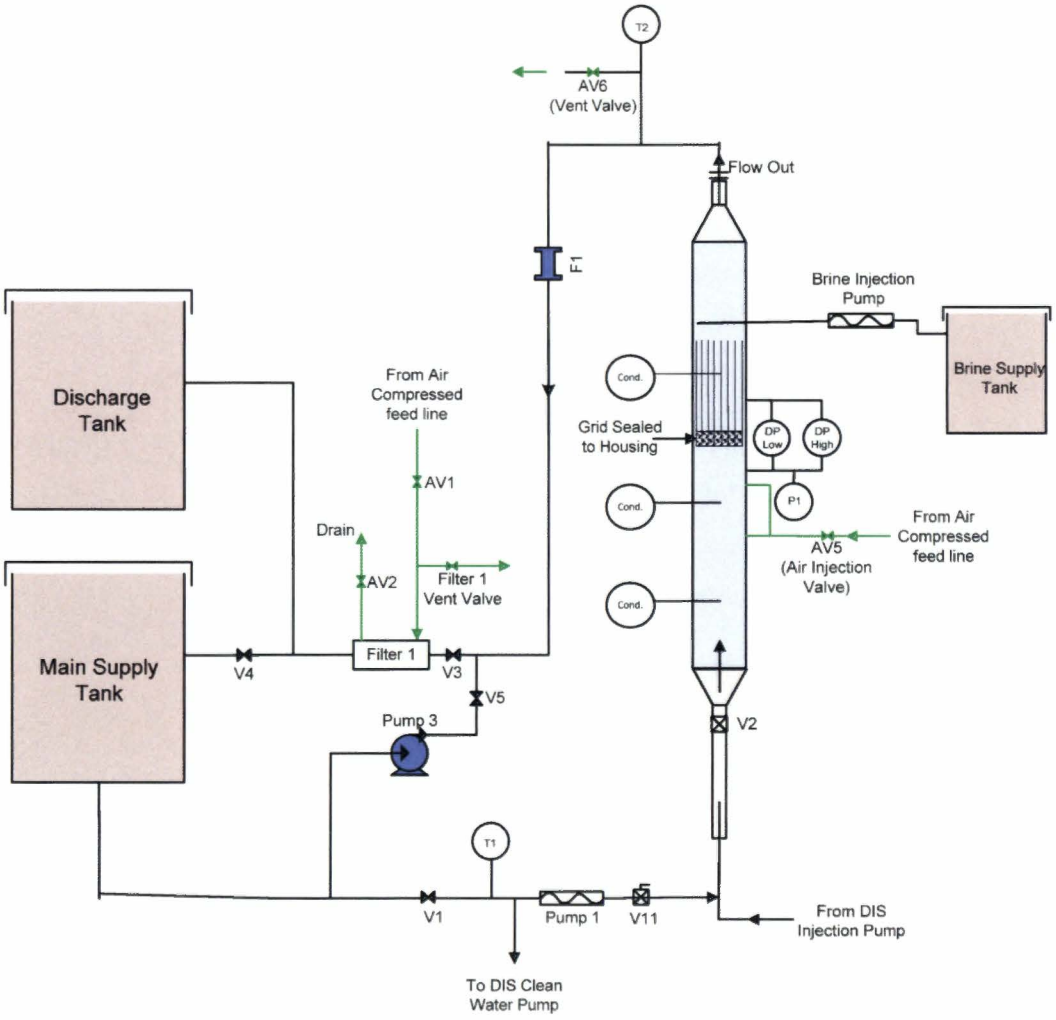

Figure 5-1 Subscale Brine Test Facility Process Flow Diagram

For all brine testing, the primary flow rate was set using the debris injection system (DIS) injection pump, which was controlled throughout each test using a variable frequency drive. The DIS injection pump drive was controlled to follow a predetermined flow rate curve based on decay heat. The main coolant loop pump (Pump 1) was only used during pre- and post-test operations.

Downstream of the test column, all debris that penetrated the test geometry was collected in a high capture efficiency bag filter (Filter 1). Post-test weight from the bag filter allowed debris penetration to be directly quantified. Given the low flow rates through the test column, pump 3 was used as a booster pump to increase the flow rate through the filter, which was required to achieve efficient capture by the bag filter.

Brine testing was completed using a once-through configuration. De-ionized water supplied by the main coolant tank was used as the source coolant and was injected by the DIS into the test column inlet. Brine solution exiting the test column was collected in the discharge tank. The brine supply tank provided the source for the brine injection system. The brine injection tank was mixed to ensure uniform brine concentration during the test duration.

5.2 DEBRIS INTRODUCTION

In general, industry testing of sump strainers and fuel components has not included debris concentration as a controlled variable. However, some efforts have been made to control debris injection such that slugs of debris did not reach the filtering area. For example, NUREG/CR-6917 (Reference 5-1) described a series of tests performed for sump strainer conditions. The strainer inlet conditions were maintained at somewhat controlled concentrations by distributing the debris along a flexible pipe segment and shaking the pipe segment to suspend the debris before initiating flow. However, this method of debris addition likely resulted in an uncontrolled distribution of debris along the pipe segment. In addition, re-circulating debris within the loop would have resulted in a time-varying concentration profile.

The WCAP-16793-NP-A, Revision 2 fuel assembly test program (Reference 5-2) controlled the concentration of fibrous debris with manual additions to a tank with uncontrolled mixing patterns. This method of debris addition resulted in non-uniform debris concentrations reaching the test assembly. The variation of concentration with time was likely a saw-tooth pattern in which peak concentrations would be difficult to calculate. Furthermore, since the method of debris addition was manual, the impact on test-to-test variation may have been significant.

To address these issues, a DIS that controls the concentration of debris reaching the test column at any point in time was designed. One of the design requirements of the DIS was to allow controlled injections over time intervals consistent with those expected during recirculation mode of a PWR. To meet this objective, an online dilution system that allowed control of debris injection over time was designed.

Figure 5-2 and Figure 5-3 show schematics of the DIS. Debris was injected to the test column with an online dilution system that provided a predetermined concentration feed of particulate and fiber debris. The main components of the DIS included two tanks with mixers, an injection

pump, a clean water addition pump, a circulation pump and a 4-way solenoid-operated control valve.

Each tank was stirred with an impeller mounted 15 degrees off axis and centered at one-third of the tank diameter from the bottom of the tank. All piping and fittings within the DIS maintained a 0.5 inch inside diameter (ID) throughout. Clear fluorinated ethylene propylene (FEP) tubing was selected for smooth inner surface and ability to evaluate potential debris trapping with good optical access. Figure 5-4 shows a photograph of the DIS.

The DIS was operated in either an injection mode, shown in Figure 5-2, or a circulation mode shown in Figure 5-3. During injection, contents from the high concentration tank (HCT) were pumped to the low concentration tank (LCT) and into the test column. During circulation mode, the LCT continued to inject to the test column, while the HCT remained isolated. Turning the 4-way valve shown in Figure 5-2 and Figure 5-3 switched between the injection and circulation mode and modulation of the 4-way valve controlled the dilution rate and injection concentration. In this manner, flow was maintained through all of the DIS tubing at all times, which prevented any settling in the tubing.

Before each test, both tanks were filled with water from the primary test loop. For ideal mixing, the DIS tanks were filled to a depth equal to the tank diameter. Before debris introduction into the system, all pumps were circulated at max flow for a period of time, which purged the DIS of any air pockets. All the previous actions were accomplished with the DIS operating in injection mode. After purging the lines, the DIS was switched to circulation mode such that the HCT was isolated from the test loop. Debris was then prepared and added to the HCT. The HCT mixer impeller was turned on at high speed to disperse the debris homogenously in the tank. During this operation, air bubbles could be intentionally entrained into the tank to enhance mixing. After debris dispersion, the HCT and LCT impellers were set at a low speed, sufficient to maintain a homogenous debris suspension without settling, but low enough to prevent vortexing and air entrainment in the un-baffled tanks. During this phase, the circulation pump continued re-circulating the contents of the HCT, which was isolated from the test loop by the 4-way valve shown in Figure 5-3. This allowed any air transported to the sample lines during the high speed mixing process to be swept out.

Once this process was complete, all three pumps shown in Figure 5-3 were set to the desired initial flow rate with the DIS still in circulation mode. At this point, no debris had been injected into the test loop. To initiate debris injection, the 4-way valve was turned and DIS switched to injection mode. Debris was pumped from the HCT to the LCT as shown in Figure 5-2. Concurrently, the clean water addition pump was switched from the LCT to the HCT. This prevented debris settling in the circulation loop piping.

The DIS flow rate was automatically controlled by a control program after starting each experiment. The software used a predetermined input file that defined the flow rate throughout the course of each experiment.

Figure 5-2 Debris Injection Schematic (Injection Mode Alignment)

Figure 5-3 Debris Injection Schematic (Circulation Mode Alignment)

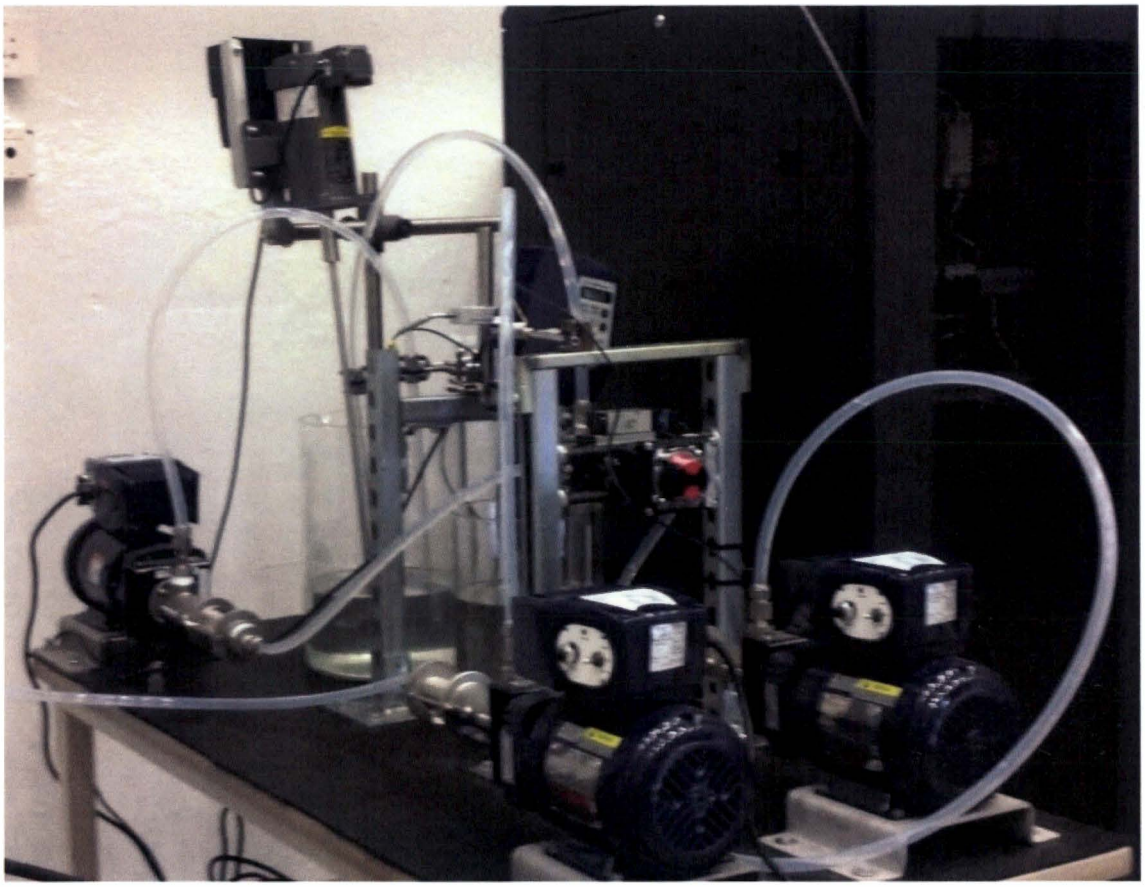

Figure 5-4 Debris Injection System

5.2.1 Debris Constituents

The brine testing utilized fibrous and particulate debris constituents. Chemical debris was not considered because the focus of this testing is on the time period before hot leg switchover (or other active boron dilutions actions). The chemical effects testing provided in WCAP-17788, Vol. 5 (Reference 5-3) has demonstrated that the formation of chemical products occurs after the time period considered in this testing. The fibrous debris constituent was **NUKON®** base wool supplied by Performance Contracting Incorporated (PCI) and was from the same batch used in the subscale head loss test program (Reference 2-1). The method for preparing the fibrous debris for introduction into the test was identical to the method used by the subscale head loss program which is described in detail in Reference 2-1.

NUKON is a registered trademark of Performance Contracting Inc. Other names may be trademarks of their respective owners

The particulate debris selected is identical to that used in the subscale head loss program as well. The particulate is a black silicon carbide powder supplied by UK Abrasives. A particulate size distribution was used in the brine testing as shown in Table 5-1. This size distribution was defined based on test results documented in Section 5.2.6 of Reference 2-1. Evidence was provided that the [ ]^{a,c} particulate resulted in the most restrictive debris bed since these particle sizes maximized the effects of particle straining and packing density. This distribution is a broad size distribution that is weighted more heavily with particulate diameters of [ ]^{a,c} Furthermore, the particulate size distribution also included a tail of smaller particulate in an attempt to further maximize particle packing.

Table 5-1 Mixed Particulate Size Distribution

Particle ID	Particle Size (µm)	Particle Mass (%)
		a,c
	Total:	100

5.3 BRINE INTRODUCTION

A brine injection system was used to introduce brine solution into the test column. The brine supply system consists of a 100 gallon brine supply tank, a tank mixer, a positive displacement pump, and a sparger used to inject brine into the test column. All piping and fittings within the brine injection system maintained a 0.5 inch inside diameter (ID) throughout. Clear fluorinated ethylene propylene (FEP) tubing was selected, consistent with that used in the DIS.

The sparger used for dispersing the brine solution into the core region was be made from 1/8 in. schedule 40 stainless steel pipe with a cap on one end. The pipe has an OD of 0.405 in. and inside diameter of 0.269 in. For injecting the brine solution, the pipe contains 6 drilled holes, oriented at 45° off vertical, to evenly disperse the brine solution throughout the core region. The 6 holes were sized to control the exiting fluid velocity through the holes to be less than 2 ft/s.

At an injection rate of 1 gpm, this yields a volumetric flow rate of:

$$1\frac{gal}{\min}\times\frac{1ft^3}{7.48gal}\frac{1}{60}\frac{\min}{\sec}=2.228\times10^{-3}\ ft^3/\sec$$

For a hole diameter of 3/16 in, the total flow area is:

$$6 \times \frac{\pi}{4} \cdot \left(\frac{0.1875}{12} \right)^2 = 1.15 \times 10^{-3} \; ft^2$$

Dividing the total flow rate by the flow area yields a fluid exit velocity of 1.94 ft/sec. This value is sufficient to induce mixing in the subscale core region but is low enough to minimize any impact on the buoyancy-driven process being studied.

5.4 FLOW CONTROL

5.4.1 Main Flow

For the main column flow, two flow curves were defined for the brine testing. The first flow decay curve was defined to reduce the flow from a starting value of 0.8 gpm to [ ]a,c during the debris injection phase of the test. The starting value scaled to the prototypic system is roughly 3 gpm/FA while the end value is roughly [ ]a,c These flow rates are consistent with those expected during large CLB conditions. The second flow curve was defined to follow the same trend of the first flow control curve only that it continued to decrease after [ ]a,c was reached. Both flow control curves are shown in Figure 5-5.

[a,c]

Figure 5-5 Subscale Main Flow Control for Brine Testing

5.4.2 Brine Injection Flow

The brine injection flow rate was held constant during the experiments. The brine injection flow rate was controlled by the brine injection pump speed. Since a positive displacement pump was used for brine injection, the flow rate is accurately relatable to the pump speed. Testing completed during the shakedown phase determined the pump speed necessary to achieve the prescribed brine injection flow rate of 0.5 gpm. The pump speed corresponding to 0.5 gpm was programmed into the pump controller and used during the duration of the test program.

5.5 TEST COLUMN

The debris-laden flow from DIS is injected directly upstream of the test column as shown in Figure 5-6. Debris was delivered from the DIS as described in Section 5.2 via a 0.5 inch inner diameter tube to the 1 inch test column inlet. This geometry aided in mixing and provided a uniform distribution of debris entering the test column. For the brine tests, there is no flow from the primary loop piping shown in Figure 5-6 expect during pre- and post-test activities.

a,c

Figure 5-6 Debris Injection Mixing Upstream of Test Column

The debris-laden flow was then passed through a custom 1 inch circular to 4 inch inner-dimension, square cross section diffuser as shown in Figure 5-6. This provided a smooth, steep transition to prevent debris from settling on the bottom surface of the diffuser. This geometry also prevented recirculation regions and promoted a uniform debris distribution entering the test column.

Dimensions for the test column are provided in Figure 5-7. The test column was designed to maintain a length-to-diameter (L/D) ratio of 10, corresponding to approximately 40 inches, upstream and downstream of the capture geometry.

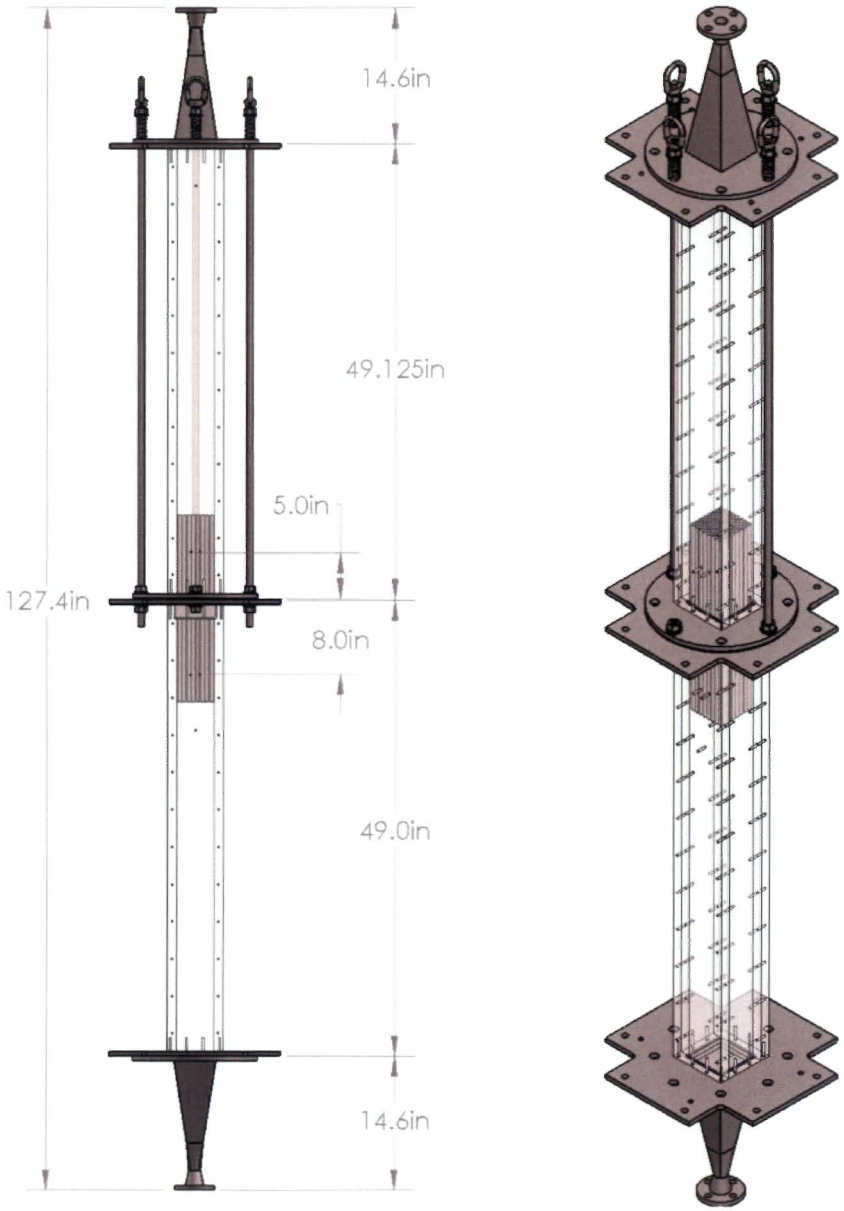

Figure 5-7 Dimensioned Drawing of Test Column

5.6 TEST GEOMETRY

5.6.1 Westinghouse Core Inlet Geometry

A center cut of the bottom nozzle (BN), which underlays an 8 x 8 P-grid cut-out, was used for the Westinghouse core inlet geometry brine tests. Several options for a BN cut-out from a full-area BN were considered. However, a single cut-out, with the same dimensions of the subscale test column, would not provide an optimal match of the open flow area ratio. Therefore, a design including [ ]^{a,c} flow holes with a diameter of [ ]^{a,c} which is within the tolerance of the Westinghouse RFA BN design was selected. The design includes blocked areas consistent with the location of thimble tubes within the fuel assembly. Table 5-2 shows important dimensions of the tested BN. Figure 5-8 through Figure 5-12 show drawings of the BN and assembled test geometry with grids installed.

Table 5-2 Summary of Tested Westinghouse Bottom Nozzle

	Value	Units
BN flow hole diameter	[ ]^{a,c}	in
Total number of BN flow holes	[ ]	
Total open flow area	[ ]	in^2
Open flow area ratio	[ ]	%
Test column flow area	[ ]	in^2
Ratio of test column inlet flow area to installed FA inlet flow area[1]	[ ]	%

Note: [1]This value is used to scale results from the test geometry to a full-area fuel assembly

5.6.2 AREVA Core Inlet Geometry

Similar to the Westinghouse test geometry, a central section of a prototypic AREVA lower end fitting was utilized in the brine testing. The AREVA lower end fitting is essentially a screen that serves the same purpose of the Westinghouse BN/P-grid combination in that it is intended to provide structural integrity for the fuel assembly and is designed to capture debris under normal operating conditions. Above the lower end fitting was the same 8 x 8 rod bundle used for the Westinghouse core inlet geometry tests. The rod bundle contained a central region of a prototypic HMP grid properly distanced from the lower end fitting. The rod bundle also contained a Westinghouse RFA grid at the top of the bundle to provide structural support and to keep the rods aligned.


a,c

Figure 5-8 Selected Westinghouse Bottom Nozzle Section


a,c

Figure 5-9 Test Section Top View Showing BN Flow Holes with Respect to Simulated Fuel Rods

a,c

Figure 5-10 Test Section Bottom View Showing BN Flow Holes with Respect to Grid Straps

a,c

Figure 5-11 Cross-Sectional View of Test Column


a,c

Figure 5-12 8x8 Central Region P-Grid Cut-Out

5.7 DEBRIS FILTRATION

Downstream of the 1 inch test column outlet, a single bag filter housing and filter insert were placed in-line for capturing all debris that penetrated the test geometry. Due to the requirement to maintain reasonable pressures in the test column, and considering the small particulate debris filtration requirements, a #2 bag filter and housing were selected. Based on the requirement that the filtration system should efficiently capture debris with size distributions at or below 10 μm, an Eaton **TOPLINE™** filter housing fitted with **ACCUGAF™** bag filters was selected. The **TOPLINE** housing is assembled from cast 304 stainless steel components, which results in a smooth internal surface with no weld seems. The entrance design to the housing essentially eliminates debris trapping locations and the bag seal prevents debris bypass.

All tests used Eaton **ACCUGAF** polypropylene bag filters. Specifications for the selected bag types are provided in Table 5-3. Bag selection for individual tests was based on injected particle size distribution.

TOPLINE and ACCUGAF are trademarks or registered trademarks of Eaton Filtration, LLC. Other names may be trademarks of their respective owners.

Table 5-3 ACCUGAF Bag Filter Specifications					
	Particle Size at Common Removal Efficiencies (μm)				
Filter Model	>60%	>90%	>95%	>99%	>99.9%
AGF-51	0.2	0.6	0.8	1.5	5
AGF-55	1	2	3	5	15

Commercially-available #2 bag filter housings with guaranteed 1μm particulate capture come standard with a 2 inch diameter inlet pipe. As a result, it was necessary to provide additional flow upstream of the bag filter housing such that debris could not settle within the piping entering the housing at the lowest tested flow rates. This was accomplished without generating additional debris capture locations by combining a small flow rate from Pump 3, as shown in Figure 5-1, upstream of the bag filter housing with the primary loop flow. The flow was combined in an annular passage with the primary flow entering on the inner portion of the piping. This prevented the velocity in the bag filter housing inlet from dropping below the settling velocity for entrained debris.

5.8 WATER CHEMISTRY

5.8.1 Main Coolant Supply

Testing was conducted using de-ionized (DI) water as the primary fluid. The main test loop supply tank was filled with 250 gallons of DI water before filling any other piping segments or the test column. Therefore, the total water inventory in the system is 250 gallons. At room temperature conditions, this corresponds to a total mass of 944.7 kg of DI water.

5.8.2 Brine Solution

Based on the conclusions in Section 4.5, potassium bromide (KBr) was used for the brine solution.

The KBr was provided in dried granular form and was added to DI water in the brine supply tank for mixing. To determine the appropriate KBr mass to be added, the mass of the water must be determined. Using 75 gallons of DI water, the volume of water is:

$$75\ gal \times \frac{1}{7.48052} \cdot \frac{ft^3}{gal} = 10.026\ ft^3$$

At ambient conditions (68°F, 14.7 psia), water has a density of 62.32 lbm/ft^3. At 2.2046 lbm/kg, this results in:

$$10.026\ ft^3 \times 62.32\ \frac{lb_m}{ft^3} \times \frac{1}{2.2046}\ \frac{kg}{lb_m} = 283.417\ \text{kg of water}$$

With the water mass known, the amount of KBr addition needed to reach the desired source concentration can be calculated. For example, in order to create a 20.0 wt% KBr solution, x kg of KBr need to be dissolved into the 75 gallons of DI water:

$$\frac{x}{x + 283.417 \cdot kg} = 0.2 \Rightarrow x = 70.85\ \text{kg KBr}$$

5.9 POST-TEST INSPECTION AND CLEANUP

Back-flushing the test loop after each test aided in the loop cleanup process and was also used to characterize debris trapped on the capture geometry. After completion of each experiment, the inlet and outlet of the test column were realigned such that flow could be reversed through the test column. Pumped flow was initiated and the back-flow was directed through a second bag filter housing. During this phase, pulsed air injections were performed, injecting compressed air just below the test geometry, through dedicated taps located on the wall of the test column to aid in breaking up the debris bed.

After back-flushing, the upper flange of the test column was disconnected and a pressure washer wand was inserted through the flange into the test column. The pressure washer was used to remove any debris remaining trapped on the test geometry after back flushing. After pressure washing was completed, the configuration was restored and the column back-flushed again to force debris dislodged by the pressure washer to the bag filter housing.

If debris was still visible on the test geometry, the geometry was removed from the column and cleaned. Debris removed from the test geometry during this process was collected and filtered using the same bag filter used for back-flushing.

Particular attention was made to cleaning and inspection of the DIS. After each test was completed, the content of debris in the DIS tanks was calculated to be lower than 0.1% of the content at the beginning of the test. Such content is negligible in terms of impact on the test results, since it is of the same order of the precision achieved when debris is weighted for addition in the HCT.

5.10 INSTRUMENTATION

Table 5-4 provides a list of the instrumentation used for this test program. The location of flow and temperature instrumentation did not change throughout the course of testing. The location of these instruments with respect to the main test facility components is shown in Figure 5-1. The HCT and LCT level sensors monitored the DIS tank levels continuously throughout each experiment and provided feedback for tank level control.

The location of differential pressure instrumentation was modified throughout the course of the test program. For the Westinghouse core inlet geometry tests, DP1H and DP1L measured differential pressure across the bottom nozzle/P-grid combination and DP2H measured the differential pressure across the first spacer grid. For the AREVA core inlet geometry tests, DP1H and DP1L measured differential pressure across the lower end fitting and the first spacer grid. DP2H was not used to measure differential pressure in the AREVA core inlet geometry tests.

Conductivity probes were used to measure brine concentration in the brine supply tank and test column. As shown in Table 5-5, three conductivity probe calibrations were performed throughout the test program and the range and accuracy is dependent on the calibration. In Table 5-5, Calibration 1 is applicable to tests completed from 2/10/2015 to 3/2/2017, Calibration 2 applies to tests completed from 3/3/2015 to 4/7/2015, and Calibration 3 applies to tests completed from 4/8/2015 to 4/15/2015.

Table 5-4 Instrumentation Summary

ID #	Description	Type	Range	Accuracy[1]
F1	Primary flow rate	Magnetic flow meter	0 - 100 gpm	± 0.258% rate
P1	Upstream pressure	Pressure transducer	0 - 36 psid	± 0.289 psi
DP1H	High-range differential pressure	Pressure transducer	0 - 20 psid	± 0.169 psi
DP2H	High-range differential pressure	Pressure transducer	0 - 36 psid	± 0.289 psi
DP1L	Low-range differential pressure	Pressure transducer	0 - 2 psid	± 0.0206 psi
Level 1	HCT level	Ultrasonic	1.0 - 14.125 in	± 0.17 in
Level 2	LCT level	Ultrasonic	1.25 - 12.25 in	± 0.16 in
T1	DIS inlet temperature	T-type thermocouple	32 - 201°F	± 2.394°F
T2	Downstream temperature	T-type thermocouple	32 - 201°F	± 2.394°F
CP1/CP1a	24 in column conductivity	Conductivity Probe	Table 5-5	
CP2	36 in column conductivity	Conductivity Probe		
CP3	55.25 in column conductivity	Conductivity Probe		
CP4	42 in column conductivity	Conductivity Probe		
CP5	12 in column conductivity	Conductivity Probe		
CP6	61.25 in column conductivity	Conductivity Probe		
CP7	83.75 in column conductivity	Conductivity Probe		
CP8	Brine tank conductivity	Conductivity Probe		

Note 1: These values account for instrument measurement accuracy and analog to digital converter accuracy.

Table 5-5 Conductivity Probe Range and Accuracy

ID #	Calibration 1		Calibration 2		Calibration 3	
	Range (wt% KBr)	Accuracy	Range (wt% KBr)	Accuracy	Range (wt% KBr)	Accuracy
CP1/CP1a	20	± 0.5 wt% KBr	20	± 0.5 wt% KBr, ≤ 10 wt% KBr ± 0.75 wt% KBr, > 10 wt% KBr	20	± 0.5 wt% KBr, ≤ 6 wt% KBr ± 12% of Reading, > 6 wt% KBr
CP2	20	± 0.5 wt% KBr	20	± 12% of Reading	20	± 0.5 wt% KBr
CP3	20	± 0.5 wt% KBr	20	± 21% of Reading	20	± 0.5 wt% KBr, ≤ 11 wt% KBr ± 10% of Reading, > 11 wt% KBr
CP4	20	± 0.5 wt% KBr	20	± 23% of Reading	20	± 0.5 wt% KBr
CP5	15	± 0.5 wt% KBr	15	± 20% of Reading	15	± 0.5 wt% KBr
CP6	20	± 0.5 wt% KBr	20	± 13% of Reading	20	± 0.5 wt% KBr
CP7	20	± 0.5 wt% KBr	20	± 15% of Reading	20	± 0.5 wt% KBr
CP8	20	± 0.5 wt% KBr	20	± 20% of Reading	15	± 0.5 wt% KBr, ≤ 6 wt% KBr ± 0.75 wt% KBr, > 6 wt% KBr

5.10.1 Concentration Measurement

An evaluation of methods of on-line detection of solution concentration was performed that considered auto-titration, inductive-coupled plasma-mass spectrometry (ICP-MS), Raman spectroscopy, and conductivity. The evaluation concluded that, based on the functional requirements for the brine testing, conductivity has the greatest potential for measuring solute concentration because of the ability to perform on-line measurements without removing a sample, the relatively inexpensive costs, and the ability to use multiple sensors in a relatively simple fashion.

5.10.1.1 Measurement Principal

The principal of measuring concentration variations in a liquid via conductivity is well established. Commercial concentration sensors are normally used to measure the concentration of bulk liquid and are large in size. In the current application, physical size restrictions require a miniature sensor.

When two electrodes are inserted into a solution as shown in Figure 5-13, the conductance between the two electrodes is proportional to the number of ions present in the conducting solution. Therefore, a measure of the conductance will give a direct reading of the solution concentration. If DC voltage is applied to the electrodes, the results can be interpreted simply because only the resistance between the two electrodes is included. However, these two electrodes are under a continuous oxidizing or deoxidizing condition and the solution composition is changing by electrolysis. If alternating voltage is applied to the electrodes, both resistance between the electrodes and inductance in the circuit must be included, which is quite difficult to be determined. To minimize these problems, a low frequency rectangular wave is utilized. In both positive and negative portions of the wave, the voltage can be taken as DC which eliminates the need to include circuit inductance, but the electrodes are under an alternating oxidizing and deoxidizing condition, which limits the effects of electrolysis on the solution composition.

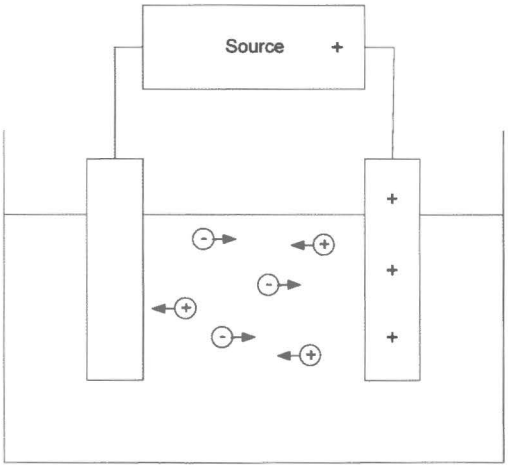

Figure 5-13 Principal of Concentration Measurement

A fast response micro-conductivity probe supplied by Micro Electrodes Inc. was selected for the brine tests. The MI-915 conductivity probe has an 1/8 inch body diameter that can be easily installed in the subscale flow column. The probes have a measurement range that corresponds to an extrapolated KBr concentration that exceeds the solubility limit of KBr. Integration hardware supplied with the conductivity probe allows the raw signal to be input directly into the existing subscale data acquisition system where the data will be added to the subscale data record.

Calibration of the probes was completed using 500 mL standards at KBr concentrations of 1, 5, 10, 15, and 20 wt%. The probes were dipped in the standards and at least 5 data points were collected after the probe reading stabilized. In most cases, more than 10 data points were collected, and during the original calibration 30 data points were collected. The data points were then averaged to determine a single value for each KBr concentration and the values were used to generate calibration curves that correlate the probe output signal to wt% KBr.

As shown in Table 5-4, eight conductivity probes were used in the subscale brine testing. Seven conductivity probes were used to measure brine concentration in the subscale test column and an eighth probe was used to measure the brine supply tank concentration. Figure 5-14 shows the location of the conductivity probes in the test column.

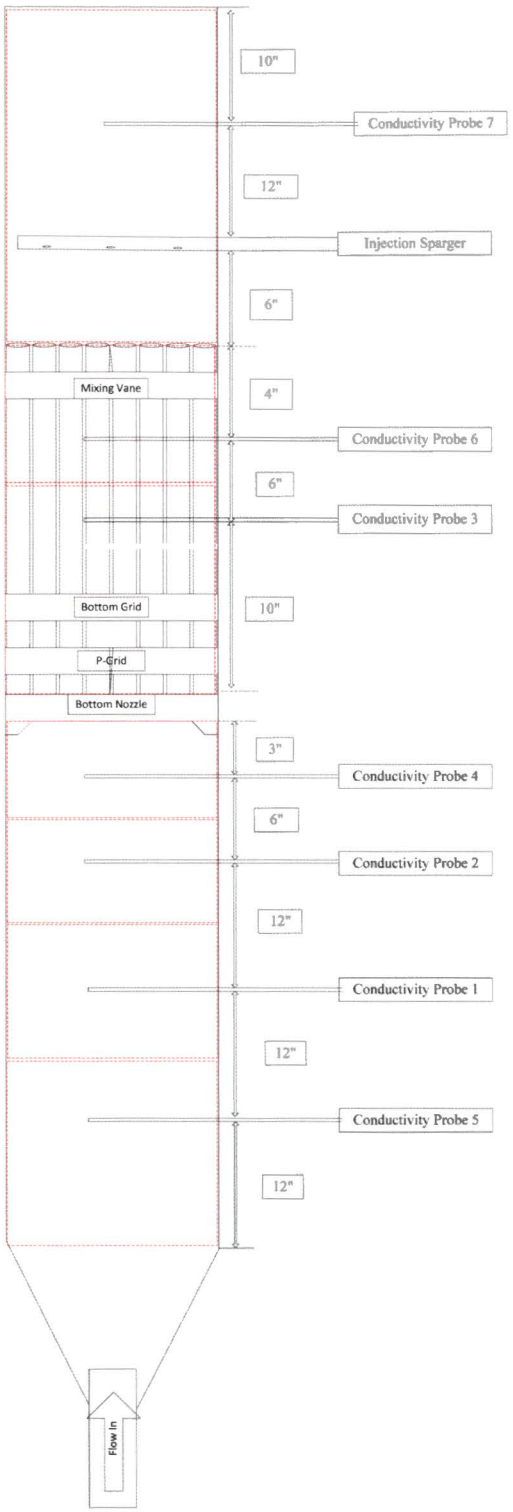

Figure 5-14 Axial Location of Conductivity Probes in Test Column

5.11 REFERENCES

5-1 NUREG/CR-6917, "Experimental Measurements of Pressure Drop across Sump Screen Debris Beds in Support of Generic Safety Issue 191," Pacific Northwest National Laboratory, 2007.

5-2 WCAP-16793-NP-A, Rev. 2, Evaluation of Long-Term Cooling Considering Particulate, Fibrous and Chemical Debris in the Recirculating Fluid," July 2013.

5-3 WCAP-17788-P/NP (Proprietary/Non-Proprietary), "Comprehensive Analysis and Test Program for GSI-191 Closure (PA-SEE-1090) – Autoclave Chemical Effects Testing for GSI-191 Long-Term Cooling," July 2015.

6 TEST MATRIX

A total of 46 production experiments were completed using the subscale brine test facility. The test program was broken into two test series. Each test series is described below.

6.1 TEST SERIES 1

Test Series 1 consists of 20 tests conducted using the Westinghouse core inlet geometry described in Section 5.6.1. Table 6-1 below provides a summary of the completed experiments. In the table, the *Flow Control Version* column identifies the flow control profile used during the testing. Flow Control Version 1 was the original flow control defined for the test program. After completing 7 experiments, the original flow control was modified such that the column flow would continue to decrease. A description of the two flow controls used for testing is provided in Section 5.4.1.

6.2 TEST SERIES 2

Test series 2 consisted of 26 tests conducted using the AREVA core inlet geometry described in Section 5.6.2. Table 6-2 provides a summary of the completed experiments for this test series. For this test series, Flow Control Version 2 was used in all experiments except those completed without brine injection. For tests completed without brine injection, the inlet flow rate was held constant at the initial flow rate. A description of the two flow controls used for testing is provided in Section 5.4.1.

Table 6-1 Test Series 1 Westinghouse Core Inlet Geometry Test Matrix

Test ID	Date	Rep. #	Test Duration (min)	Brine Injection (gpm)	Brine Injection Delay (min)	Source Conc. (wt% KBr)	Initial Column Flow (gpm/FA)	Flow Control Version	Fiber Load (g/FA)	p:f Ratio
T012	2/23/15	1	38	0.5	0	10	3.43	1	0	0
T013	2/23/15	1	38	0.5	0	10	3.43	1	5	0
T014	2/23/15	1	38	0.5	20	10	3.43	1	5	0
T015	2/24/15	1	57	0.5	0	10	3.43	1	7.5	0
T016	2/24/15	1	64	0.5	20	10	3.43	1	7.5	0
T017	2/25/15	2	45	0.5	0	10	3.43	1[1]	7.5	0
T018	2/26/15	1	47	0.5	0	10	3.43	1[1]	10	0
T019	2/27/15	1	75	0.5	20	10	3.43	2	10	0
T020	2/27/15	1	70	0.5	20	10	3.43	2	7.5	2
T021	3/2/15	1	75	0.5	20	10	3.43	2	15	1
T022	3/3/15	2	79	0.5	0	10	3.43	2	10	0
T023	3/3/15	2	73	0.5	20	10	3.43	2	10	0
T024	3/6/15	1	73	0.5	0	15	3.43	2	10	0
T025	3/6/15	1	95	0.5	0	15	3.43	2	15	0
T026	3/6/15	1	92	0.5	0	5	3.43	2	5	0
T027	3/9/15	1	76	0.5	0	5	3.43	2	2.5	0
T028	3/10/15	1	100	0.5	0	15	3.43	2	20	0
T029	3/10/15	3	73	0.5	0	10	3.43	2	7.5	0
T030	3/11/15	2	52	0.5	0	15	3.43	2	10	0
T031	3/11/15	2	100	0.5	0	15	3.43	2	15	0

Note: [1] The flow was manually reduced at the end of these tests.

Table 6-2 Test Series 2 AREVA Core Inlet Geometry Test Matrix

Test ID	Date	Rep. #	Test Duration (min)	Brine Injection (gpm)	Brine Injection Delay (min)	Source Conc. (wt% KBr)	Initial Column Flow (gpm/FA)	Flow Control Version	Fiber Load (g/FA)	p:f Ratio
T032	3/19/15	1	40	0.5	0	10	3.43	2	0	0
T033	3/19/15	1	40	0	0	0	3.43	Const. Flow	22.5	0
T034	3/20/15	1	40	0	0	0	3.43	Const. Flow	22.5	12
T035	3/20/15	1	73	0.5	0	10	3.43	2	7.5	0
T036	3/23/15	1	67	0.5	0	10	3.43	2	7.5	2
T037	3/24/15	1	45	0	0	0	3.43	Const. Flow	10	0
T038	3/24/15	1	85	0.5	0	10	3.43	2	15	0
T039	3/24/15	1	33	0	0	0	3.43	Const. Flow	15	1
T040	3/26/15	1	76	0.5	0	10	3.43	2	15	1
T041	3/26/15	1	43	0.5	0	10	3.43	2	10	0
T042	3/30/15	2	46	0.5	0	10	3.43	2	7.5	0
T043	3/30/15	2	92	0.5	0	10	3.43	2	15	0
T044	3/31/15	1	48	0.5	0	15	3.43	2	10	0
T045	3/31/15	1	49	0.5	0	15	3.43	2	15	0
T046	4/1/15	1	45	0.5	0	5	3.43	2	5	0
T047	4/1/15	1	67	0.5	0	5	3.43	2	7.5	0
T048	4/2/15	2	55	0.5	0	10	3.43	2	10	0
T049	4/2/15	1	83	0.5	0	10	3.43	2	15	2
T050	4/7/15	2	52	0.5	0	15	3.43	2	15	0
T051	4/7/15	2	70	0.5	0	10	3.43	2	0	0
T052	4/14/15	3	95	0.5	0	10	3.43	2	10	0
T053	4/14/15	3	56	0.5	0	10	3.43	2	7.5	0
T054	4/15/15	4	70	0.5	0	10	3.43	2	10	0
T055	4/15/15	4	60	0.5	0	10	3.43	2	7.5	0

7 OVERVIEW OF TEST RESULTS

At the start of the experiment, the temperature of the DI water in the main supply tank and brine solution in the brine supply tank was measured to ensure that each liquid was in the desired temperature range. DI water from the main supply tank was then circulated to fill the facility, including the DIS. The HCT was isolated for debris addition and debris was prepared according to the test procedures, added to the HCT and the contents uniformly mixed. To start the experiment, the operator set the specified flow control for the column inlet flow, opened the HCT isolation valve to begin injecting debris-laden coolant into the test column. For tests with concurrent debris and brine injection, the brine injection pump was started when the HCT isolation valve was opened. For tests with delayed brine injection, the brine injection pump was started 20 minutes after the HCT isolation valve was opened.

The following test results are generated for each experiment:

- Test column pressure
- Test column inlet and outlet temperature
- High and low concentration debris injection tank liquid levels
- Test column inlet and outlet flow rates
- Brine injection flow rate
- Cumulative fiber mass
- Pressure drop across fuel components
- Test column and brine tank solute concentrations
- Volume-averaged core and lower plenum region solute concentrations with uncertainty

7.1 TEST COLUMN PRESSURE

The test column pressure was measured during each test in the lower section of the test column, several inches upstream of the capture geometry. There was no prescribed initial column pressure required for the brine testing and there was some variance throughout the test program. The average initial test section pressure was 5.16 psig. The minimum initial pressure was 1.68 psig (T033) and the maximum initial pressure was 8.2 psig (T047). In general, the pressure trends seen throughout the test program include a small pressure spike corresponding to the start of brine injection and a reduction in pressure during each experiment, consistent with the reduction in column inlet flow rate.

Figure 7-1 shows a typical pressure measurement recorded during test T029. As seen in the figure, the column pressure trend is characterized by an initial spike in column pressure, which

is consistent with the initiation of the brine injection. After the initial spike, the column pressure reduces throughout the duration of the experiment consistent with the reduction in column inlet flow rate. In general, these trends are seen consistently in all tests with concurrent brine and debris injection.

Figure 7-2 shows a typical pressure measurement recorded during test T021, which was a delayed brine injection test. As seen in the figure, the column pressure trend is characterized by a reduction in pressure with a step change that occurs when the brine injection is started. In general, these trends are seen consistently in all tests with delayed brine introduction.

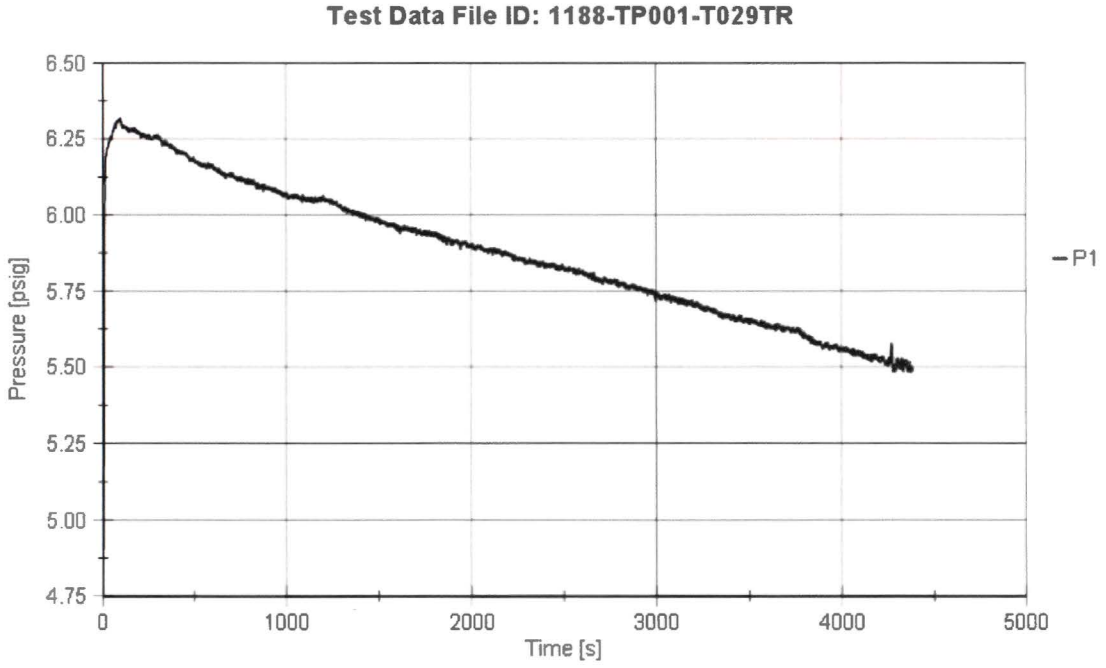

Figure 7-1 Test Column Pressure Measured during Test T029

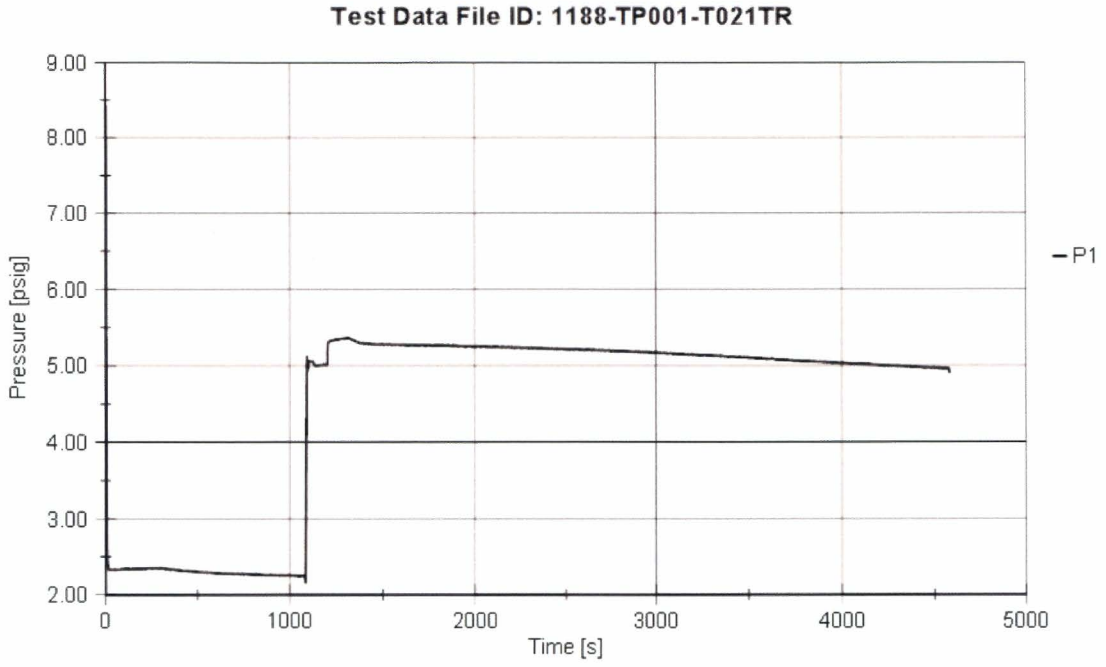

Figure 7-2 Test Column Pressure Measured during Test T021

7.2 TEST COLUMN INLET AND OUTLET TEMPERATURE

The test column inlet and outlet fluid temperatures were measured throughout the duration of each experiment. In addition, the DI water and brine solution temperature were measured before the start of each experiment. The inlet temperature was measured in the main coolant circulation loop piping at the off-take pipe for the DIS coolant source, which is upstream of the test column inlet. The column outlet temperature is measured on the main coolant circulation loop just downstream from the test column outlet diffuser. The inlet and outlet column fluid temperatures were prescribed to be in the range of 64 - 72°F during the test duration. In most experiments, this was the case; however, there were several experiments in which the fluid temperature was outside the desired temperature range. Table 7-1 lists tests that had fluid temperatures outside the desired range. The highest fluid temperature was measured during test T017, which was 81.3°F. The lowest fluid temperature was measured during test T032, which was 60°F.

The prescribed temperature range was established to ensure that the conductivity probes are operating in their calibrated temperature range. If a given experiment has a fluid temperature outside this range, the uncertainty on the conductivity probe measurements will be higher. If the fluid temperature is low, the conductivity measurement will be low. If the fluid temperature is high, the conductivity measurement will be high.

The temperature gradient between the DI water and brine solution is also important. Since the tests were designed to investigate mass transport due to a concentration gradient, any density differences due to temperature should be minimized. Table 7-1 summarizes the temperature gradient for each test. The majority of tests had a temperature gradient less than 4°F. As shown in the table, two tests had a brine temperature that was more than 4°F greater than the DI water temperature and eight tests had a DI water temperature that was more than 4°F greater than the brine. For tests that had a higher brine temperature, the concentration gradient required to induce buoyancy-driven mass transport from the core to the lower plenum will be higher since the temperature gradient is opposing the concentration gradient. The opposite is true for tests with a higher DI water temperature.

Table 7-1 Summary of DI Water and Brine Solution Temperatures
Tests with DI Water Temperature > 72°F
T017, T018, T021, T022, T023, T024, T025
Tests with DI Water Temperature < 64°F
T032, T033
Test with Brine Temperature > 72°F
None
Test with Brine Temperature < 64°F
T044, T045, T046, T047
Tests with a Positive (Brine > DI Water) Temperature Gradient ≤ 2°F
T014, T015, T020, T030, T031, T051
Tests with a Positive (Brine > DI Water) Temperature Gradient ≤ 4°F
T019
Tests with a Positive (Brine > DI Water) Temperature Gradient > 4°F
T026, T032
Tests with a Negative (Brine < DI Water) Temperature Gradient ≤ 2°F
T016, T022, T023, T025, T027, T029, T035, T042, T043, T050, T052, T053, T054
Tests with a Negative (Brine < DI Water) Temperature Gradient ≤ 4°F
T012, T013, T018, T021, T024, T028, T038, T048, T049, T055
Tests with a Negative (Brine < DI Water) Temperature Gradient > 4°F
T017, T036, T040, T041, T044, T045, T046, T047

Figure 7-3 shows typical column outlet and inlet fluid temperatures measured during test T051. As the figure shows, the inlet and outlet temperatures remain similar throughout the test duration. The outlet temperature is higher than the inlet temperature which indicates that the brine solution being injected into the test column is slightly hotter.

Figure 7-4 shows the inlet and outlet fluid temperatures from test T026 which had a brine temperature that was 8°F hotter than the DI water temperature. This test had the highest positive temperature gradient. As a result, the column outlet temperature increased during the test because the hotter brine solution injected into the test column was mixing with the colder DI water. Similar temperature trends were seen in other tests that had a brine solution temperature that was hotter than the DI water.

Figure 7-5 shows the inlet and outlet fluid temperatures from test T044 which had a brine temperature that was 13°F colder than the DI water temperature. This test had the highest negative temperature gradient. As a result, the column outlet temperature decreased during the test because the colder brine solution injected into the test column was mixing with the hotter DI water. Similar temperature trends were seen in other tests that had a brine solution temperature that was colder than the DI water.

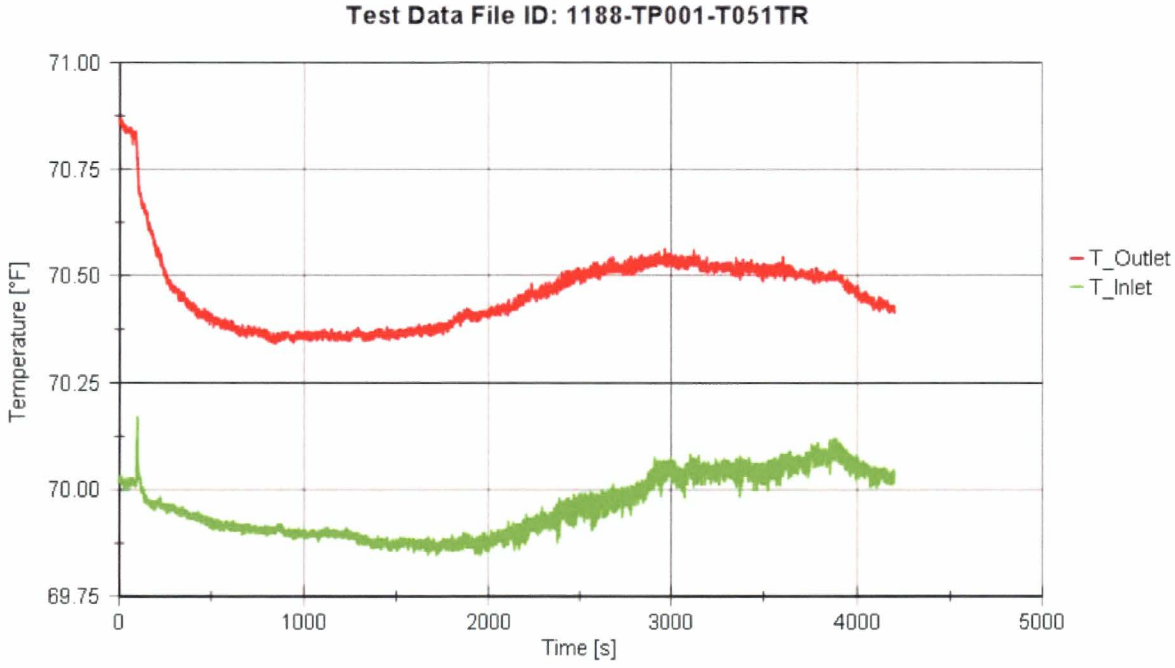

Figure 7-3 Test Column Liquid Temperature Measured during Test T051

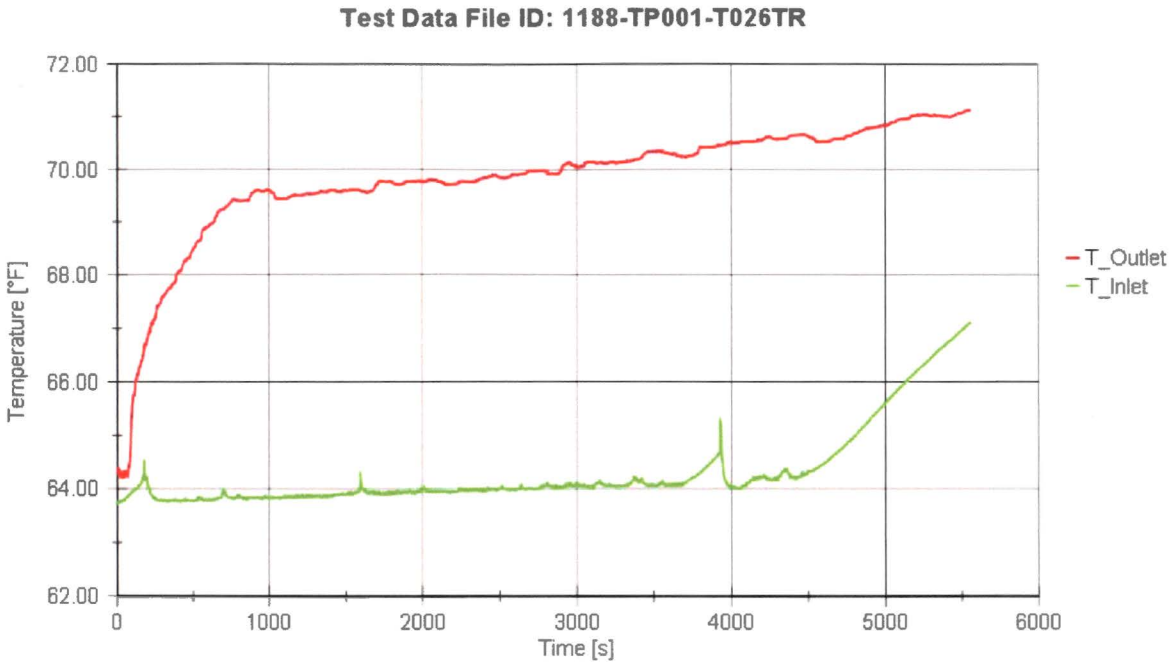

Figure 7-4 Test Column Liquid Temperature Measured during Test T026

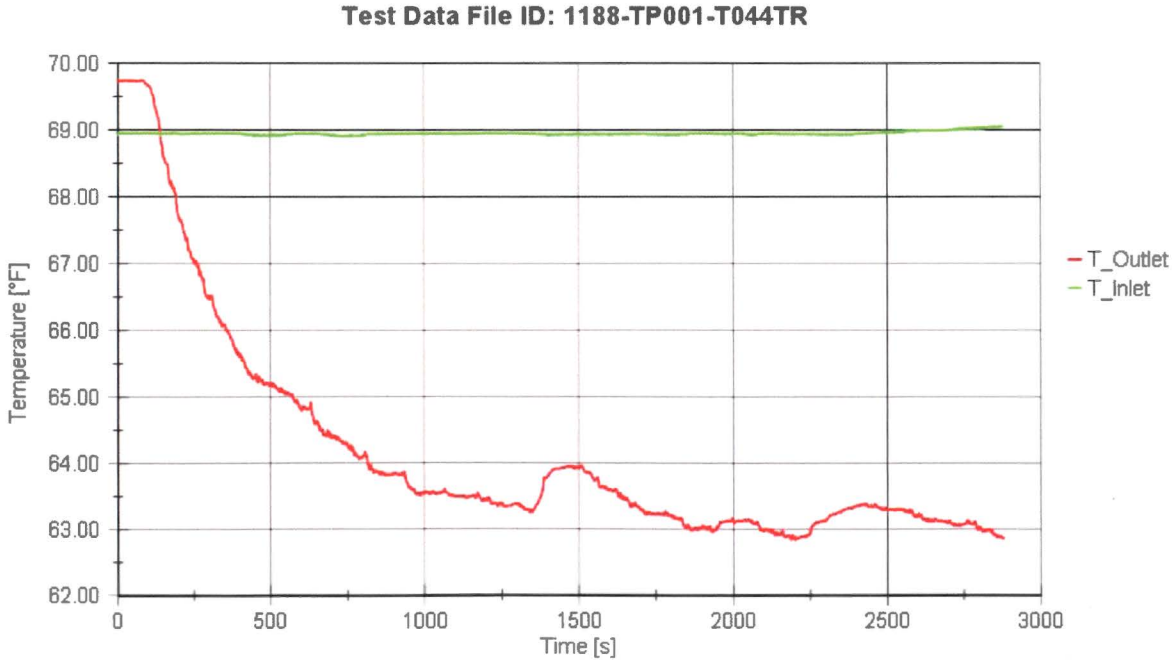

Figure 7-5 Test Column Liquid Temperature Measured during Test T044

7.3 DEBRIS INJECTION SYSTEM TANK LIQUID LEVELS

The DIS HCT and LCT tanks levels were measured during the test using ultrasonic level sensors. The level measurements are used to calculate the cumulative fiber mass injected during each experiment. The desired tank levels are prescribed by the facility control system. The HCT level starts at a nominal level of 12 inches and drains to 6 inches over the first 3 minutes of the experiment. The HCT level remains at 6 inches until the end of the test. In some cases, the HCT was drained completely at the end of the test. The LCT level is controlled to be nominally 8 inches throughout the duration of the test. In some cases, the LCT is drained at the end of the test as well. Figure 7-6 shows typical HCT and LCT levels from test T029. In general, most level data is consistent with that shown in Figure 7-6; however, there were several tests that had erroneous level measurements. For example, Figure 7-7 shows the DIS level measurements from test T026. As the figure shows, the HCT level does not follow the expected trend. This is most likely due to water droplets deposited on the level sensor during the debris preparation process.

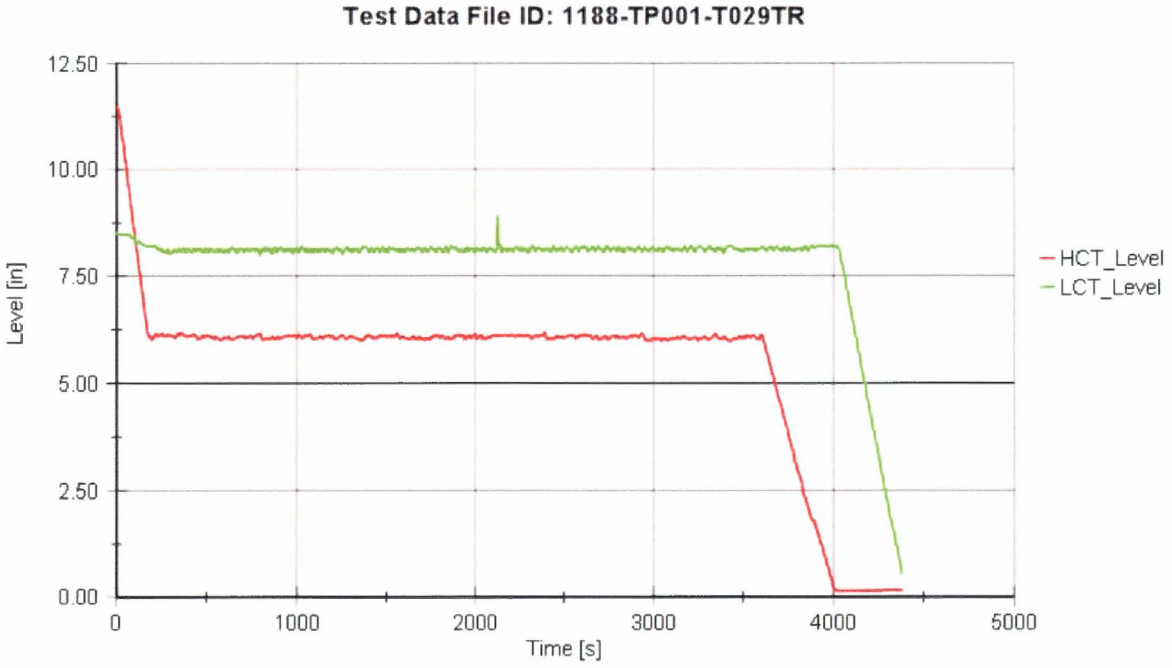

Figure 7-6 DIS Tank Levels Measured during Test T029

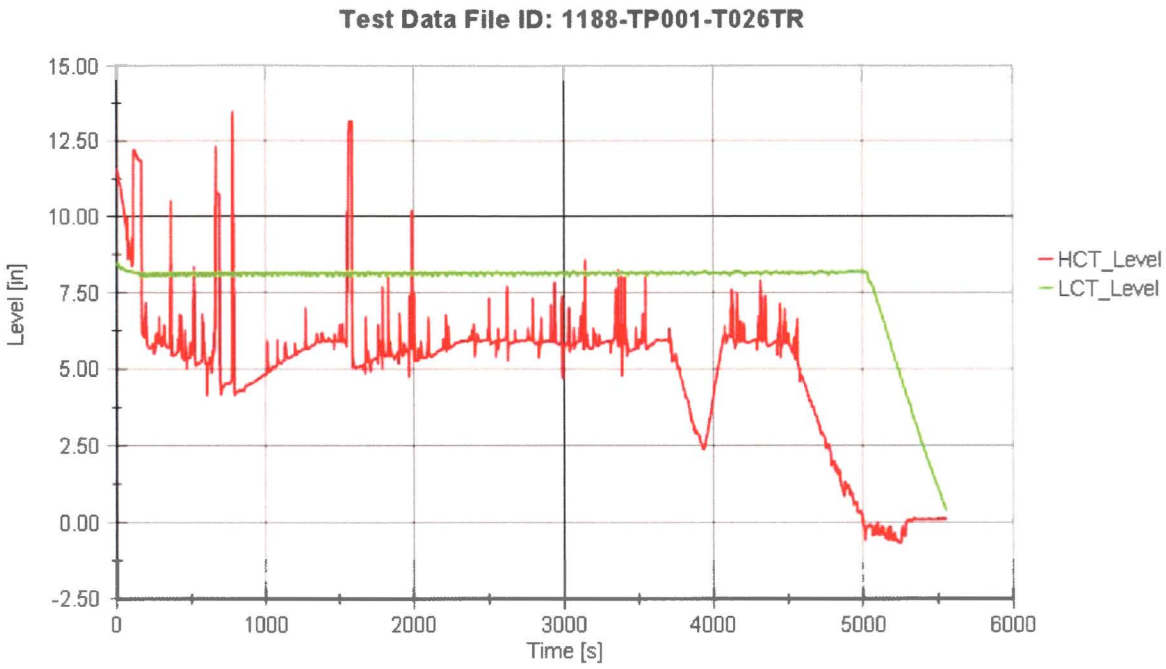

Figure 7-7 DIS Tank Levels Measured during Test T026

7.4 TEST COLUMN FLOW RATES

The outlet flow rate, which is the combination of inlet and brine injection flow rates, is measured during each experiment. The inlet flow rate is calculated by subtracting the brine injection flow rate from the outlet flow rate. The desired inlet flow rate is prescribed by the facility control system. Two different flow control profiles were used during the test program. The flow control profile used in tests T012 – T018 was the original specification for the test program. Following test T018, it was decided that the inlet flow rate should continue to reduce as the test progressed. As a result, a second flow control profile was defined as shown in Figure 5-5. The only difference is that instead of the flow reducing to [ ]^{a,c} and remaining constant, as was the case with the first flow control, the flow rate continues to decrease at a linear rate after reaching [ ]^{a,c} For the four AREVA tests (T033, T034, T037, and T039), conducted without brine injection, the inlet flow rate was held constant at 0.8 gpm nominal and did not use one of the flow control profiles described above.

Erroneous outlet flow measurements were measured at the start of some experiments. These flow measurements were confirmed to be erroneous because the measured values were outside the injection and brine pump capacity. Further, because the pumps used in the facility are positive displacement pumps, the flow rate is accurately related to the pump speed. During the tests that erroneous flow measurements were made, no change in the facility pump speeds were observed. The source of the erroneous flow measurements is most likely due to air in the

downstream circulation loop piping where the flow meter is located. Erroneous flow measurements were collected in tests T025, T036, T038, T040, T042 – 48, T050, and T051.

The column inlet flow rate, calculated using the measured outlet flow rate, is used to determine the cumulative fiber mass injected for each test. Using the outlet flow rate for tests that had the erroneous flow measurements resulted in the total cumulative fiber mass reaching the test column over an unrealistic duration. For this reason, flow rates from tests with similar test conditions were used to calculate the cumulative fiber mass for experiments that experienced erroneous flow measurements.

The brine injection flow rate was not measured during the experiments. The brine injection flow rate was controlled by the brine injection pump speed. Since a positive displacement pump was used for brine injection, the flow rate is accurately relatable to the pump speed. Testing completed during shakedown testing determined the pump speed necessary to achieve the prescribed brine injection flow rate of 0.5 gpm. The pump speed corresponding to 0.5 gpm was programmed into the pump controller and used during the duration of the test program. When calculating the column inlet flow rate, the brine flow is assumed constant at 0.5 gpm when injecting into the column.

Figure 7-8 shows typical flow rates for test T029 which was conducted with concurrent brine injection. Figure 7-9 shows typical flow rates from test T014 which was conducted with delayed brine injection. Figure 7-10 shows flow rates from test T048 which was one of the tests that experienced erroneous flow measurements at the beginning of the test. The inlet flow rate shown in the figure has the same erroneous values because it was calculated using the measured outlet flow rate.

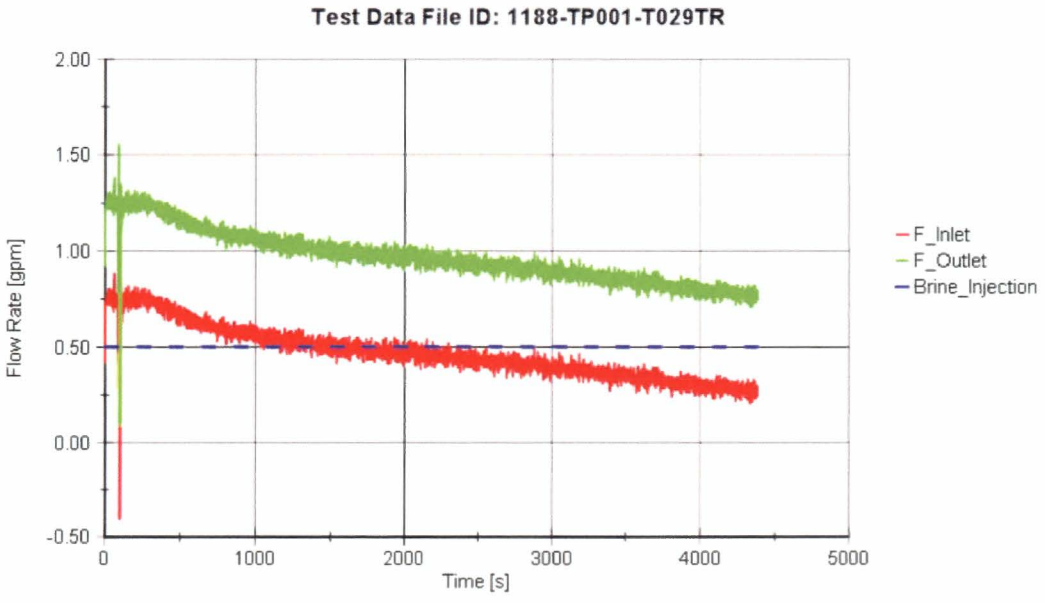

Figure 7-8 Test Column Flow Rates during Test T029

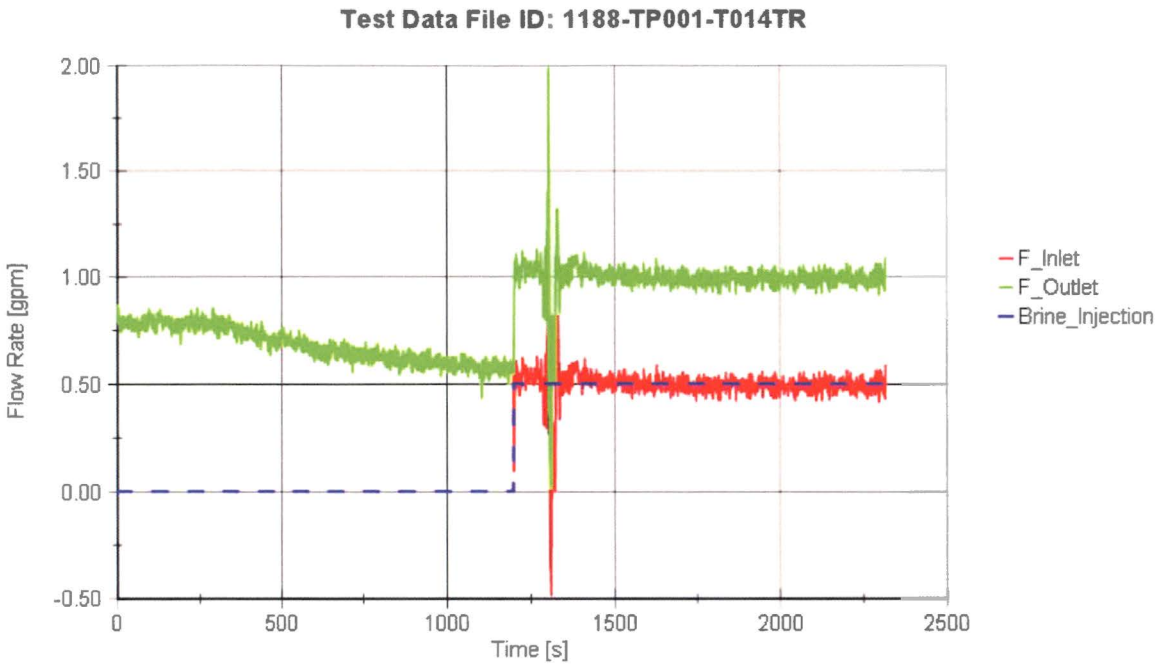

Figure 7-9 Test Column Flow Rates during Test T014

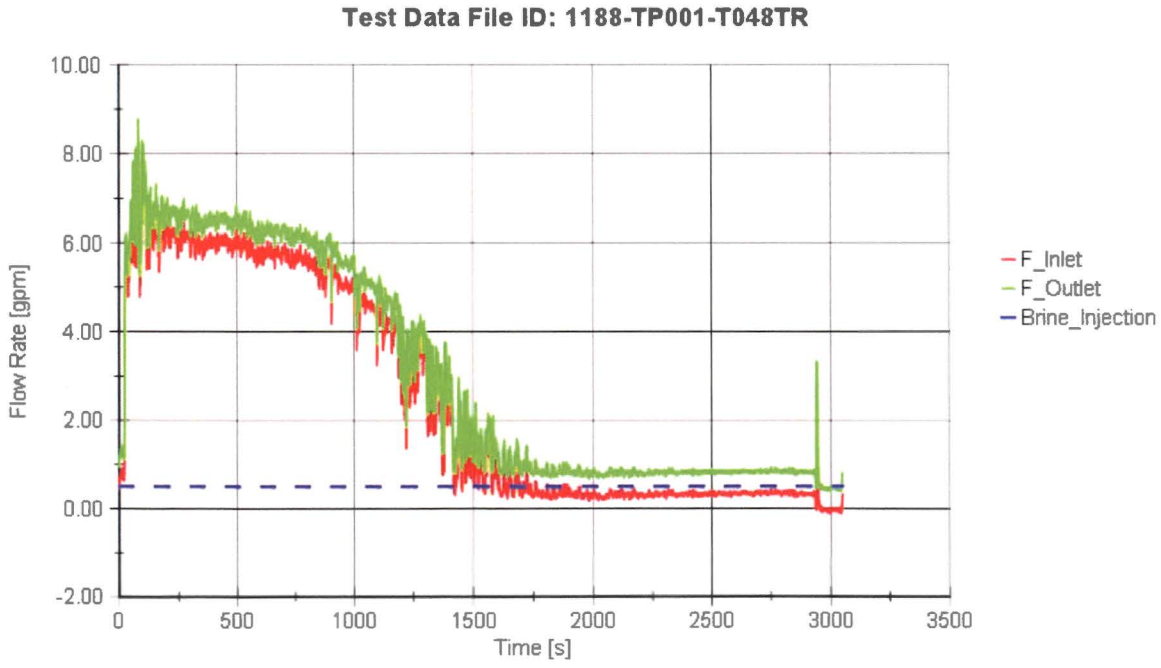

Figure 7-10 Test Column Flow Rates during Test T048

7.5 CUMULATIVE FIBER MASS

The calculation of cumulative fiber mass transported to the test column is made for each experiment. This calculation is completed using the calculated inlet flow rate, the measured DIS tanks levels, and the total mass of fiber prepared for the experiment.

First, the HCT and LCT water volume is calculated:

$$V_{HCT} = \frac{\pi}{4} {D_{HCT}}^2 \times HCT\_Level \quad \text{Eq. 7-1}$$

and

$$V_{LCT} = \frac{\pi}{4} {D_{LCT}}^2 \times LCT\_Level \quad \text{Eq. 7-2}$$

where:

D_{HCT} = 11.22 in, which is the outer diameter of the HCT

D_{LCT} = 8.86 in, which is the outer diameter of the LCT

Since only the outer diameter is reported for the HCT and LCT, it will be used to calculate the tank volumes. Using the outer diameter to calculate volume will result in some error, however, since the beakers are thin-walled, the error due to use of the outer diameter is small when compared to the total uncertainty expected in the calculated cumulative debris load.

Initially, the entire fiber load is contained in the HCT and the fiber load in the LCT and test column is zero. Tables 6-1 and 6-2 provide the total fiber load prepared in the HCT for each experiment. As the test progresses, fiber from the HCT is pumped at the inlet flow rate to the LCT where it is mixed and pumped to the test column at the inlet flow rate.

Therefore, for any given point in time, the masses of fiber in the HCT, the LCT, and the test column are:

$${M_{f,HCT}}^t = {M_{f,HCT}}^{t-1} - {C_{f,HCT}}^{t-1} \times F\_Inlet^{t-1} \quad \text{Eq. 7-3}$$

$${M_{f,LCT}}^t = {M_{f,LCT}}^{t-1} + \left({C_{f,HCT}}^{t-1} - {C_{f,LCT}}^{t-1}\right) \times F\_Inlet^{t-1} \quad \text{Eq. 7-4}$$

and

$$Fiber\_Mass^t = Fiber\_Mass^{t-1} + {C_{f,LCT}}^{t-1} \times F\_Inlet^{t-1} \quad \text{Eq. 7-5}$$

where:

M_f^{t-1} = The mass of fiber in the tanks at the previous time step

C_f^{t-1} = The concentration of fiber in the tanks at the previous time step

Figure 7-11 shows the cumulative fiber mass transported to the test column for the seven debris loads tested. Since the column inlet flow rate and DIS tank levels are similar from test-to-test, the cumulative fiber masses for other tests will be similar to those shown in Figure 7-11 with the same total fiber load.

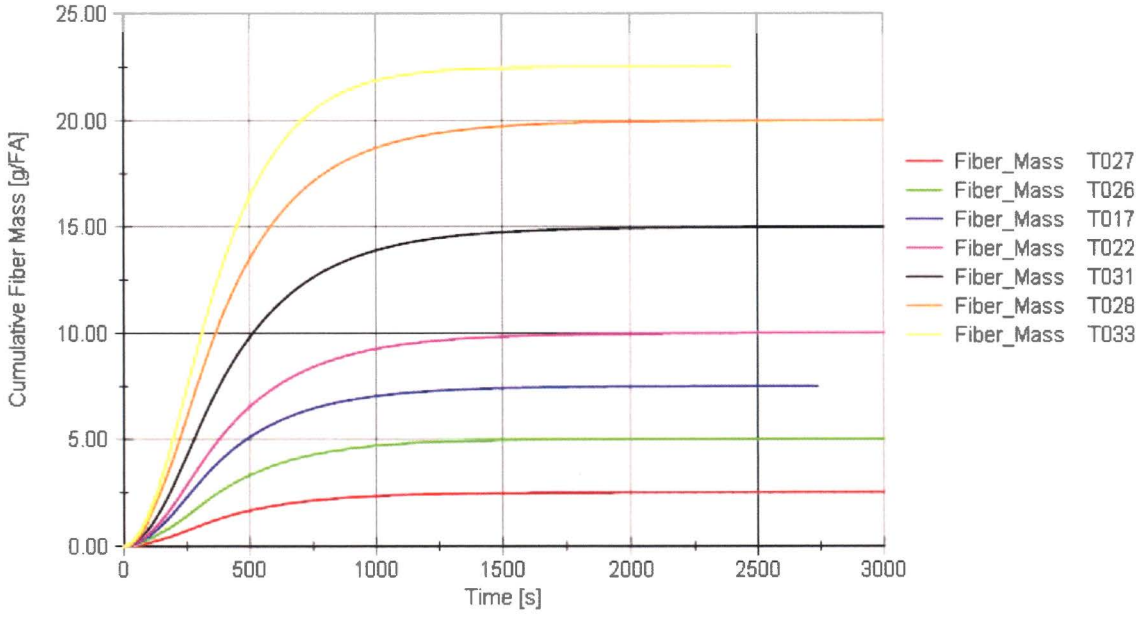

Figure 7-11 Cumulative Fiber Mass Transported to the Test Column

7.6 PRESSURE DROP ACROSS FUEL COMPONENTS

Various pressure drop measurements were made during the test program. For tests completed using the Westinghouse core inlet geometry, high and low range pressure transducers (DP1L and DP1H) were used to measured pressure drop across the bottom nozzle and P-grid combination. A third pressure transducer (DP2H) was used to measure the pressure drop across the first spacer grid.

For tests completed using the AREVA core inlet geometry, high and low range pressure transducers (DP1L and DP1H) were used to measured pressure drop across the lower end

fitting and first spacer grid combination. The third pressure transducer (DP2H) was not used for the AREVA tests.

Figure 7-12 shows typical pressure drop measurements from test T013. Since this was a test conducted using the Westinghouse core inlet geometry, there are three pressure drop measurements. For this test, DP1L and DP2H agree well. This was expected given that the pressure drop measured by these transducers is across the same elevation. DP2H is measured across the first spacer grid.

Figure 7-13 shows typical pressure drop measurements from test T042. Since this test was conducted using the AREVA core inlet geometry, there are two pressure drop measurements both made across the lower end fitting and first spacer grid. As the figure shows, the measurement from DP1H is slightly higher compared to DP1L; however, the difference is well within the accuracy of the pressure transducers.

The discrepancy between the low range pressure transducer (DP1L) and the high range (DP1H) was seen in a number of experiments. Figure 7-14 shows the pressure drop data from test T029 which shows that DP1H is measuring a pressure drop approximately 0.02 psid higher than DP1L. Again, this difference is well within the high range pressure transducer accuracy and deviations like this are not unexpected given the relatively low pressure drops being measured.

a,c

Figure 7-12 Pressure Drops Measured across Fuel Components during Test T013

a,c

Figure 7-13 Pressure Drops Measured across Fuel Components during Test T042

a,c

Figure 7-14 Pressure Drops Measured across Fuel Components during Test T029

7.7 TEST COLUMN AND BRINE TANK CONCENTRATIONS

The brine solution concentration is measured at seven locations in the test column and in the brine supply tank. The location of the conductivity probes in the test column is shown in Figure 5-14.

Figure 7-15 shows the measured brine concentrations from test T012, which was conducted without debris. In the figure, the brine supply tank concentration (CP8) remains constant during the experiment. The concentrations measured in the core region (CP7, CP6, and CP3) are similar throughout the test duration and a concentration gradient is seen in the lower plenum region (CP4, CP2, CP1, and CP5). In general, similar trends were seen throughout the test program.

a,c

Figure 7-15 Brine Concentrations Measured during Test T012

The measured brine concentration is used to calculate the equivalent boric acid concentration in the test column and supply tank using Eq. 4-5. Figure 7-16 shows the equivalent boric acid concentrations from test T012. As seen in the figure, the calculated boric acid concentration begins at a negative value. This is because Eq. 4-5 is also accounting for differences in solution temperature. The brine testing was completed using brine solution at an average temperature of 68°F. The equivalent boric acid concentration calculated using Eq. 4-5 is for boric acid at a temperature of 212°F.

a,c

Figure 7-16 Equivalent Boric Acid Concentrations Calculated for Test T012

7.8 VOLUME-AVERAGED CONCENTRATIONS

Both the measured brine concentrations and the calculated boric acid concentrations are volume-averaged based on the test column geometry to determine a core region and lower plenum region average concentration.

The volume-averaged concentration of the lower plenum region is calculated as follows:

$$\bar{C}_{LP} = C_{CP5}\frac{V_{CP5}}{V_{LP}} + C_{CP1}\frac{V_{CP1}}{V_{LP}} + C_{CP2}\frac{V_{CP2}}{V_{LP}} + C_{CP4}\frac{V_{CP4}}{V_{LP}} \quad \text{Eq. 7-6}$$

where:

C = the concentration in the subscript region

V = the volume of the subscript region

Similarly, the volume-averaged concentration of the core region is calculated as follows:

$$\bar{C}_{core} = C_{CP3}\frac{V_{CP3}}{V_{core}} + C_{CP6}\frac{V_{CP6}}{V_{core}} + C_{CP7}\frac{V_{CP7}}{V_{core}} \quad \text{Eq. 7-7}$$

The uncertainty in the volume-averaged concentrations is obtained by taking the partial derivative of the volume average with respect to each variable, multiplication with the accuracy in that variable, and addition of these individual terms in quadrature. For the lower plenum volume average:

$$\delta\bar{C}_{LP} = \sqrt{\left(\frac{\partial\bar{C}_{LP}}{\partial C_{CP5}} \times \delta C_{CP5}\right)^2 + \left(\frac{\partial\bar{C}_{LP}}{\partial C_{CP1}} \times \delta C_{CP1}\right)^2 + \left(\frac{\partial\bar{C}_{LP}}{\partial C_{CP2}} \times \delta C_{CP2}\right)^2 + \left(\frac{\partial\bar{C}_{LP}}{\partial C_{CP4}} \times \delta C_{CP4}\right)^2} \quad \text{Eq. 7-8}$$

or:

$$\delta\bar{C}_{LP} = \sqrt{\left(\frac{V_{CP5}}{V_{LP}} \times \delta C_{CP5}\right)^2 + \left(\frac{V_{CP1}}{V_{LP}} \times \delta C_{CP1}\right)^2 + \left(\frac{V_{CP2}}{V_{LP}} \times \delta C_{CP2}\right)^2 + \left(\frac{V_{CP4}}{V_{LP}} \times \delta C_{CP4}\right)^2} \quad \text{Eq. 7-9}$$

where:

∂C = the uncertainty in the concentration in the subscript region.

Similarly, for the volume-averaged core concentration:

$$\delta\bar{C}_{core} = \sqrt{\left(\frac{V_{CP3}}{V_{core}} \times \delta C_{CP3}\right)^2 + \left(\frac{V_{CP6}}{V_{core}} \times \delta C_{CP6}\right)^2 + \left(\frac{V_{CP7}}{V_{core}} \times \delta C_{CP7}\right)^2} \quad \text{Eq. 7-10}$$

Figure 7-17 shows the brine volume-averaged concentrations calculated for test T012 and Figure 7-18 shows the equivalent boric acid volume-averaged concentrations calculated for test T012. The volume-averaged boric acid concentration plots will be used in the following sections to provide comparisons of the various test conditions investigated.

a,c

Figure 7-17 Calculated Brine Volume-averaged Concentrations from Test T012

a,c

Figure 7-18 Calculated Boric Acid Volume-averaged Concentrations from Test T012

8 TESTS WITHOUT BRINE INJECTION

Four tests were completed without brine injection (debris only) using the AREVA core inlet geometry. As identified in Table 8-1, the debris only tests were conducted using fibrous debris loads ranging from 10 – 22.5 g/FA and particulate-to-fiber (p:f) ratios ranging from 0:1 – 12:1. The column inlet flow, supplied by the DIS, was held constant at 0.8 gpm (3.43 gpm/FA) during these tests as shown in Figure 8-1. Using column inlet flow rate and the DIS tank level measurements, the cumulative fiber mass arriving to the test column is calculated for the four debris only tests, as shown in Figure 8-2.

Table 8-1 Summary of Debris Only Tests

Test ID	Test Duration (min)	Column Flow Rate (gpm/FA)	Fiber Load (g/FA)	p:f Ratio
T033	40	3.43	22.5	0
T034	40	3.43	22.5	12
T037	45	3.43	10	0
T039	33	3.43	15	1

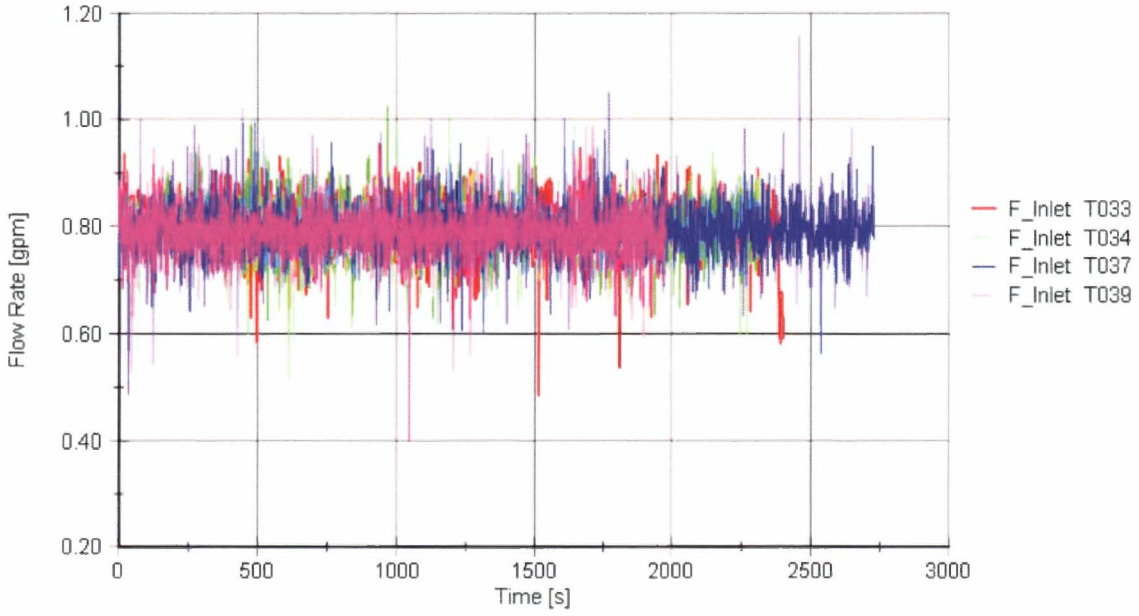

Figure 8-1 Column Inlet Flow Rate from Tests Conducted without Brine Injection

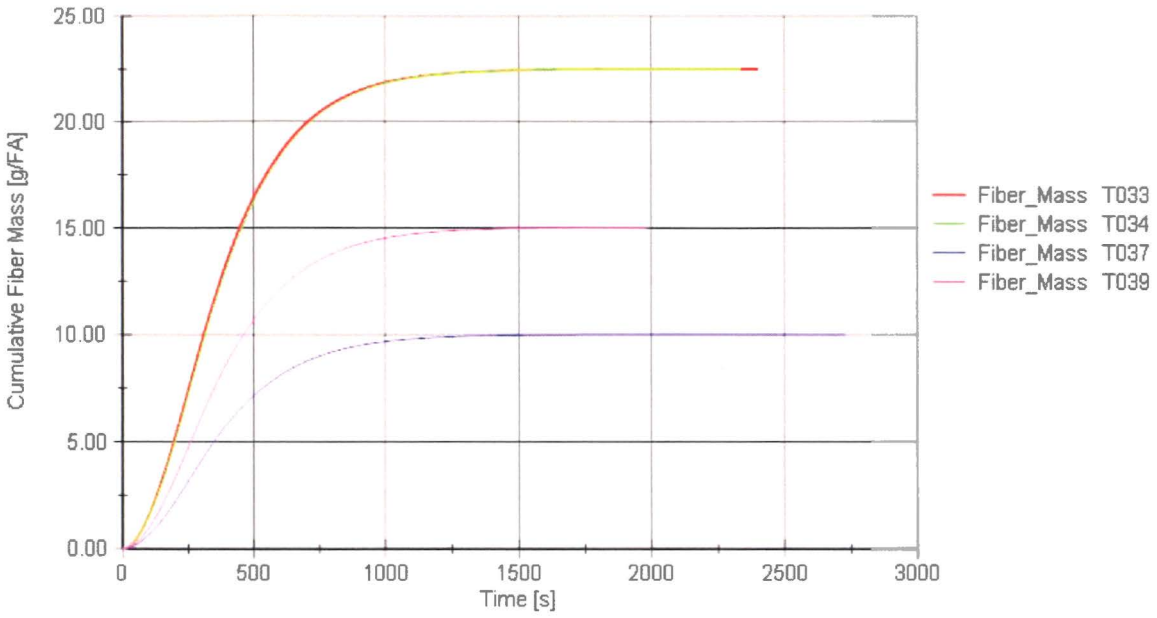

Figure 8-2 Cumulative Fiber Mass from Tests Conducted without Brine Injection

The purpose of conducting debris only tests was to determine the head loss due to the formation of a low-fiber load debris bed under low-flow conditions. In the AREVA core inlet geometry tests, the pressure drop was measured across the lower end fitting and first spacer grid. Observations from these tests indicate that [

]^{a,c} The measured pressure drop from the low range pressure transducer (DP1L) is shown in Figure 8-3 for the four debris only tests. As the figure indicates, a maximum pressure drop of approximately [ ]^{a,c} occurred during test T033 which had a 22.5 g/FA fiber load with a 0:1 p:f ratio. It is noted that the accuracy of the pressure transducer is ±0.0206 psi, which is [ ]^{a,c} from test T033. Considering the instrument accuracy, the maximum pressure drop that could have been achieved during the debris only tests is [ ]^{a,c} Given the low-flow condition and the low fiber loads at which these tests were conducted, the low pressure drops achieved during these tests were expected.

Given the low pressure drops obtained in the AREVA core inlet geometry tests, debris only production tests were not necessary for the Westinghouse core inlet geometry because the same trends would be expected. The subscale head loss testing (Reference 2-1) has shown that under low-flow conditions like those expected following a large CLB, [ ]^{a,c} Given that the debris bed formation will be similar for both fuel geometries, the AREVA debris only pressure drop results are also applicable to the Westinghouse inlet geometry. Pressure drop measurements from test T028, which was

conducted using the Westinghouse core inlet geometry and a fibrous debris load of 20 g/FA support this assertion. In this test [ ]a,c The measured pressure drop from the low range pressure transducer (DP1L) across the bottom nozzle shortly after [ ]a,c was approximately [ ]a,c which is comparable to the maximum pressure drop measured during the AREVA debris only tests.

It is also of interest to compare tests T033 and T034. These tests were both conducted with 22.5 g/FA fiber. Test T033 was conducted with a p:f ratio of 0:1 and test T034 with a p:f ratio of 12:1. Although the accuracy of the pressure transducer at these low pressures makes it difficult to compare results with any certainty, the trends in Figure 8-3 clearly show that test T034 had a [ ]a,c when compared to T033. This trend indicates that at these [

]a,c

[a,c]

Figure 8-3 Measured Pressure Drop across Core Inlet Geometry from Tests Conducted without Brine Injection

9 TESTS WITHOUT DEBRIS INJECTION

Three tests were completed without debris injection (brine only). The brine only tests were conducted using a nominal brine source concentration of 10 wt% KBr, injected into the test column at 0.5 gpm. As identified in Table 9-1, the core inlet geometry and the flow control version were varied. The column inlet flow, supplied by the DIS, started at 0.8 gpm (3.43 gpm/FA) and decayed during these tests as shown in Figure 9-1. As discussed in Section 7.4, test T051 experienced erroneous flow measurements at the beginning of the test and the flow profile used for test T501 was taken from test T054.

Table 9-1 Summary of Brine Only Tests

Test ID	Test Duration (min)	Core Inlet Geometry	Flow Control Version
T012	38	Westinghouse	1
T032	40	AREVA	2
T051	70	AREVA	2

The brine only tests serve as a baseline for determining the impact that debris collection at the core inlet has on the mass transport from the core to the lower plenum. Results from these tests will be compared to test results that include debris injection. Since these tests were done using different core inlet geometries, the results can also be used to assess the impact geometry has on the transport process.

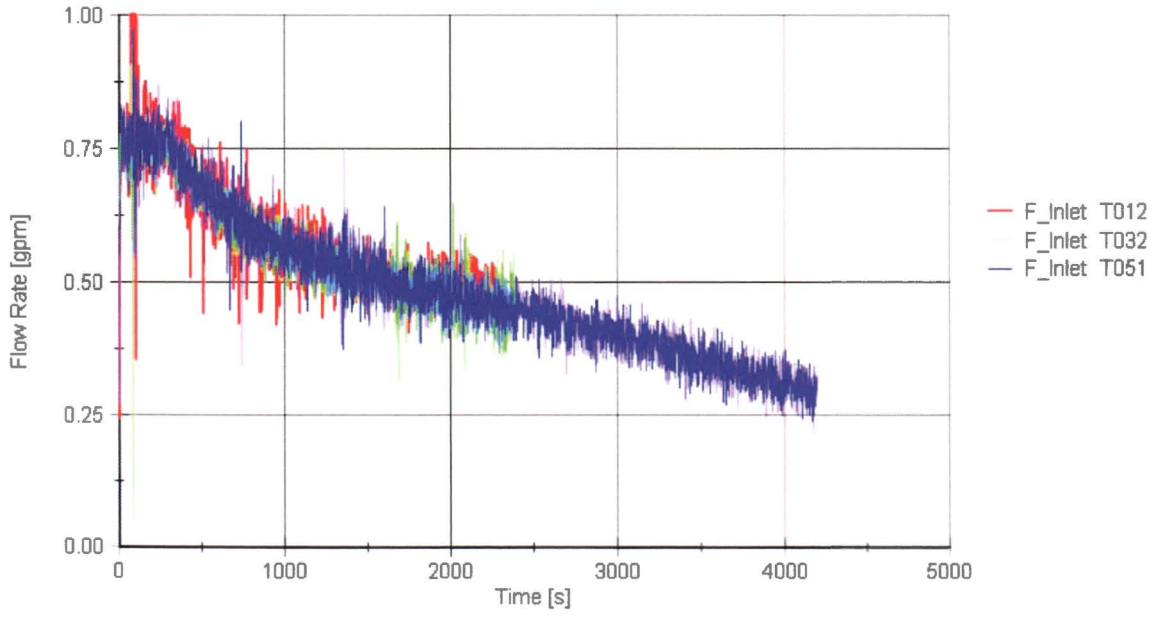

Figure 9-1 Column Inlet Flow Rate from Tests Conducted without Debris Injection

Figure 9-2 shows the calculated equivalent boric acid (BA) volume-averaged core and lower plenum region concentrations from test T012. The figure also provides uncertainty bands for the concentrations that are based on conductivity probe accuracy. The trends seen in the plot are expected. Initially, the core region concentration increases quickly. After a short delay, the density gradient between the core and the lower plenum regions becomes large enough to overcome the inertia due to the upward flow through the test column and mass transfer from the core to the lower plenum begins. This mass transport is indicated by an increase in the lower plenum region concentration and a decrease in the rate at which the core region concentration is increasing. Figure 9-3 shows the same data from test T012, zoomed-in to the first 200 seconds. The figure indicates that the onset of density-driven mass transport begins after approximately 50 seconds when the core region concentration is [ ]^{a,c}

Figure 9-4 shows the calculated equivalent BA volume-averaged core and lower plenum region concentrations from test T032. The figure also provides uncertainty bands for the concentrations that are based on conductivity probe accuracy. The trends seen in the plot are expected and similar to those seen in test T012. Figure 9-5 shows the same data from test T032, zoomed-in to the first 200 seconds. The figure indicates that the onset of density-driven mass transport begins at roughly 45 seconds when the core region concentration is [ ]^{a,c} which is similar to test T012.

Figure 9-6 shows the calculated equivalent BA volume-averaged core and lower plenum region concentrations from test T051. The figure also provides uncertainty bands for the concentrations that are based on conductivity probe accuracy. The trends seen in the plot are expected and similar to those seen in tests T012 and T032. Figure 9-7 shows the same data from test T051, zoomed-in to the first 200 seconds. The figure indicates that the onset of density-driven mass transport begins at roughly 55 seconds when the core region concentration is [ ]^{a,c} which is slightly higher compared to tests T012 and T032 but the agreement is reasonable.

Figure 9-8 is generated to provide a direct comparison of the volume-averaged BA concentrations obtained during tests T012, T032, and T051. In this figure, the uncertainty bands have been removed to aid in comparison of the data. As the figure indicates, there are some differences in the test results. Namely, test T051 has higher average concentrations when compared to tests T012 and T032. This difference can be explained by reviewing the brine source concentrations from these tests as shown in Figure 9-9. As the figure indicates, the brine source concentration is approximately 2.5 wt% BA higher in tests T032 and T051. This explains why the core and lower plenum region volume-averaged concentrations are higher in test T051 when compared to test T012 but it does not explain why test T032, with a brine source concentration comparable to test T051, has lower core and lower plenum region concentrations.

To understand the differences between tests T032 and T051, a review of the water and brine supply temperatures is completed. Table 9-2 lists the liquid temperatures recorded at the beginning of tests T012, T032, and T051. As seen in the table, the water supply temperature in test T032 is lower than the desired range of 64 - 72°F. This temperature range was defined based on the temperature range that was considered for the conductivity probe calibration.

Conductivity is dependent on temperature and lower temperatures result in lower measured conductivities. Figure 9-10 shows the test column inlet and outlet temperatures measured during test T032. As seen in the figure, the inlet temperature is approximately 60°F throughout the test duration, consistent with the water supply temperature. The test column outlet temperature increases from approximately 60 to 64°F during the test duration, which is consistent with a 66°F injected brine solution mixing with the colder water in the test column.

Given the above discussion, the concentrations seen in test T032 are expected to be higher than the measurements suggest due to the lower fluid temperature, which would make test T032 more comparable to test T051.

Table 9-2 Summary of Water and Brine Supply Temperatures from Brine Only Tests

Test ID	Water Supply Temperature (°F)	Brine Supply Temperature (°F)
T012	71	68
T032	60.1	66
T051	69.8	69.6

[a,c]

Figure 9-2 Volume-averaged Core and Lower Plenum Boric Acid Concentrations from Test T012

a,c

Figure 9-3 Volume-averaged Core and Lower Plenum Boric Acid Concentrations from Test T012 (zoomed-in to first 200 seconds)

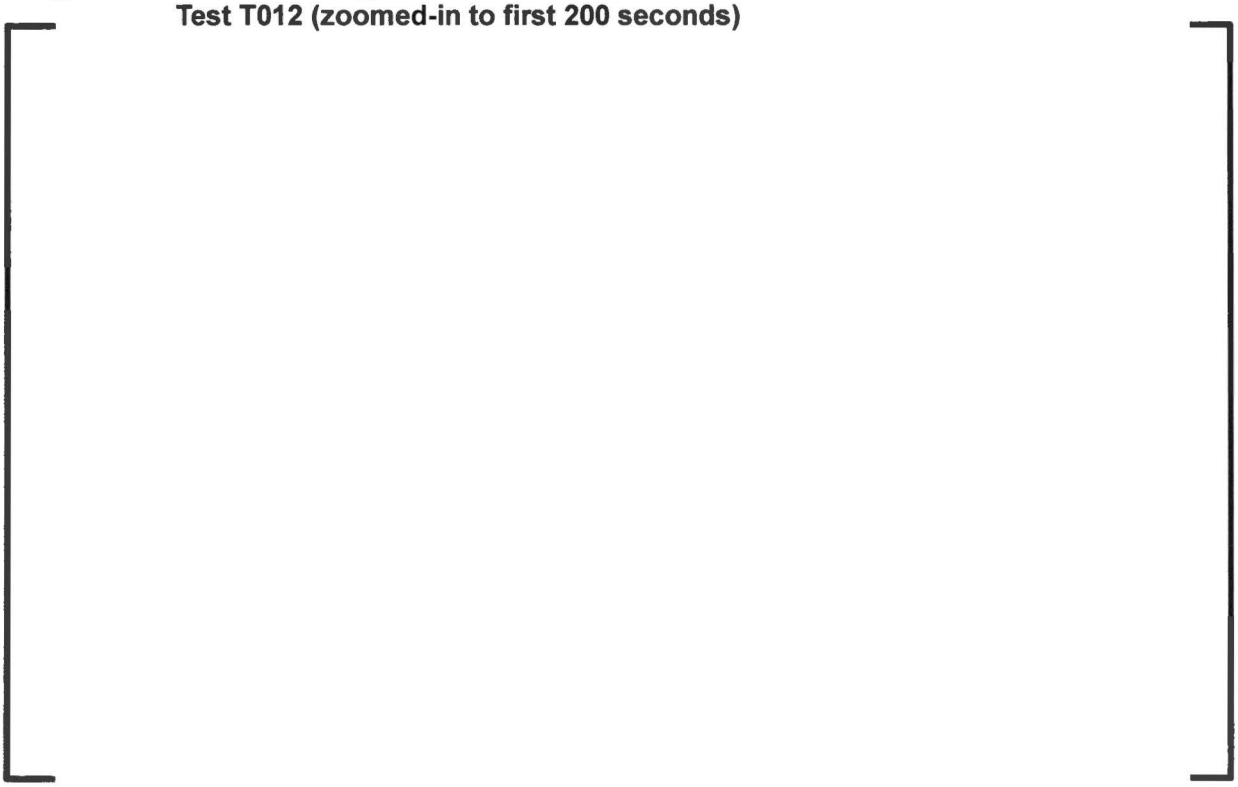

a,c

Figure 9-4 Volume-averaged Core and Lower Plenum Boric Acid Concentrations from Test T032

a,c

Figure 9-5 Volume-averaged Core and Lower Plenum Boric Acid Concentrations from Test T032 (zoomed-in to first 200 seconds)

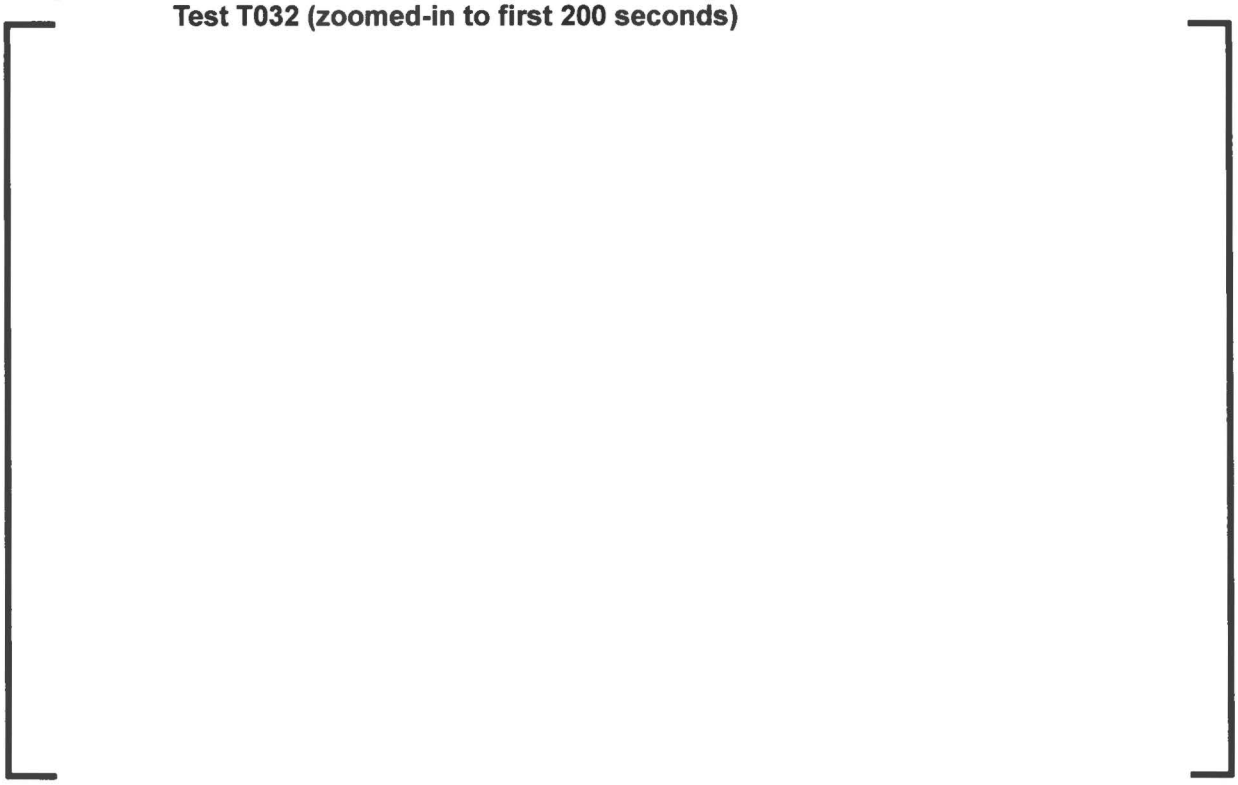

a,c

Figure 9-6 Volume-averaged Core and Lower Plenum Boric Acid Concentrations from Test T051

a,c

Figure 9-7 Volume-averaged Core and Lower Plenum Boric Acid Concentrations from Test T051 (zoomed-in to first 200 seconds)

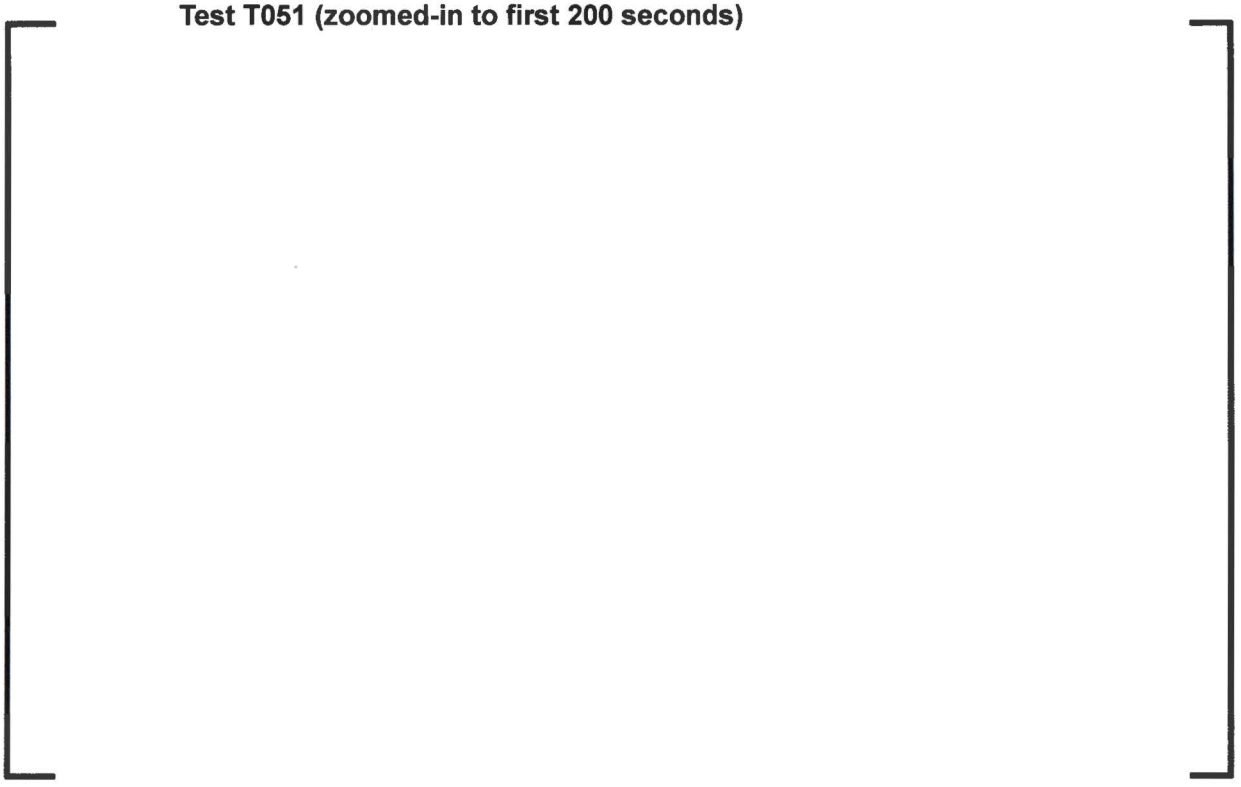

a,c

Figure 9-8 Comparison of Volume-averaged Core and Lower Plenum Boric Acid Concentrations from Tests Conducted without Debris Injection

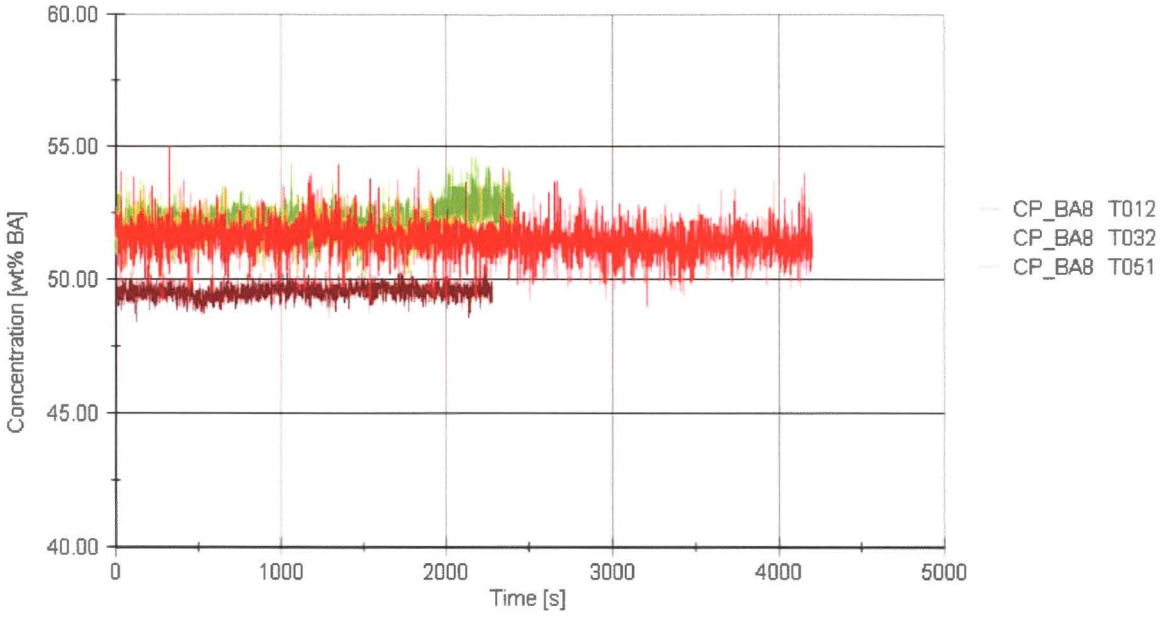

Figure 9-9 Comparison of Brine Source Concentrations from Tests Conducted without Debris Injection

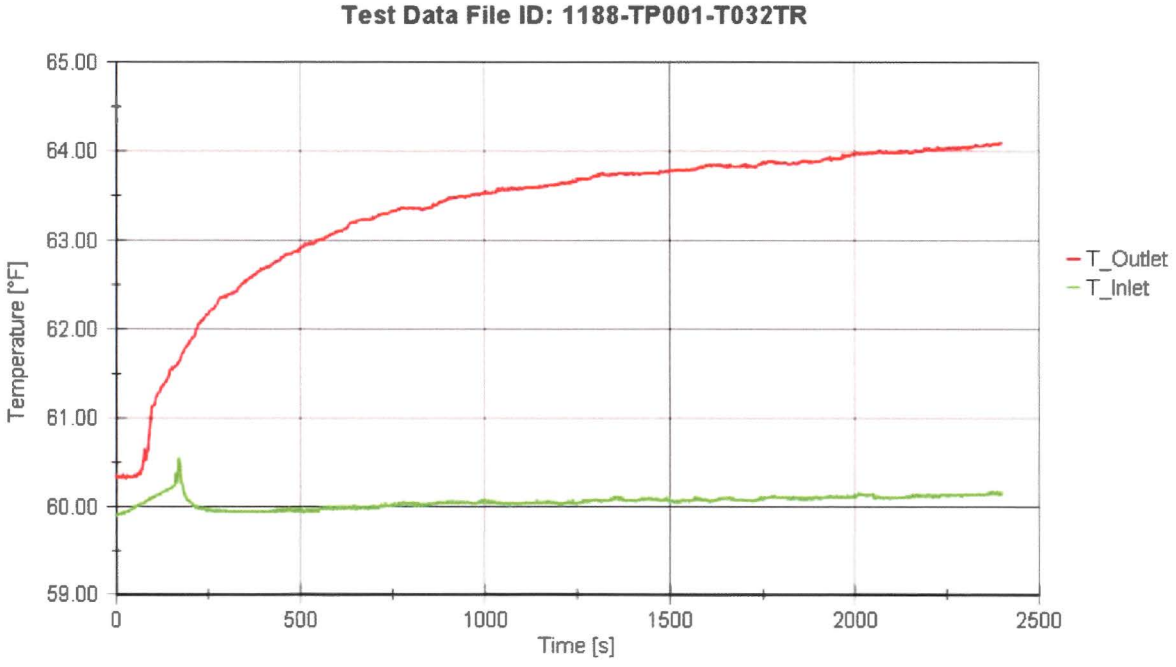

Figure 9-10 Test Column Fluid Temperatures Measured during Test T032

9.1 CALCULATION OF EXCHANGE FLOW RATE

Using results from the brine only tests described above, it is possible to determine the core-to-lower plenum exchange flow rate (i.e., the rate at which mass is transported form the core to the lower plenum) when debris is not present. Figure 9-11 provides the control volumes for the subscale facility along with the required geometric information and boundary conditions.

Performing a mass balance on the core region (V1) yields:

$$V_1 \frac{d\rho_1}{dt} = Q_B\rho_B + Q_{21}\rho_2 - Q_{out}\rho_1 - Q_{BF}\rho_1 \quad \text{Eq. 9-1}$$

where V_1 is the volume of the core region, ρ_1 and ρ_2 the core and lower plenum region densities, respectively, Q_B the volumetric brine injection flow, Q_{out} the volumetric outlet flow, and Q_{BF} the volumetric exchange flow (back flow) from the core to the lower plenum.

A volumetric flow balance across the bottom nozzle requires:

$$Q_{21} = Q_{in} + Q_{BF} \quad \text{Eq. 9-2}$$

where Q_{in} is the volumetric inlet flow.

Substituting Eq. 9-2 into Eq. 9-1 and solving for the volumetric exchange flow, Q_{BF}, produces:

$$Q_{BF} = \frac{-V_1 \frac{d\rho_1}{dt} + Q_B\rho_B + Q_{in}\rho_2 - Q_{out}\rho_1}{(\rho_1 - \rho_2)} \quad \text{Eq. 9-3}$$

Since all the variables on the right hand side of Eq. 9-3 can be determined from the experimental results, the volumetric exchange flow can be calculated for each test.

Figure 9-12 shows the experimental volumetric exchange flow from the three brine only tests (tests T012, T032, and T051). As the figure shows, the volumetric exchange flow remains fairly constant for each experiment; however, there is some variation from test-to-test with the average volumetric exchange flow from the three tests being approximately [ ]^{a,c}

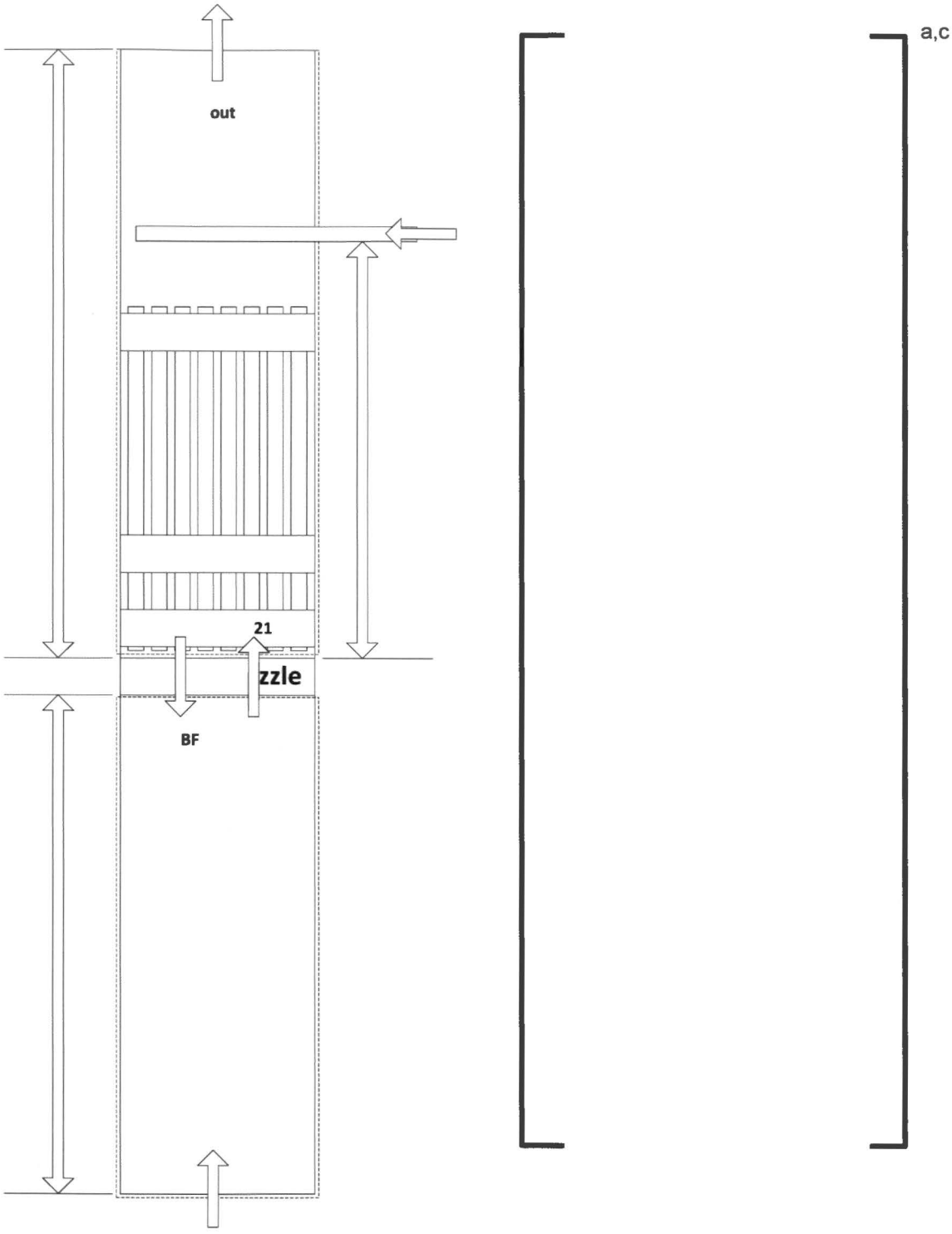

Figure 9-11 Subscale Facility Control Volumes used to Determine Exchange Flow Rate

a,c

Figure 9-12 Experimental Volumetric Exchange Flow from Tests T012, T032, and T051

9.2 PREDICTION OF EXCHANGE FLOW RATE

As described in Section 3.2, Epstein and Kenton (Reference 3-2) have developed a model to predict the buoyancy-driven exchange flow through small, multiple, openings in a horizontal partition with an externally imposed upward flow. The procedure as recommended by Epstein and Kenton (Reference 3-2), for solving such a problem is as follows: The volumetric exchange flow is calculated by first assuming unidirectional flow throughout the system (see Figure 3-1). In this manner a Q_u is calculated for each opening using Eq. 3-2. Then each opening is checked for countercurrent natural convection flow by calculating the flooding flow rate, q using Eq. 3-4. If openings are found such that $Q_u < q$, then the exchange flow rates in these openings will be bidirectional and are recomputed using the relation provided in Eq. 3-6 where Q_u to be input into this relation is already calculated from the initial, purely unidirectional analysis. If openings are found such that $Q_u > q$, then the exchange flow will remain unidirectional and the volumetric exchange flow is Q_u.

Following this procedure, Q_u is first calculated using Eq. 3-2 for the brine only experiments. In the calculation, it is assumed that [ ]^{a,c} of the bottom nozzle holes have downward flow while the remaining [ ]^{a,c} holes have upward flow. This assumption is justified based on experimental observations which indicated that only a [ ]^{a,c} Also in Eq. 3-2, the length L, which is used to determine the gravitational head for the system, is the distance between the [ ]^{a,c}

The flooding flow rate, q is calculated using Eq. 3-4 for the brine only experiments. In the calculation, the bottom nozzle geometry provided in Figure 9-11 is used to calculate the aspect ratio (L/D) for the bottom nozzle holes.

Figure 9-13 shows the calculated unidirectional flow, Q_u, and the flooding flow, q, for test T012. Here, the unidirectional flow is divided by the number of bottom nozzle holes experiencing downward flow since the flooding flow is calculated for a single hole. As the figure shows, [ ]a,c Similar results are obtained for tests T032 and T051 even though the core inlet geometry is different than that used in test T012.

[a,c

Figure 9-13 Unidirectional and Flooding Volumetric Flows Calculated for Test T012

Now that it has been determined that mass transport in the subscale facility is governed by a [ ]a,c This comparison is shown in Figure 9-14 for tests T012, T032, and T051. In the figure, the volumetric exchange rate is determined using densities obtained from test T051 since it was the longest duration test. Using densities from the other two tests conducted at this condition produces similar results. The comparison shows that the [ ]a,c reasonably represents the average of the experimental exchange rates from the brine only tests.

a,c

Figure 9-14 Comparison of Unidirectional Volumetric Exchange Rate to Experimental Exchange Rates from Tests T012, T032, and T051

10 TESTS WITH CONCURRENT BRINE AND DEBRIS INJECTION

The majority of brine tests were completed with concurrent brine and debris injection. That is, brine was injected into the test column starting at the beginning of the test consistent with the start of debris injection. As seen in Table 10-1, 13 concurrent tests were completed using the Westinghouse core inlet geometry and 18 concurrent tests were completed using the AREVA core inlet geometry. All of the tests shown in Table 10-1 were conducted with a 0.5 gpm brine injection rate and an initial column inlet flow rate of 3.43 gpm/FA.

In these tests, a debris bed [ ]^{a,c}
The core region brine concentration increased quickly and the onset of buoyancy-driven exchange flow was reached within the first minute of the experiment. For tests conducted with lower debris loads, [ ]^{a,c} In these tests, the debris bed [
]^{a,c} As the debris load was increased, the formation of the debris bed was [ ]^{a,c} As the tests continued, the upward flow rate reduced and the density gradient between the core and lower plenum increased, thus increasing the potential for exchange flow. For tests in which a debris bed was [

]^{a,c}

This behavior is discussed in detail in the following sections.

Table 10-1 Summary of Concurrent Brine and Debris Introduction Tests

Test ID	Core Inlet Geometry	Brine Source Conc. (wt% KBr)	Fiber Load (g/FA)	p:f Ratio
T027	Westinghouse	5	2.5	0
T026	Westinghouse	5	5	0
T046	AREVA			
T047	AREVA	5	7.5	0
T013	Westinghouse	10	5	0
T015 / T017 / T029	Westinghouse	10	7.5	0
T035 / T042 / T053 / T055	AREVA			
T036	AREVA	10	7.5	2
T018 / T022	Westinghouse	10	10	0
T041 / T048 / T052 / T054	AREVA			
T038 / T043	AREVA	10	15	0

Table 10-1 Summary of Concurrent Brine and Debris Introduction Tests (cont.)				
Test ID	**Core Inlet Geometry**	**Brine Source Conc. (wt% KBr)**	**Fiber Load (g/FA)**	**p:f Ratio**
T040	AREVA	10	15	1
T049	AREVA	10	15	2
T024 / T030	Westinghouse	15	10	0
T044	AREVA			
T025 / T031	Westinghouse	15	15	0
T045 / T050	AREVA			
T028	Westinghouse	15	20	0

10.1 TESTS CONDUCTED WITH 5 WEIGHT PERCENT POTASSIUM BROMIDE SOURCE CONCENTRATION

Four tests were conducted using a nominal 5 wt% KBr source concentration. This section presents results from these tests in the order from least to highest debris load.

Test T027 was conducted with the Westinghouse core inlet geometry and a 2.5 g/FA fibrous debris load. Figure 10-1 shows the volume-averaged BA concentrations for the core and lower plenum regions from test T027. The figure also provides uncertainty bands for the concentrations that are based on conductivity probe accuracy. As seen in the figure, [

]^{a,c} During this test, it was noted that [

]^{a,c}

Tests T026 and T046 were conducted with the Westinghouse and AREVA core inlet geometries, respectively. Both tests applied a 5 g/FA debris load. Figure 10-2 shows the volume-averaged BA concentrations for the core and lower plenum regions from tests T026 and T046. The figure also provides uncertainty bands for the concentrations that are based on conductivity probe accuracy. As seen in the figure, [

]^{a,c}

During test T046, [

]a,c The differences in test T026 and T046 is most likely due to [

]a,c Even though these tests were conducted with different core inlet geometries, the brine only tests showed that there was [

]a,c The other difference in these tests is that T046 had a higher core region concentration. This is because the brine source concentration was higher in test T046, as shown in Figure 10-3. [

]a,c

Test T047 was conducted with the AREVA core inlet geometry and a 7.5 g/FA fibrous debris load. Figure 10-4 shows the volume-averaged BA concentrations for the core and lower plenum regions from test T027. The figure also provides uncertainty bands for the concentrations that are based on conductivity probe accuracy. As seen in the figure, [

]a,c

[a,c

Figure 10-1 Volume-averaged Core and Lower Plenum Boric Acid Concentrations from Test T027

a,c

Figure 10-2 Volume-averaged Core and Lower Plenum Boric Acid Concentrations from Tests T026 and T046

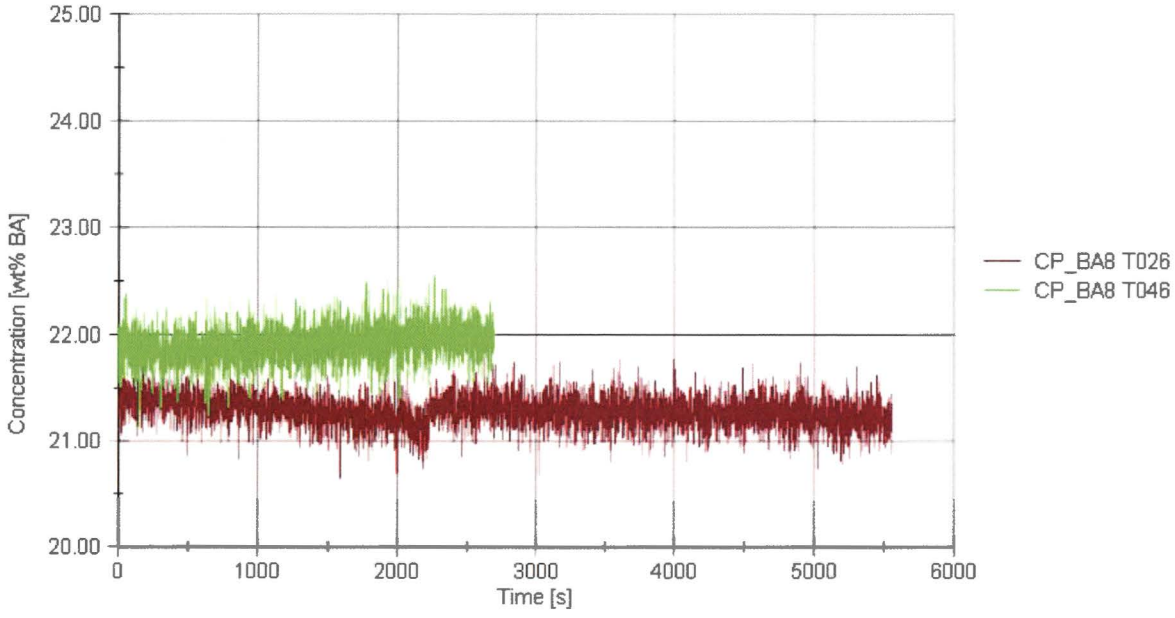

Figure 10-3 Boric Acid Source Concentrations from Tests T026 and T046

[a,c

]

Figure 10-4 Volume-averaged Core and Lower Plenum Boric Acid Concentrations from Test T047

10.2 TESTS CONDUCTED WITH 10 WEIGHT PERCENT POTASSIUM BROMIDE SOURCE CONCENTRATION

Nineteen tests were completed using a nominal 10 wt% KBr source concentration. This section presents results from these tests in the order from least to highest debris load.

Test T013 was conducted with the Westinghouse core inlet geometry and a 5 g/FA fibrous debris load. Figure 10-5 shows the volume-averaged BA concentrations for the core and lower plenum regions from test T013. The figure also provides uncertainty bands for the concentrations that are based on conductivity probe accuracy. As seen in the figure, [

]a,c

A number of tests were conducted using a 7.5 g/FA fibrous debris load and a 10 wt% KBr source concentration. In addition, one test was completed with a 2:1 p:f ratio. First, the Westinghouse core inlet geometry tests will be discussed, followed by the AREVA core inlet geometry tests.

Tests T015, T017, and T029 were conducted using the Westinghouse core inlet geometry. Figure 10-6 shows the volume-averaged BA concentrations for the core and lower plenum

regions from these three tests. The uncertainty bands from these tests have been removed from this figure to make comparisons easier. As the figure shows, [

]a,c

Tests T035, T042, T053, and T055 were conducted using the AREVA core inlet geometry. Figure 10-7 shows the volume-averaged BA concentrations for the core and lower plenum regions from these three tests. The uncertainty bands have also been removed from this figure to make comparisons easier. As the figure shows, [

]a,c

Test T036 was also completed using the AREVA core inlet geometry. In this test, 7.5 g/FA of fibrous debris was injected into the test column with a p:f ratio of 2:1. In Figure 10-8, the volume-averaged BA concentrations from this test are compared to results from test T042 which was conducted with the same fiber load but without particulate. As seen in the figure, [

]a,c

[a,c]

Figure 10-5 Volume-averaged Core and Lower Plenum Boric Acid Concentrations from Test T013

a,c

Figure 10-6 Volume-averaged Core and Lower Plenum Boric Acid Concentrations from Tests T015, T017, and T029

a,c

Figure 10-7 Volume-averaged Core and Lower Plenum Boric Acid Concentrations from Tests T035, T042, T053, and T055

[a,c

]

Figure 10-8 Volume-averaged Core and Lower Plenum Boric Acid Concentrations from Tests T036 and T042

Two tests were completed using the Westinghouse core inlet geometry with a fibrous debris load of 10 g/FA. Figure 10-9 shows the volume-averaged BA concentrations from tests T018 and T022. As seen in the figure, [

]a,c This difference can be explained by reviewing the column inlet flow for these tests, as seen in Figure 10-10. As Figure 10-10 indicates, the column inlet flow rate was different during these two tests. [

]a,c

Four tests were completed using the AREVA core inlet geometry with a fibrous debris load of 10 g/FA. Figure 10-11 shows the volume-averaged BA concentrations from tests T041, T048, T052, and T054. Comparison of these results is interesting in that the tests with [

]a,c

a,c

Figure 10-9 Volume-averaged Core and Lower Plenum Boric Acid Concentrations from Tests T018 and T022

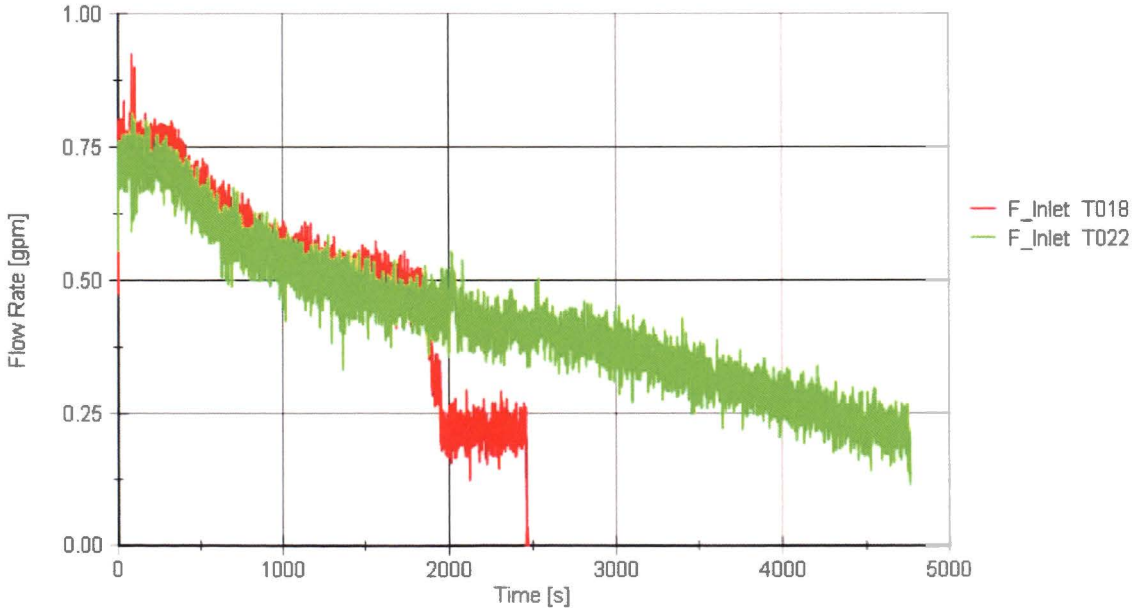

Figure 10-10 Test Column Inlet Flow Rate from Tests T018 and T022

[ ] a,c

Figure 10-11 Volume-averaged Core and Lower Plenum Boric Acid Concentrations from Tests T041, T048, T052, and T054

Four tests, all using the AREVA core inlet geometry, were completed at this source concentration with a fibrous debris load of 15 g/FA. Tests T038 and T043 were conducted without particulate, while test T040 was conducted with a p:f ratio of 1:1, and test T049 with a p:f ratio of 2:1. The volume-averaged BA concentrations from these four tests are shown in Figure 10-12. As the figure indicates, the trends in all four tests are similar. [

]^{a,c} In test T049, which was conducted with a p:f ratio of 2:1, [

]^{a,c} In test T040, which was conducted with a p:f ratio of 1:1, [ ]^{a,c} For test T038 and T043, which were conducted without particulate, [

]^{a,c}

a,c

Figure 10-12 Volume-averaged Core and Lower Plenum Boric Acid Concentrations from Tests T038, T043, T040, and T049

10.3 TESTS CONDUCTED WITH 15 WEIGHT PERCENT POTASSIUM BROMIDE SOURCE CONCENTRATION

Eight tests were completed using a nominal 15 wt% KBr source concentration. This section presents results from these tests in the order from least to highest debris load.

Tests T024, T030, and T044 were conducted using a fibrous debris load of 10 g/FA. Tests T024 and T030 were conducted with the Westinghouse core inlet geometry and test T044 was conducted using the AREVA core inlet geometry. Figure 10-13 shows the volume average boric acid concentrations from these three tests. As the figure indicates, [

]^{a,c} The difference between this test and the two conducted with the Westinghouse core inlet geometry is that the core region concentration is considerably higher. It does however indicate that the AREVA inlet geometry is [ ]^{a,c} as was also seen in tests conducted with lower fibrous debris loadings.

Four tests were completed using a fibrous debris load of 15 g/FA. Tests T025 and T031 were conducted using the Westinghouse core inlet geometry and tests T045 and T050 were conducted using the AREVA core inlet geometry. Figure 10-14 shows the volume-averaged BA

concentrations from these tests. As seen in the figure, tests T024 and T030 agree well but do not agree with tests T045 and T050 because the core region concentration is higher in these tests. As a result, [ ]a,c

Test T028 was completed using the Westinghouse core inlet geometry and a fibrous debris load of 20 g/FA. The volume-averaged BA concentrations from this test are shown in Figure 10-15. As seen in the figure, [

]a,c

a,c

Figure 10-13 Volume-averaged Core and Lower Plenum Boric Acid Concentrations from Tests T024, T030, and T044

a,c

Figure 10-14 Volume-averaged Core and Lower Plenum Boric Acid Concentrations from Tests T025, T031, T045, and T050

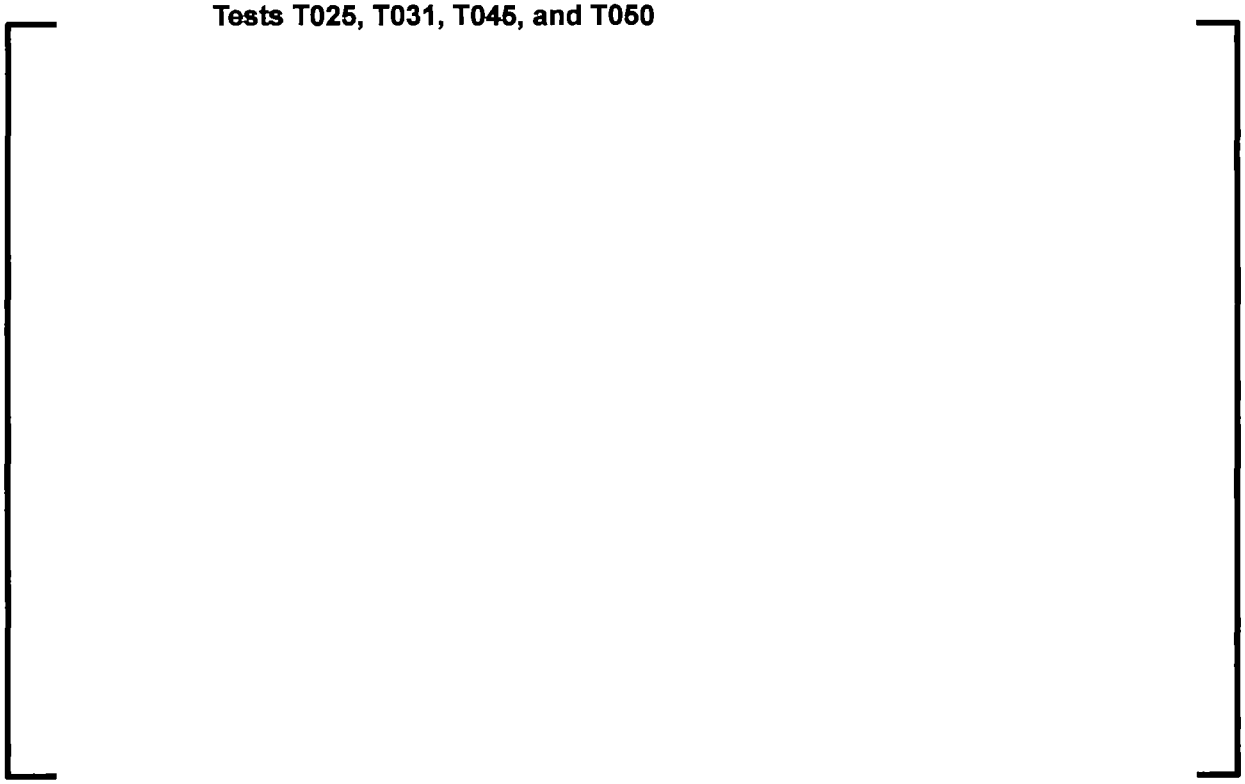

a,c

Figure 10-15 Volume-averaged Core and Lower Plenum Boric Acid Concentrations from Test T028

10.4 CALCULATION OF EXCHANGE FLOW RATE

In this section, the exchange rate is calculated using the same approach as that described in Section 9.1. Results from these calculations are compared to results obtained in Section 9.1 as a means to quantify the impact that debris has on the exchange process. Table 10-2 lists the concurrent debris tests used to calculate the exchange flow rate. As shown in the table, three tests conducted with 5 wt% KBr source concentration were used with varying fiber loads. Similarly, three tests conducted using 10 wt% KBr source concentration were used and two tests conducted using 15 wt% KBr source concentration were used.

Figure 10-16 shows the calculated exchange flow rates from tests conducted with a 5 wt% KBr source concentration. As the figure shows, [

]^{a,c} Figure 10-17 shows the exchange flow rate from the tests conducted with 10 wt% KBr. Also provided in this figure is the exchange flow rate from test T051 which was completed without fibrous debris. As the figure shows, [

]^{a,c} Figure 10-18 shows results from tests conducted with a 15 wt% KBr source concentration. Again, these tests show that [

]^{a,c}

Table 10-2 Summary of Concurrent Brine Tests used to Calculate The Exchange Flow Rate

Test ID	Brine Source Conc. (wt% KBr)	Fiber Load (g/FA)
T027	5	2.5
T026	5	5
T047	5	7.5
T013	10	5
T015	10	7.5
T022	10	10
T024	15	10
T025	15	15

a,c

Figure 10-16 Experimental Volumetric Exchange Flow from Tests T027, T026, and T047

a,c

Figure 10-17 Experimental Volumetric Exchange Flow from Tests T051, T013, T015, and T047

[a,c

]

Figure 10-18 Experimental Volumetric Exchange Flow from Tests T024 and T025

10.5 PREDICITON OF EXCHANGE FLOW RATE

With the experimental exchange flow rates calculated for the concurrent brine and debris injection tests, it is interesting to see if a relation can be developed that relates [ ]a,c For tests completed without debris, it was shown in Section 9.2 that the exchange flow rate could be reasonably predicted by [ ]a,c To investigate this hypothesis, [ ]a,c for the tests shown in Table 10-2. In these calculations, [ ]a,c Results from this calculation are shown in Figure 10-19 which shows [ ]a,c

a,c

Figure 10-19 Number of Holes In Bottom Nozzle that Experience Downflow

10.6 PREDICTION OF DEBRIS BED BREAK-THROUGH

A number of test conditions resulted in a situation in which [

]a,c

As described in Section 3.3, the inception of buoyancy-driven exchange flow is governed by several factors. First, the density gradient between the core and lower plenum due to solute concentration differences must overcome any density gradient caused by the temperature difference between the core and lower plenum. Second, since there is upflow, the buoyancy-driven exchange flow in the downward direction must be larger than the flow rate in the upward direction such that there is net mass exchange between the core and lower plenum. [

]a,c

Considering this, Froude number was calculated using Eq. 4-3 at [

]^{a,c} For the calculation of Froude number, the length used is the height of the core region (4 ft) and velocity is calculated using the flow areas of the bottom nozzle and lower end fittings used in the subscale facility. Table 10-3 summarizes results from this calculation and Figure 10-20 presents the results graphically.

These results can be used to predict [

]^{a,c} For the Westinghouse core inlet geometry, the Froude number [

]^{a,c} For the AREVA core inlet geometry, the Froude number [

]^{a,c}

Table 10-3 Summary of Froude Number Calculation

Test ID	a,c
T015	
T017	
T018	
T022	
T024	
T025	
T026	
T028	
T029	
T030	
T031	
T038	
T040	
T043	
T049	
T052	

a,c

Figure 10-20 Froude Number Calculation

11 TESTS WITH DELAYED BRINE INJECTION

Several tests were completed using the Westinghouse core inlet geometry that had delayed brine injection. In these tests, the injection of brine was delayed 20 minutes after the injection of debris began. This allowed for a debris bed to form prior to creating the density gradient between the core and lower plenum regions. As seen in Table 11-1, six delayed brine injection tests were completed. All of the tests shown in Table 11-1 were conducted with a 0.5 gpm brine injection rate and an initial column inlet flow of 3.43 gpm/FA.

In these tests, a debris bed [ ]^{a,c} In all tests, the introduction of brine resulted [

]^{a,c} This section presents results from these tests in the order from least to highest debris load.

Table 11-1 Summary of Concurrent Brine and Debris Introduction Tests

Test ID	Core Inlet Geometry	Brine Source Conc. (wt% KBr)	Fiber Load (g/FA)	p:f Ratio
T014	Westinghouse	10	5	0
T016	Westinghouse	10	7 5	0
T020	Westinghouse	10	7 5	2:1
T019 / T023	Westinghouse	10	10	0
T021	Westinghouse	10	15	1·1

Test T014 was conducted with a 5 g/FA debris load. Figure 11-1 shows the volume-averaged BA concentrations from this test. As the figure shows, [

]^{a,c} The core and lower plenum region BA concentrations are comparable to those seen in test T013, which was conducted at similar conditions but with concurrent brine injection.

Tests T016 and T020 were conducted with a 7.5 g/FA debris load. Test T016 was conducted without particulate and test T020 was conducted with a p:f ratio of 2:1. Figure 11-2 shows the volume-averaged BA concentrations from these tests. As the figure shows, [

]^{a,c} Test T020, which was conducted with a p:f ratio of 2:1, [

]^{a,c}

Tests T019 and T023 were both conducted with a 10 g/FA debris load. Figure 11-3 shows the volume-averaged BA concentrations from these tests. As the figure shows, [

]a,c

Test T021 was conducted with a fibrous debris load of 15 g/FA and a p:f ratio of 1:1. Figure 11-4 shows the volume-averaged BA concentrations from this test. The trends in the figure are expected in that [

]a,c

[a,c]

Figure 11-1 Volume-averaged Core and Lower Plenum Boric Acid Concentrations from Test T014

a,c

Figure 11-2 Volume-averaged Core and Lower Plenum Boric Acid Concentrations from Tests T016 and T020

a,c

Figure 11-3 Volume-averaged Core and Lower Plenum Boric Acid Concentrations from Tests T019 and T023

[a,c

]

Figure 11-4 Volume-averaged Core and Lower Plenum Boric Acid Concentrations from Test T021

11.1 MODEL PREDICTIONS OF DELAYED BRINE INJECTION TESTS

In this section, relations for the volumetric exchange flow rate and [ ]^{a,c} are used in conjunction with the empirical relation for unidirectional flow developed by Epstein (Reference 3-1) to predict the time-histories of the core and lower plenum brine concentrations. First, mass balances are written for the brine concentration, Y_i, for each region shown in Figure 9-11.

Starting with the core region (V1):

$$V_1 \frac{dY_1}{dt} = Q_B Y_B + Q_{in} Y_2 + Q_u (Y_2 - Y_1) - Q_{out} Y_1 \qquad \text{Eq. 11-1}$$

And for the lower plenum region (V2):

$$V_2 \frac{dY_2}{dt} = Q_u (Y_1 - Y_2) - Q_{in} Y_2 \qquad \text{Eq. 11-2}$$

In the above equations, V_1 and V_2 are the core and lower plenum liquid volumes, respectively. Q_B is the brine injection volumetric flow rate, Y_B the brine injection concentration, Q_{in} the

volumetric flow of fresh water entering the lower plenum, and Q_{out} the volumetric flow exiting the core which is equal to $Q_{ln} + Q_B$.

Eqs. 11-1 and 11-2 are solved numerically to obtain Y_1 and Y_2 as a function of time. Since a debris bed [ ]^{a,c} the first step in performing the simulations is to calculate the Froude number based on Eq. 4-3. The calculated Froude number at each time step is then compared to the critical Froude numbers listed in Table 10-3 for the given debris bed load. Once the critical Froude number is reached, [ ]^{a,c} When calculating the unidirectional exchange flow, the trend line in Figure 10-19 is used to determine [ ]^{a,c} The results of the numerical simulations are discussed below for each of the delayed brine tests.

Test T014 was conducted with a fibrous debris load of 5 g/FA. Based on Table 10-3, the critical Froude number for a 5 g/FA debris bed with Westinghouse core inlet geometry is [ ]^{a,c} Using the inlet flow rate from test T014 and the volume-averaged brine concentrations predicted by the model, the critical Froude number is reached in the simulation [ ]^{a,c} after the start of the test. This time agrees well with [ ]^{a,c} Figure 11-5 shows the volume-averaged KBr concentrations from the test and compares them to those predicted by the model. As seen in the figure, the lower plenum concentration predicted by the model is within the uncertainty of the experimental lower plenum concentration. The core concentration predicted by the model is within 20% of the experimental core concentration.

Test T016 was conducted with a fibrous debris load of 7.5 g/FA. Based on Table 10-3 the critical Froude number for a 7.5 g/FA debris bed with Westinghouse core inlet geometry is [ ]^{a,c} Using the inlet flow rate from test T016 and the volume-averaged brine concentrations predicted by the model, the critical Froude number is reached in the simulation [ ]^{a,c} after the start of the test. In this case, the predicted [ ]^{a,c} Figure 11-6 shows the volume-averaged KBr concentrations from the test and compares them to those predicted by the model. As seen in the figure, the lower plenum concentration predicted by the model is within the uncertainty of the experimental lower plenum concentration. The core concentration predicted by the model is within 16% of the experimental core concentration.

Test T019 was conducted with a fibrous debris load of 10 g/FA. Based on Table 10-3 the critical Froude number for a 10 g/FA debris bed with Westinghouse core inlet geometry is [ ]^{a,c} Using the inlet flow rate from test T019 and the volume-averaged brine concentrations predicted by the model, the critical Froude number is reached in the simulation [ ]^{a,c} after the start of the test. In this case, the predicted [ ]^{a,c} Figure 11-7 shows the volume-averaged KBr concentrations from the test and compares them to those predicted by the model. As seen in the figure, the lower plenum

concentration predicted by the model falls just outside the uncertainty band of the experimental lower plenum concentration. The core concentration predicted by the model is within 22% of the experimental core concentration.

Test T021 was conducted with a fibrous debris load of 15 g/FA. Based on Table 10-3 the critical Froude number for a 15 g/FA debris bed with Westinghouse core inlet geometry is [ ]^{a,c} however, when this value is applied [ ]^{a,c} As a result, a critical Froude number of [ ]^{a,c} is selected for the simulation such that better agreement to the experimental result is obtained. Using the inlet flow rate from test T021 and the volume-averaged brine concentrations predicted by the model, the critical Froude number is reached in the simulation [ ]^{a,c} after the start of the test. In this case, the predicted [ ]^{a,c} Figure 11-8 shows the volume-averaged KBr concentrations from the test and compares them to those predicted by the model. As seen in the figure, [ ]^{a,c} However, the final lower plenum concentration predicted agrees well with experimental value. The core concentration predicted by the model is within 10% of the experimental core concentration.

[a,c]

Figure 11-5 Volume-averaged Core and Lower Plenum Boric Acid Concentrations from Test T014 Compared to Model Predictions

a,c

Figure 11-6 Volume-averaged Core and Lower Plenum Boric Acid Concentrations from Test T016 Compared to Model Predictions

a,c

Figure 11-7 Volume-averaged Core and Lower Plenum Boric Acid Concentrations from Test T019 Compared to Model Predictions

a,c

Figure 11-8 Volume-averaged Core and Lower Plenum Boric Acid Concentrations from Test T021 Compared to Model Predictions

Overall, the predictions of the delayed brine tests were reasonable with the maximum difference between the predicted and the experimental concentrations being 22% at the end of test T019 in the core region. In general, the core region concentration had the highest difference which can be attributed to the concentration of brine assumed to be exiting the core. In the predictions, it is assumed that the brine concentration exiting the test column is at the core average. Given that the brine injection point is at the top of the core volume and that the sparger orientation is such that the higher source concentration is injecting upwards, it is reasonable to expect that the concentration exiting the test column is greater than the core average concentration.

To investigate this effect, a sensitivity case is performed for test T019. In the sensitivity case, the brine concentration exiting the test column is increased to 120% of the core volume-averaged concentration. Results from this case are shown in Figure 11-9. As the figure shows, both the core and lower plenum region predicted brine concentrations are within the experimental uncertainty.

a,c

Figure 11-9 Volume-averaged Core and Lower Plenum Boric Acid Concentrations from Test T019 Compared to Model Predictions Showing the Effect of Increased Brine Concentration Exiting the Test Column

12 SUMMARY OF RESULTS AND CONCLUSIONS

The subscale brine test program was successful in improving the state of knowledge of density-driven mass transport between the core and the lower plenum in the presence of in-vessel debris. The testing considered a broad range of conditions prototypic of those expected to occur following a postulated large CLB LOCA and considered both Westinghouse and AREVA core inlet geometries by using prototypic fuel components.

In the testing, the density gradient that develops between the core and the lower plenum due to the build-up of boron solutes in the core was simulated using a potassium bromide solution. Flow through the test column was scaled based on the boil-off rate calculated for prototypic Post-LOCA conditions. For tests that had brine injection, the flow rate was reduced during each test consistent with the decay heat curve. For tests conducted with debris only (no brine injection) the flow rate was held constant at a value consistent with decay heat boil-off calculated at 20 minutes post-LOCA. Fibrous debris loadings of 2.5 – 22.5 grams per full-area fuel assembly (g/FA) arriving at the core inlet were considered in the testing, which is consistent with the range of debris loads expected to enter the reactor vessel following a large CLB scenario. A limited number of tests were completed with fibrous and particulate debris to understand the impact that particulate debris has on the resulting debris bed and the core-to-lower plenum buoyancy-driven exchange process.

For the range of debris loads tested, it was shown that debris beds formed under low-flow conditions prototypic of a large CLB scenario result in minimal head loss. Section 8 presents pressure drop results from tests completed without brine injection which show that the maximum pressure drop achieved across the debris bed was less than [ ]^{a,c} when experimental uncertainty was considered. The maximum pressure drop was achieved during test T033 which was conducted with a fibrous debris load of 22.5 g/FA and no particulate. The second highest pressure drop from the debris only tests was achieved in test T034 which was also conducted with a fibrous debris load of 22.5 g/FA but included a particulate load with a p:f ratio of 12:1. Although the accuracy of the pressure transducer at these low pressures makes it difficult to compare results with any certainty, the trends in Figure 8-3 clearly show that [

]^{a,c} This observation is consistent with that seen in the subscale head loss testing documented in Reference 2-1 which showed that [

]^{a,c}

Data from tests conducted without debris injection presented in Section 9 are used to calculate the volumetric exchange flow rate that occurs across the core inlet geometry used in the subscale facility. Comparison of the exchange flow rates from the test conducted with the Westinghouse core inlet geometry to tests conducted with the AREVA core inlet geometry show that both geometries [ ]^{a,c} When the experimental exchange flow rate from the Westinghouse core inlet geometry test is compared to theoretical values predicted by empirical relations previously developed by Epstein (Reference 3-1) and Epstein and Kenton (Reference 3-2), it is determined that the exchange flow process [

]a,c

For tests conducted with concurrent brine and debris injection, it was shown in Section 10 that [

]a,c Densimetric Froude number provides the relative importance of inertia to buoyancy forces. As Froude number reduces buoyancy forces become more dominant. In this scenario, a reduction in upward liquid velocity or an increase in density difference results in a reduction in Froude number.

As the Froude number [

]a,c

In Section 11, results from tests with delayed brine injection are presented. In these tests, [

]a,c Concentration estimates from simulations of the delayed brine injection tests were shown to be within 22% of the volume-averaged experimental core and lower plenum concentrations. The largest differences between the simulations and the experimental results were for the core region concentration, and it was shown that the difference is most likely due to the assumption that the brine concentration exiting the test column is equal to the volume average core concentration. If the brine concentration exiting the test column is increased to 120% of the average core concentration, the simulation results match the experimental results to within 5%.

The brine test results demonstrate that [

]a,c